GROUNDWATER DISCHARGE FROM THE LEEWARD HALF

OF THE BIG ISLAND, HAWAI‘I

THESIS SUBMITTED TO THE GRADUATE DIVISION OF THE
UNIVERSITY OF HAWAI‘I IN PARTIAL FULFILLMENT
OF THE REQUIREMENTS FOR THE DEGREE OF

MASTER OF SCIENCE

IN

GEOLOGY AND GEOPHYSICS

AUGUST 2008

By
Adam G. Johnson

Thesis Committee

Craig Glenn, Chair
Jeffrey Gillis-Davis
Paul Lucey
Frank Sansone

We certify that we have read this thesis and that, in our opinion, it is satifactory in scope and quality as a thesis for the degree of Master of Science in Geology and Geophysics.

THESIS COMMITTEE

Chairperson

Acknowledgements

Throughout the process of this research I was very fortunate to have worked with and been helped along by so many people. I would first like to thank my advisor, Craig Glenn, for providing me with the opportunity to come to Hawaii to work on this project. His support, guidance, patience, and sacrifices in all phases of our research have made the completion of this thesis successful. I am grateful to my committee members, Jeff Gillis-Davis, Paul Lucey, and Frank Sansone for their valuable input, timely help, and encouragement.

This project has been a collaborative effort, with our colleagues Bill Burnett and Ricky Peterson from Florida State University being an essential part of our great team. Many thanks to George Wilkins for not only providing the inspiration and direction for this project, but also for the hospitality, cold beer, and great steaks.

The aerial surveys were a major component of this research, and were accomplished through the efforts of many people. Matt Barbee, Josh Cahill, Jeff Gillis-Davis, Dave Hampton, Will Koeppen, Paul Lucey, Mike Winter, and Mark Wood were all extraordinarily helpful throughout all phases the aerial surveys and data processing.

Fieldwork would not have been possible without the substantial aid from Bill Walsh, Brent Carman, and staff at the Kona Division of Aquatic Resources. We are most indebted to Sallie Beavers, Rebecca Most, and the staff at Kaloko-Honokohau National Historical Park, and Bob Ravenscroft and Owen Suzuki at the Department of Water Supply. Mahalo to Vergi and Kai Rojas at Kahauloa Bay and David and Sandy Esperanza at Manini Beach. I was very fortunate to have assistance from Henrieta Dulaiova, Jesse Favia, Dave Gremminger, Eric Grossman, Jacque Kelly, Carrie Plath, Isaac Santos, Axel

Schmidt, and Benjamin Sellers- all who helped in various ways including fieldwork preparations, sampling, and manuscript revisions. Finally, this thesis would never have been realized without the enthusiasm and encouragement from my family, friends, and fellow students in the Geology and Oceanography departments.

Abstract

Fluxes of dissolved nutrients and other species via groundwater pathways are now recognized as important components of coastal marine biogeochemical budgets and ecological systems. Unfortunately, determining groundwater discharge locations and associated fluxes over wide areas has remained, until now, highly problematic. We report on the first large-scale quantitative application of integrating precise aerial thermal infrared mapping of groundwater input locations and their oceanic dispersal patterns with ground-based nutrient and radiochemically-measured water flux estimates along the majority of the dry, western half of the large volcanic island of Hawaii. Our high-resolution imagery (<0.1^{o}C; 1.3m/pixel) depicts the locations and relative magnitudes of more than 50 cold, but buoyant, submarine groundwater discharge (SGD) "plumes" dispersing into the ocean. The plumes are cool, brackish, nutrient-rich groundwaters injected into and floating on top of the ocean. These inputs represent the only source of new nutrients into the region's nutrient-poor coastal waters. Based on time-series measurements of ^{222}Rn and salinity, we estimate a total daily load of ~26,000, 3,800, and 160 moles of dissolved inorganic Si, N, and P, respectively, for six of the larger discharge plumes. These fluxes are similar in magnitude to those discharged from heavily populated coastlines, (e.g. northeast U.S. and Korea), but along west Hawaii nutrients exhibit conservative mixing. We use a proportionality between plume surface area and discharge rate to approximate individual flux estimates for each of the groundwater plumes we mapped. For 65 km of coastline, we estimate a cumulative total groundwater (mixed fresh and marine) flux from 42 point-source groundwater inputs to be about 260,000 m^3 d^{-1}.

Table of Contents

Acknowledgements……iii

Abstract……....v

List of Tables……..ix

List of Figures……..x

List of Panels…….xii

CHAPTER 1: REGIONAL ASSESSMENTS AND UPSCALING OF SUBMARINE GROUNDWATER DISCHARGE TO THE OCEAN: BIG ISLAND HAWAII AS THE "PRISTINE" ENDMEMBER……...1

1.1 Introduction……..2

Setting of West Hawaii…….4

1.2 Methods…….……....7

Aerial Thermal Infrared Surveys…….7

Water Column Profiles……..10

Regional Nutrient Sampling……...11

Groundwater Discharge Fluxes…….11

1.3 Results and Discussion…...……..……..12

Aerial Thermal Infrared Surveys.....…….12

Water Column Profiles……..18

Regional Nutrient Characteristics……22

Groundwater Discharge Fluxes ...…..……...25

Up-Scaling Groundwater Fluxes…..…….26

Nutrient Flux Estimates…..……...31

1.4 Conclusions……...……..36

CHAPTER 2: AERIAL INFRARED IMAGING REVEALS LARGE NUTRIENT-RICH GROUNDWATER INPUTS TO THE OCEAN……..38

Abstract…….39

2.1 Introduction……39

2.2 Methods……...43

Aerial TIR Surveys……43

Temperature and Salinity Profiles and Nutrients...….…….…….43

Groundwater Discharge Fluxes...……..44

2.3 Results and Discussion……...45

2.4 Conclusions…….50

APPENDIX A: August 2005 Aerial Thermal Infrared Survey……...52

Overview……...52

Survey Details……...52

Post-flight Image Processing……...54

Initial temperature calibrations…….54

Image spatial corrections……..54

Patching procedure……56

Ground-truthing temperature calibrations……57

APPENDIX B: April/May 2007 Aerial TIR Survey: Kawaihae to Hookena…….59

Overview……...59

Survey Details……...59

Post-flight Image Processing……...65

Overview……65

Initial temperature calibrations……65

Correcting sensor drift……...66

Atmospheric and skin-layer corrections……68

Other sources of temperature error……...69

Sunglint and edge effects……...69

Heating artifacts and reduced water temperature contrast……...70

APPENDIX C: Mass Balance Model to Quantify SGD…...……73

APPENDIX D: Anthropogenic Phosphate in Honokohau Harbor…….78

APPENDIX E: Nutrient Sample Tables……81

APPENDIX F: Aerial TIR Survey Imagery……..91

REFERENCES……...135

List of Tables

Table 1. Locations of point-source and diffuse groundwater inputs to west Hawaii identified in aerial TIR surveys…….14

Table 2. Total SGD fluxes and plume areas of six groundwater discharges…….....26

Table 3. Comparison of groundwater discharge nutrient inputs to different regions …...33

Table 4. Comparison of independent estimates of groundwater nutrient inputs to west Hawaii……...34

Table A1. August 16, 2005 aerial TIR survey flight line times…….……53

Table B1. April 30, 2007 aerial TIR survey flight line times……..…. 63

Table B2. May 1, 2007 aerial TIR survey flight line times……..…….64

Table E1. Freshwater wells nutrient samples……82

Table E2. Brackish wells nutrient samples……83

Table E3. WWTP and brackish wells inland from Honokohau Harbor……84

Table E4. Brackish ponds nutrient samples……...85

Table E5. Kiholo Bay nutrient samples…….86

Table E6. Honokohau Harbor nutrient samples…….87

Table E7. Kailua Bay nutrient samples……..88

Table E8. Kealakekua Bay nutrient samples…….89

Table E9. Kealakekua Bay samples (Kahauloa Inlet)……...90

List of Figures

Figure 1. Location map of Hawaiian Islands and west Hawaii survey area……5

Figure 2. Schematic cross section of west Hawaii groundwater system……7

Figure 3. Sea surface temperature image of Kiholo Bay……...13

Figure 4. Sea surface temperature image of Kailua Bay……...16

Figure 5. Sea surface temperature image of Kealakekua Bay……...18

Figure 6. Kiholo and Kailua Bay water column temperature and salinity profiles……...20

Figure 7. Kealakekua Bay water column temperature and salinity profiles……..21

Figure 8. Nutrient characteristics of west Hawaii……..23

Figure 9. Temperature transect in TIR imagery to define SGD plume boundary…….28

Figure 10. Relationship between groundwater discharge flux and plume area……29

Figure 11. SST map of Kaloko-Honokohau National Historical Park…….……42

Figure 12. Honokohau Harbor water column temperature and salinity profiles……...46

Figure 13. West Hawaii nutrient characteristics and temperature/salinity relationships...48

Figure A1. Relationship between water temperatures determined from AHI instrument and *in-situ* temperature measurements……..58

Figure B1. Flight line locations in northern section of 2007 aerial TIR survey region….61

Figure B2. Flight line locations in southern section of 2007 aerial TIR survey region….62

Figure B3. Correlation between water temperatures in overlapping areas between two adjacent flight lines……...67

Figure B4. Relationship between water temperatures determined from Merlin instrument and *in-situ* temperature measurements……..69

Figure B5. Flight line images with erroneous warm surface water areas and limited temperature contrast……..71

List of Figures (continued)

Figure C1. Diagram of mass balance model variables used to determine groundwater discharge fluxes……74

Figure D1. Dissolved phosphate concentrations for all samples collected in west Hawaii region……79

Figure D2. Comparison of phosphate concentrations in Honokohau Harbor before and after continuous disposal of treated wastewater effluent inland from harbor……...80

List of Panels

Panel 1. Kawaihae Bay……..92

Panel 2. Mauna Kea Beach……93

Panel 3. Hapuna Beach……..94

Panel 4. Puako Bay……95

Panel 5. Puako Pt……...96

Panel 6. Waima Pt……..97

Panel 7. Pauoa Bay……98

Panel 8. Makaiwa Bay……...99

Panel 9. Honokaope Bay……..100

Panel 10. Waiulua Bay……101

Panel 11. Anaehoomalu Bay……102

Panel 12. Weliweli……...103

Panel 13. Keawaiki Bay……...104

Panel 14. Ohiki Bay……105

Panel 15. NE Kiholo Bay (Apr. 30)……106

Panel 16. SW Kiholo Bay (Apr. 30)……....107

Panel 17. Kiholo Bay (Apr. 30)……...108

Panel 18. NE Kiholo Bay (May 1)……...109

Panel 19. SW Kiholo Bay (May 1)……..110

Panel 20. Kiholo Bay (May 1)……111

Panel 21. 1801 lava flow……..112

Panel 22. Mano Pt……113

Panel 23. Ala Kahakai……..114

Panel 24. Kahuwai Bay……115

Panel 25. Kukio Bay……116

Panel 26. Kua Bay……117

Panel 27. Awakee Bay…….118

Panel 28. Mahaiula Bay……...119

Panel 29. Makolea Pt……...120

Panel 30. Puu Kala Pt……..121

Panel 31. Kona Airport……122

Panel 32. Keahole Pt……123

Panel 33. Kalihi Pt……...124

Panel 34. Wawaloli Beach……...125

Panel 35. Wawahiwaa Pt…….126

Panel 36. Kaloko Pond…….127

Panel 37. Aimakapa Pond……128

Panel 38. Honokohau Harbor……...129

Panel 39. Kaiwi Pt……130

Panel 40. Keahu o Lu Pt……..131

Panel 41. Old Kona Airport…….132

Panel 42. Kuka'ilimoku Pt……...133

Panel 43. Kailua Bay……134

CHAPTER 1. REGIONAL ASSESSMENTS AND UPSCALING OF SUBMARINE GROUNDWATER DISCHARGE TO THE OCEAN: BIG ISLAND HAWAII AS THE "PRISTINE" ENDMEMBER

Adam G. Johnson[1], Craig R. Glenn[1], William C. Burnett[2], Richard N. Peterson[2], Paul G. Lucey,[3] and Jeffrey J. Gillis-Davis[3]

[1]*Dept. of Geology and Geophysics, School of Ocean and Earth Science and Technology, University of Hawaii, Honolulu, Hawaii 96822, USA*
[2]*Dept. of Oceanography, Florida State University, Tallahassee, Florida 32306, USA*
[3]*Hawaii Institute of Geophysics and Planetology, School of Ocean and Earth Science and Technology, University of Hawaii, Honolulu, Hawaii 96822, USA*

Submitted to Limnology and Oceanography

1.1 Introduction

Submarine groundwater discharge (SGD) is not a pure freshwater flux, but is the combined seaward propagating flux of fresh terrestrial groundwater that has mixed with seawater circulating within coastal aquifers (Burnett et al. 2003). Relative to rivers, the net *freshwater* component of SGD may be low, yet, in volume, *total* SGD flow (freshwater + recirculated seawater) to the ocean may exceed that delivered by rivers. As based on radium isotope inventories (Moore et al. 2008), the total SGD flux to the Atlantic Ocean is estimated to be between 80 and 160% of the river flux.

Because of its sustained residence time and recirculation in the subsurface, and due to its direct bypassing of chemical adsorption in estuarine filters, the "subterranean estuary" of SGD thus has the potential to rival or surpass rivers in its ability to discharge both pristine and anthropogenically-enhanced fluxes of C, nutrients, trace metals and bacteria directly to the oceans (Krest et al. 2000; Moore et al. 2002; Burnett et al. 2007). SGD-derived nutrients have been shown to be important in near-shore ecosystems in sustaining new primary productivity (Giblin and Gaines 1990; Valiela et al. 1990; Valiela et al. 1992) as well as even promoting coastal eutrophication and harmful algal blooms (Paerl 1997; Hu et al. 2006; Lee and Kim 2007), which can have cascading effects throughout intercoupled food webs (Anderson and Garrison 1997; Bowen et al. 2007).

Recognizing its significance, our understanding of SGD has advanced considerably through development and improvements of assessment methods including seepage meters (Lee 1977), piezometers, various natural groundwater tracers (Moore 1996; Burnett et al. 2001; Breier et al. 2005), hydrogeologic basin models (Zekster 2000) and global water balance estimates (Garrels and Mackenzie 1971). Resolving *detailed*

spatial variability of groundwater discharges for *large* coastal regions, however, has remained a deficiency in SGD assessment. This has been problematic and a persistent obstacle when attempting to determine the magnitude and significance of SGD for large regions based on localized estimates. Further, the selection of scaling factors (e.g. discharge from a length of shoreline or discharge to a bay's area) are often arbitrary and inconsistent between different investigations**,** making it difficult to impossible to compare one region to another.

Aerial thermal infrared (TIR) surveying has been utilized as an effective way to identify specific SGD locations in coastal areas (Roxburgh 1985; Banks et al. 1996; Miller and Ullman 2004; Shaban et al. 2005; Duarte et al. 2006; Mulligan and Charette 2006), but has not been implemented for large-scale groundwater study. TIR surveying remotely measures sea surface temperature (SST) and therefore can be used to map discharging groundwaters which have temperatures that contrast with ambient seawater, and that are fresh enough to buoyantly float atop denser seawater. While satellite sensors (e.g. AVHRR, MODIS, and GOES) are employed to measure global ocean SST, the spatial resolution of the imagery is typically 1 km (30 m at best) in the infrared bands (Brown et al. 2005), making them unpractical for detecting groundwater discharge on the local scale. As demonstrated here, however, TIR imaging using radiometers aboard aircraft can afford rapid $<0.1^{o}C$ surface temperature differences at sub-meter spatial resolution. Still, TIR mapping does not provide details on rates of SGD flow, nor subsurface water column structure. Our goal, therefore, was to use TIR to ascertain the input and seaward mixing character of SGD over large areas, and to use that imagery as a vehicle for upscaling multiple shore-based efforts to regional extent.

We chose the dry, western half of the Big Island of Hawaii as our "type-locality" study site since groundwater is the only major source of terrestrial freshwater to its ocean, and because it remains a relatively pristine area compared to more developed coastal regions. These factors averted most complications arising from stream flow and anthropogenic nutrient enrichments. High-resolution SST maps produced from aerial TIR surveys identified the exact locations and relative magnitudes of more than 50 groundwater discharges for the region (Fig. 1 inset). Using TIR imagery as a guide, intensive ground-based assessments were concentrated at specific SGD sites in Kiholo Bay, Honokohau Harbor, Kailua Bay, and at three discharge locations in Kealakekua Bay (Fig. 1). These included 3-dimensional water column temperature and salinity profiling, and nutrient sampling in coastal ocean surface waters and in onshore groundwaters. Peterson et al. (2008) detail the results of our time-series measurements of natural groundwater tracers (^{222}Rn and salinity) to quantify groundwater fluxes at each of these six SGD sites.

Setting of West Hawaii

The Island of Hawaii is the youngest and largest Hawaiian island, attains an altitude of 4,200 m, and is built by thousands of lava flows from five shield volcanoes, three of which are historically active (Macdonald et al. 1983). The western half of the island is shielded from the prevailing northeastly trade winds and is relatively dry, with areas along the coastal plain typically receiving less than 25 cm of rain each year (Mink et al. 1993). Most precipitation occurs at land elevations between 600-1800 m in the form of rain and fog drip associated with sea-breeze induced clouds that converge with cooler

air at higher elevations (Juvik and Ekern 1978). In addition to the arid climate, limited soil development and young porous lava flows facilitate the infiltration of precipitation into the ground, creating a situation such that streams are sparse, intermittent, and rarely reach the ocean (Mink et al. 1993). Thus, groundwater discharge is the principal source of terrestrial freshwater to the ocean bordering west Hawaii.

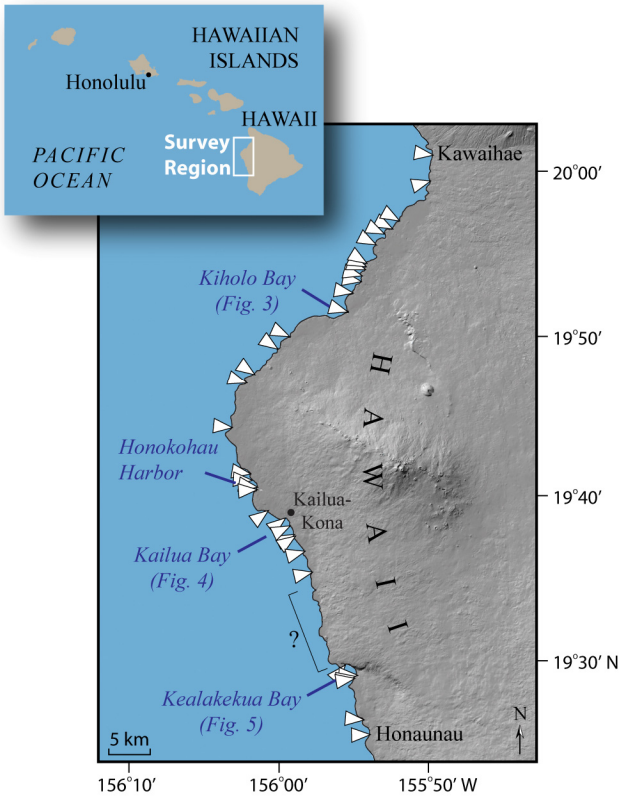

Figure 1. Map of the Hawaiian Islands and the main study region along the western half of the Island of Hawaii. August 2005 aerial survey was conducted over Kealakekua Bay and Honokohau Harbor area. May 2007 aerial survey covered the coastline between Kawaihae and Honaunau. White triangles represent locations of large point-source groundwater discharges.

The groundwater system for the region consists of a buoyant, freshwater lens (Ghyben-Herzberg lens) on top of denser, oceanic seawater with a brackish transition zone between (Fig. 2) (Oki 1999). The freshwater lens is thickest inland, where recharge is greatest, and thins toward the coastline where mixing with subterranean seawater forms brackish water that is evident in coastal wells and shallow pits dug into the ground (Oki 1999). Brackish ponds occur in depressions in lava flows along the coastline that are deep enough to extend into the brackish groundwater table (Maciolek and Brock 1974). In general, groundwater flows from inland recharge areas toward the coastline, and is transmitted though porous spaces between lava flows, fractures, and lava tubes (Stearns and Macdonald 1946; Oki 1999). The shoreline and near-shore marine bottom are dominantly composed of lava rock with limited sedimentary cover. Consequently, there is an uninhibited connection for the exchange of water and dissolved materials between the basal aquifers and the coastal ocean that is evident in tidal variations in wells nearly 4 km inland from the coast (Bauer 2003).

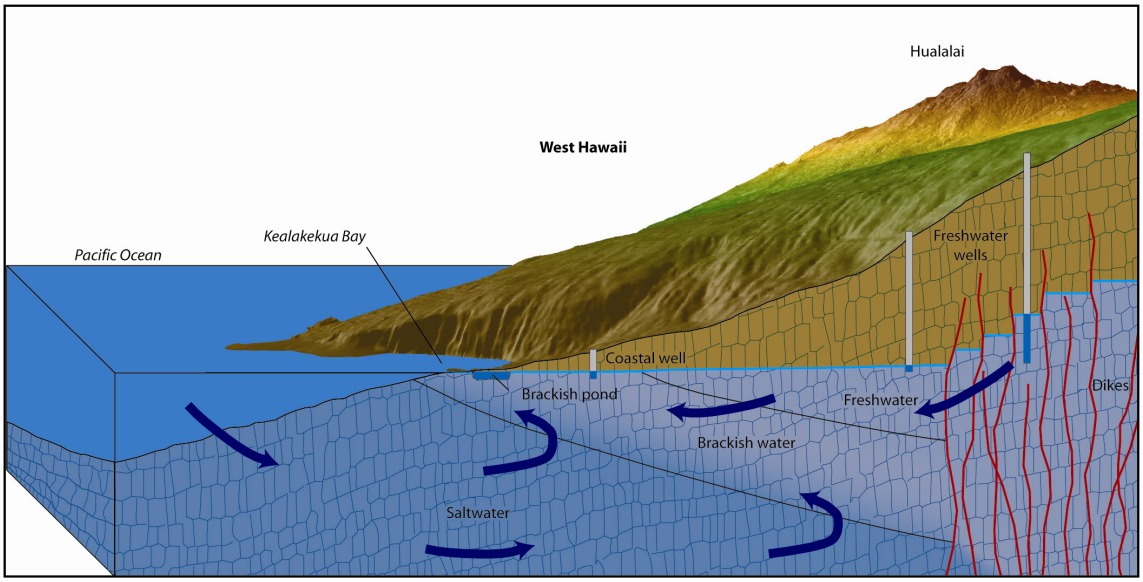

Figure 2. Schematic cross section of west Hawaii groundwater system adapted from Oki (1999), specifically for the vicinity of Kealakekua Bay. Black arrows indicate general directions of water movement. Low-permeability dikes impounding high levels of groundwater are implied (Oki, 1999). Vertical scale and thickness of lava flows are greatly exaggerated.

1.2 Methods

Aerial Thermal Infrared Surveys

Initial aerial TIR surveys were focused over Honokohau and Kealakekua Bays on 16 August 2005 between 06:00h and 10:00h HST (Hawaii Standard Time); low tide (-3.0 cm) that day was at 07:00h HST. A subsequent regional-scale survey covered >100 km of the west Hawaii coastline over a period of two days: 06:55-10:15h on 30 April 2007 and 07:53-10:30h HST on 1 May 2007. Low tide (-6.1 cm) was at 08:15h and 08:30h HST on April 30 and May 1, respectively.

Surface water temperatures were remotely determined from an infrared camera bore sighted through an opening in the fuselage of a fixed-wing aircraft. Both surveys used highly sensitive (0.1^{o}C) cameras that measured the radiance emitted from the water's surface in the thermal infrared spectral range of 8 – 12 microns and produced swath images for each flight line. The main difference between two surveys was the camera's field of view, which was about three times wider in the second survey than in the first. Since both surveys were conducted at an altitude of about 1 km, the second survey was able to cover three times more area for each flight line, and thus was able to survey a much larger region while still producing imagery with a spatial resolution (1.3 m) fully capable of resolving groundwater inputs to the ocean. Appendices A and B contain more details of the aerial TIR surveys.

After the surveys, processing of the thermal data was required. Thermal images were first converted to temperature (^{o}C) using onboard measurements to a multi-temperature flat-panel blackbody. This was done by determining a relationship between spectral radiance measured by the camera and the corresponding temperature of the blackbody. Temperature conversions for each image were completed on a pixel-by-pixel basis to account for slight differences in the camera's sensitivity across its field of view. Temperature-converted images for each flight line were next mosaicked together into a composite flight line image. Each image was then georeferenced to basemaps by selecting ground-control points such as rock outcrops, unique lava flow features, road/trail intersections, and other distinctive features at ground level near the shoreline that could be identified in both the TIR imagery and basemaps. Basemaps were ortho-

rectified, aerial photograph composites collected in 2000 at 0.85 m resolution with NAD83, UTM Zone4 datum.

After georeferencing the flight line images, corrections were made for four sources of temperature error: 1) drift in the camera's sensitivity during the survey 2) atmospheric interferences between the airborne sensor and the ocean 3) surface water skin-layer effects, and 4) assumption that water had an emissivity of 1. Sensor drift can be caused by air temperature changes in the airplane, vibrations, and other stresses. Normally, sensor drift can be corrected for by taking frequent blackbody calibration measurements during data collection, preferably before and after each flight line. Unfortunately, due to power problems on the aircraft, it was only possible to take calibration measurements prior to collecting the first line and after collecting the last line each survey day. Instead, we mitigated sensor drift between adjacent flight line images by calibrating water temperatures in one image to the other at specific locations where two images overlap. Although frequent onboard blackbody calibrations would have eliminated sensor drift more precisely, our method did yield a coherent set of overlapping thermal images that were then ground-truthed to in-situ temperature measurements.

Atmospheric scattering, emission, and attenuation of radiance between ocean's surface and airborne sensor can also cause temperature errors in the TIR imagery (Pieters and Englert 1993). For our surveys, radiance emitted from the ocean's surface was likely absorbed by water vapor and aerosols from human and volcanic activity on the island. As a result, radiance reaching the airborne sensor is reduced, leading to calculated temperatures being too low. Additionally, the TIR sensor measures the radiance emitted from the upper <1 mm ("skin") of the ocean's surface, which can be up to 0.3^{o}C cooler

that the "bulk" temperature immediately beneath the skin (Schluessel et al. 1990), and which we assumed had emissivity of 1. Atmospheric interferences, skin-layer effects, and non-uniform emissivities can all, however, be corrected to in-situ temperature measurements made during the survey (Cracknell and Hayes 1991). We thus recalibrated our TIR images to temperatures measured by thermistors (Onset HOBO® pendant, accurate to 0.5°C) stationed throughout the survey area and to direct ground-truthing temperature measurements in Kailua Bay and Honokohau Harbor.

Water Column Profiles

Transects of water column temperature and salinity profiles were measured to determine the structure and mixing characteristics of the six groundwater discharge plumes. In Kealakekua Bay, Queen's Bath, Manini Beach, and Kahauloa Bay plumes were profiled on 8/8/06, 8/10/06, and 8/4/06, respectively. Kiholo Bay and Kailua Bay profiles were measured on 5/17/07 and 5/19/07, respectively. Profile transects were measured in the early morning to coincide with low tide conditions and to minimize surface heating effects. For each transect, six to ten profiles were measured from near the shoreline to beyond the seaward extent of the cool, brackish plume. For each profile, temperature and salinity were measured between the ocean's surface to depths as low as 8 m at 0.25 m intervals using a calibrated YSI® probe accurate to ± 0.15°C and ±1% of reading for salinity. Additional salinity determinations from unfiltered water samples were made at the University of Washington using a Guildline Autosal Laboratory Salinometer.

Regional Nutrient Sampling

Water samples for chemical analysis were collected between August 2005 and May 2007 (8/05, 2/06, 8/06, 10/06, and 5/07) throughout west Hawaii to determine regional nutrient characteristics. Samples were collected in pristine freshwater wells, brackish wells and ponds along the coastline, and in coastal ocean surface waters (upper 0.15 m). All samples were collected in acid-washed, triple-rinsed, high-density polyethylene bottles. For each sample, 60 mL of water was syringe-filtered through a 0.45 micron GF/C Acetate Filter, and refrigerated until analyzed at the University of Washington's Marine Chemistry Laboratory for $Si(OH)_4$, NO_3^-, NO_2^-, NH_4^+, and PO_4^{3-} using spectrophotometric segmented flow nutrient analysis (UNESCO 1994). Here, we refer to $Si(OH)_4$ as DISi, PO_4^{3-} as DIP, and the sum of NO_3^-, NO_2^-, and NH_4^+ as dissolved inorganic nitrogen (DIN). Respective standard errors (n=10) for DISi, DIN, and DIP were 1.1%, 4.0%, and 3.4% of the measured concentration.

Groundwater Discharge Fluxes

Groundwater fluxes for our six intensively studied SGD sites were estimated using a combination of natural groundwater tracers. This was done by continuously measuring ^{222}Rn, salt, and water level for several tidal cycles at a platform stationed ~25 – 160 m from the shoreline at each SGD site. ^{222}Rn is a useful tracer of SGD because it is concentrated in groundwater, depleted in seawater, easy to measure, and behaves conservatively in the ocean (accounting for decay) (Burnett et al. 2001). Appendix C is an excerpt from Peterson et al. (2007) containing a detailed explanation of the mass balance model, measured parameters, mass balance equations, and procedures used to

calculate both freshwater and total submarine groundwater fluxes for one of the plumes (Honokohau Harbor).

1.3 Results and Discussion

Aerial Thermal Infrared Surveys

The TIR surveys collectively covered approximately 50 km^2 along the coastal west Hawaii region between Kawaihae Harbor and Honaunau Bay (Fig. 1). The high-resolution SST maps clearly depict the spatial variability of groundwater inputs to coastal waters for the region. SGD occurs as discreet point-source discharges and diffuse non-point seeps, both of which tend to be concentrated in coastal embayments, though seepage from seaward-protruding coastal points is also occasionally evident. The SGD points are patchily distributed along the coastline, with most seepage plumes occurring north of Kiholo Bay. Comparably less seepage occurs from other areas (e.g. south of Kiholo Bay to Honokohau Harbor). In total, we identified 58 point-source and 12 diffuse discharge plumes (Table 1). Many of the point-source plumes identified in Table 1 are in fact supplied by several smaller, yet distinct point-sourced inputs. The paucity of discharge sites shown in Fig. 1 (inset) for the area south of Kailua Bay is due to poor temperature resolution in the 2007 TIR data for that region, which was caused by solar-heated land oversaturating the TIR during the late morning.

Groundwater discharges are recognized as cool water plumes (blue/green-colored) dispersing from the shoreline and mixing into warmer, coastal ocean water (red-colored) (Fig. 3-5). The temperature of the discharging groundwater is almost invariably coldest at the shoreline point of discharge visible in the TIR imagery, but varies slightly from site to

site due to local spatial differences in subterranean mixing between groundwater and intruding seawater. There are noticeable repetitions of alternating warmer and colder water spatial patterns within some of groundwater discharge plumes (Fig. 3, 5), which may be related to effects of wave and/or swell pulsing at the point of discharge near the shoreline. It is important to note that ambient ocean water temperature for the region was about 3.5°C cooler in May 2007 (Figs. 3-4) than when Kealakekua Bay was surveyed in August 2005 (Fig. 5).

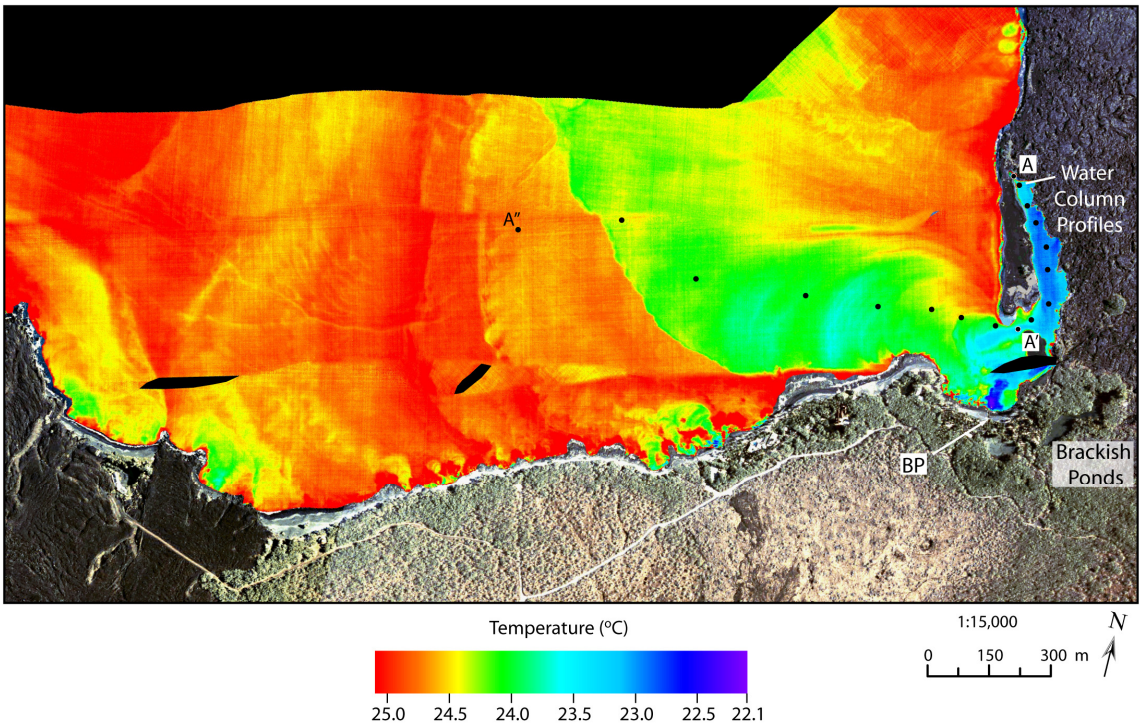

Figure 3. May 2007 sea surface temperature image of Kiholo Bay. Relatively cold groundwater discharge plumes are blue-green colored. See Fig. 6 for water column temperature and salinity profile transects A-A' (Wainanalii Lagoon) and A'A". The major SGD plume is sourced by both marine lagoon to the east (A-A'), and by drainage from brackish ponds at point BP.

Table 1. Locations of point-source (P) and diffuse (D) groundwater inputs to west Hawaii identified in aerial TIR surveys. arranged north to south. SGD flux is the estimated total (fresh groundwater + recirculated seawater) groundwater discharge rate for each plume based on its surface area extent in the TIR imagery and using the equation in Fig. 10. Plume areas of most diffuse discharges could not be accurately measured since the plume boundaries were not well-defined.

General Location	Plume	Latititude	Longitude	Point or diffuse	Plume Area (m^2)	SGD flux ($m^3 d^{-1}$)
Waikui Beach	1	20° 01' 24"	155° 49' 22"	P	30,000	3,089
Mauna Kea Beach	2	20° 00' 12"	155° 49' 32"	P	70,000	7,089
N. Hapuna Beach	3	19° 59' 32"	155° 49' 33"	P	22,000	2,289
Puako Pt.	4	19° 58' 22"	155° 50' 20"	D	50,000	-
N Waima Pt.	5	19° 58' 10"	155° 50' 46"	P	5,400	629
Waima Pt.	6	19° 58' 6"	155° 50' 57"	P	4,100	499
Kapuniau Pt.	7	19° 57' 52"	155° 51' 15"	D	79,800	-
Pauoa Bay	8	19° 57' 7"	155° 51' 43"	P	44,000	4,489
Nanuku Inlet	9	19° 56' 49"	155° 52' 07"	P	83,600	8,449
Hopeaia Fishpond	10	19° 56' 35"	155° 52' 14"	P	20,600	2,149
Manoku Fishpond	11	19° 56' 33"	155° 52' 22"	P	5,200	609
Waawaa Pt.	12	19° 56' 24"	155° 52' 37"	D	?	-
Waiulua Bay	13	19° 55' 34"	155° 53' 17"	P	22,000	2,289
Anaehoomalu Bay	14	19° 54' 48"	155° 53' 18"	P	780,000	78,089
South of Anaehoomalu Bay	15	19° 54' 21"	155° 54' 3"	D	?	-
N. Akahu Kaimu	16	19° 54' 11"	155° 54' 04"	P	28,700	2,959
S. Akahu Kaimu	17	19° 54' 01"	155° 54' 04"	P	66,900	6,779
Weliweli Pt.	18	19° 53' 52"	155° 54' 17"	D	?	-
Pueo Bay	19	19° 53' 35"	155° 54' 16"	P	121,500	12,239
Keawaiki Bay	20	19° 53' 17"	155° 54' 21"	P	112,000	11,289
S. Keawaiki Bay	21	19° 53' 7"	155° 54' 31"	P	45,600	4,649
Kaiwi Pt.	22	19° 52' 58"	155° 54' 45"	D	?	-
Ohiki Bay	23	19° 52' 33"	155° 54' 54"	D	?	-
Kiholo Bay	**24**	**19° 51' 37"**	**155° 55' 19"**	**P**	**252,000**	**25,289**
Mid-N Kiholo Bay	25	19° 51' 11"	155° 55' 40"	P	16,000	1,689
Mid-S Kiholo Bay	26	19° 51' 02"	155° 56' 4"	P	2,400	329
S Kiholo Bay	27	19° 51' 01"	155° 56' 04"	P	82,000	8,289
SS Kiholo Bay	28	19° 50' 58"	155° 56' 19"	P	63,300	6,419
Kahuwai Bay	29	19° 49' 52"	155° 59' 13"	P	55,000	5,589
Kukio Bay	30	19° 49' 09"	155° 59' 53"	P	90,000	9,089
Kikaua Pt.	31	19° 49' 04"	156° 00' 03"	P	7,700	859
Kakapa Bay	32	19° 48' 51"	156° 00' 10"	D	45,000	-
Kua to Kahoiawa Bay	33	19° 48' 30"	156° 00' 49"	D	?	-
Awakee	34	19° 47' 45"	156° 01' 20"	P	4,700	559
N. Puu Alii Bay	35	19° 47' 35"	156° 01' 36"	P	14,700	1,559
N. Mahaiula Bay	36	19° 47' 00"	156° 02' 12"	P	24,000	2,489
S. Mahaiula Bay	37	19° 46' 30"	156° 02' 49"	P	81,700	8,259
Makako Bay	38	19° 44' 09"	156° 03' 11"	P	6,000	689
Kaloko Pond beach face	39	19° 41' 13"	156° 01' 59"	P	20,000	2,089
N. Kaloko Pt. ("The Cut")	40	19° 41' 09"	156° 02' 01"	P	2,800	369
Kaloko Pt.	41	19° 40' 46"	156° 01' 51"	P	41,000	4,189
Aimakapa	42	19° 40' 29"	156° 01' 35"	D	49,000	-
N. of Aiopio Fishtrap	43	19° 40' 23"	156° 01' 35"	P	?	-
Aipio Fishtrap	44	19° 40' 18"	156° 01' 38"	P	59,400	6,029
Honokohau Harbor	**45**	**19° 40' 08"**	**156° 01' 16"**	**P**	**95,000**	**9,589**
Noio Pt.	46	19° 39' 47"	156° 01' 52"	P	4,000	489
N. old kona airport	47	19° 38' 52"	156° 01' 00"	P	9,600	1,049
S. old kona airport	48	19° 38' 29"	156° 00' 29"	P	11,000	1,189
Kailua Bay: Narrow Inlet	49	19° 38' 18"	155° 59' 52"	P	7,900	879
Kailua Bay: Swimming Beach	50	19° 38' 21"	155° 59' 51"	P	4,400	529
Kailua Bay: largest plume	**51**	**19° 38' 23"**	**155° 59' 42"**	**P**	**89,000**	**8,989**
Oneo Bay	52	19° 38' 8"	155° 59' 26"	P	4,600	549
Kahului Bay	53	19° 37' 48"	155° 59' 23"	P	?	-
Kahului Bay	54	19° 37' 41"	155° 59' 18"	P	?	-
Kahului Bay	55	19° 37' 26"	155° 59' 06"	P	?	-
S. Holualoa Bay	56	19° 36' 10"	155° 58' 29"	P	?	-
White Sands Beach	57	19° 35' 54"	155° 58' 28"	P	?	-
Kahaluu Bay	58	19° 35' 11"	155° 58' 16"	P	?	-
Kahaluu Bay	59	19° 34' 51"	155° 58' 00"	P	?	-
Keahou Bay	60	19° 33' 43"	155° 57' 43"	P	?	-
Maihi to Paaoao Bay	61	19° 33' 43"	155° 57' 43"	D	?	-
Keawekaheka Bay	62	19° 29' 45"	155° 56' 53"	P	?	-
Kealakekua Bay (Queen's Bath)	**63**	**19° 28' 57"**	**155° 55' 58"**	**P**	**18,000**	**1,889**
Kealakekua Bay (Manini Beach)	**64**	**19° 28' 16"**	**155° 55' 21"**	**P**	**64,800**	**6,569**
Kahauloa Bay	**65**	**19° 28' 11"**	**155° 55' 15"**	**P**	**20,300**	**2,119**
Kaopapa	66	19° 28' 02"	155° 55' 17"	P	13,500	1,439
N. Palemano Pt.	67	19° 27' 41"	155° 55' 31"	P	?	-
S. of Keomo Pt.	68	19° 26' 38"	155° 55' 14"	D	?	-
Honaunau Bay	69	19° 25' 22"	155° 54' 39"	P	?	-
Kauhako Bay	70	19° 24' 42"	155° 54' 19"	P	?	-

One of the largest SGD plumes for the region is discharging into Kiholo Bay (Fig. 3). This plume is supplied by groundwater seepage from the shoreline bordering the narrow marine lagoon (Wainanalii Pond) in the east part of the bay, and from a narrow channel that funnels the tidally-driven exchange of waters between a large brackish pond and the ocean (Fig. 3 labeled "BP"). The main coldwater plume in the bay extends more than 1 km from the shoreline. There are at least a dozen smaller, well-defined groundwater inputs which dot most of the bay's 2.5 km stretch of coastline, and a few larger inputs in the southeast corner of the bay. Two large brackish ponds (used by early Hawaiians as fishponds) were formerly present immediately to the south and north of Kiholo Bay, but were overlain by lava flows in 1801 and 1859, respectively (Kelly 1973).

SGD is entering Kailua Bay primarily from point-source inputs in the northeast and southeast part of the bay (Fig. 4). Ground-based efforts indicate the northernmost input is entering the bay from a submarine lava tube, several meters from the shoreline that creates a 'boil' of cold, brackish water at the ocean's surface. Groundwater also discharges from a small section of beach and a small inlet west of the pier. Warm water lineations within the cool water plume in Fig. 5 are the wakes of boats that have upwelled warmer seawater into the brackish SGD lens.

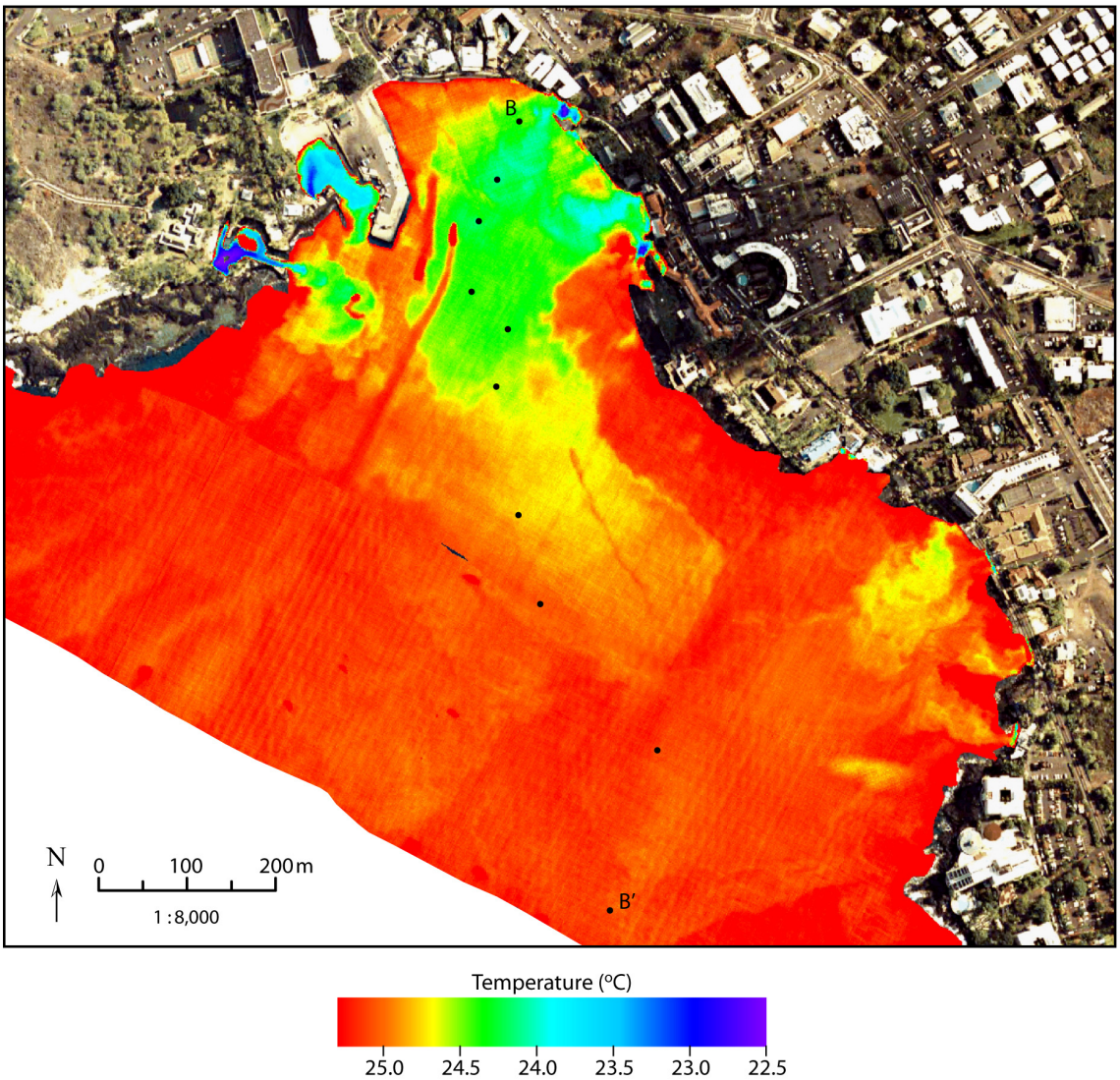

Figure 4. May 2007 sea surface temperature image of Kailua Bay. Black dots indicate locations of water column temperature and salinity profiles for transect B-B' (see Fig. 6).

In Kealakekua Bay, two groundwater discharge outlets are contributing to the SGD plume in the northwest corner of the bay (Fig. 5). We refer to this plume as "Queen's Bath" since groundwater flows into a circular depression in the rocks of along the coastline that is said to have been used by Hawaiian royalty for bathing. Several groundwater inputs contribute to a second, larger coldwater plume emanating from the

southeast corner of the bay. Our ground-based efforts for this plume were concentrated at groundwater discharging from the shoreline in the vicinity of Manini Beach. No observable groundwater seepage is evident along the 1.3-km stretch of coastline at the base of the cliff (a fault scarp) bordering the bay. Immediately south of Kealakekua Bay, groundwater discharges into a small inlet (Kahauloa Bay) forming a “Y”-shaped coldwater expression that is due to the divergence of the cold surface water plume around a large rock exposed at low tide in the middle of the inlet. Another groundwater plume is emanating from another shoreline inlet approximately 250 m south of Kahauloa Bay.

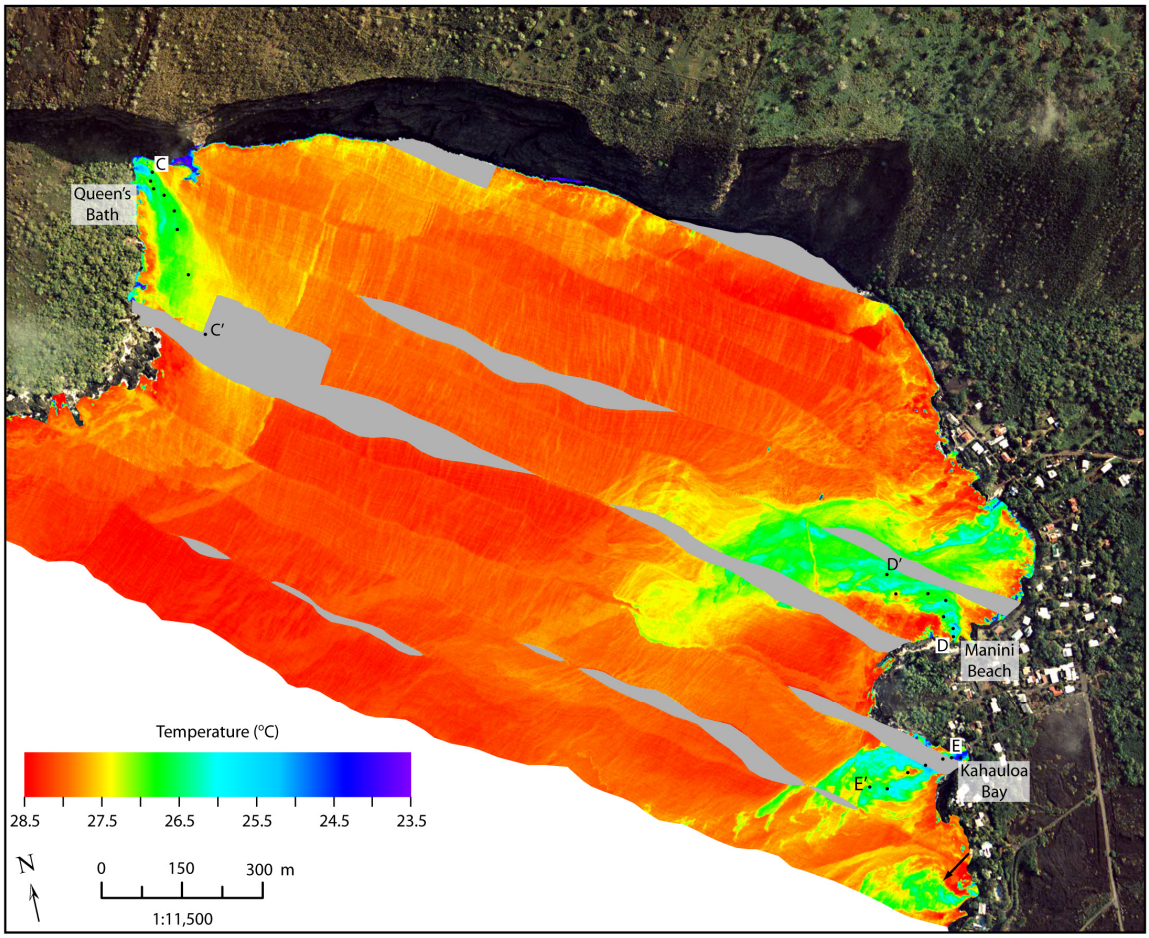

Figure 5. August 2005 sea surface temperature image of Kealakekua Bay. Ground-based efforts were concentrated at groundwater discharges at Queen's Bath, Manini Beach, and Kahauloa Bay. See Fig. 7 for water column temperature and salinity profile transects C-C', D-D', and E-E'. For reference, the southern-most SGD plume (arrow) has an area of 13,000 m^2.

Water Column Profiles

Transects of vertical water column profiles of temperature and salinity in groundwater discharge plumes of Kiholo Bay, Kailua Bay, and Kealakekua Bay are shown in Fig. 6-7. All profile transects clearly indicate a thin, buoyant lens of cold, brackish water that extends over and mixes with warmer, saltier ocean water beneath and surrounding it. Temperature and salinity both increase with increasing depth and distance

from the shoreline, indicating groundwater is discharging near the shoreline-ocean interface. At several of the sites, particularly at Honokohau Harbor and Kiholo Bay, visible currents of coldwater can be observed emerging from the coastline and flowing seaward, especially during low tide. The greatest changes in temperature and salinity in the water column generally occur at depths between 0.5 - 1.0 m, but this transition becomes less well-defined further from shore as mixing progresses.

Water column profiles in the marine lagoon in Kiholo Bay (Fig. 6, A-A') show a distinct cold, brackish lens ~0.75m thick, with the coldest and freshest water flowing into the northern part of the lagoon. The saline water beneath this lens is about 2°C warmer than ambient marine waters, which is likely due to daily heating and restricted circulation. Profiles in the main plume in Kiholo Bay (A'-A") also indicate a thin (0.5 m), cool, brackish lens. Mixing between the buoyant layer and ocean water beneath causes noticeable turbidity in the water observed as far as several hundred meters from shore. Near point A", relatively cool and less saline waters may be the signature of other SGD inputs from the shoreline further southwest. Profiling in Kailua Bay (B-B') indicate the plume extends about 600 m from the shoreline. Seaward of the Kailua Bay plume, solar surface heating is also evident in the upper few meters of the water column. Profiles in Kealakekua Bay (Fig. 7) also depict a cold, brackish surface lens at SGD sites. As revealed by water column profiling, the seaward extents of the plumes in Kealakekua were less pronounced than that observed in the infrared imagery. We suspect this is due to both relatively high (0.1^{o}C) temperature sensitivity of the TIR cameras within the upper mm of the sea surface (relative to in-situ measurements), and/or strong wind chop and wave swell during the profile measurements.

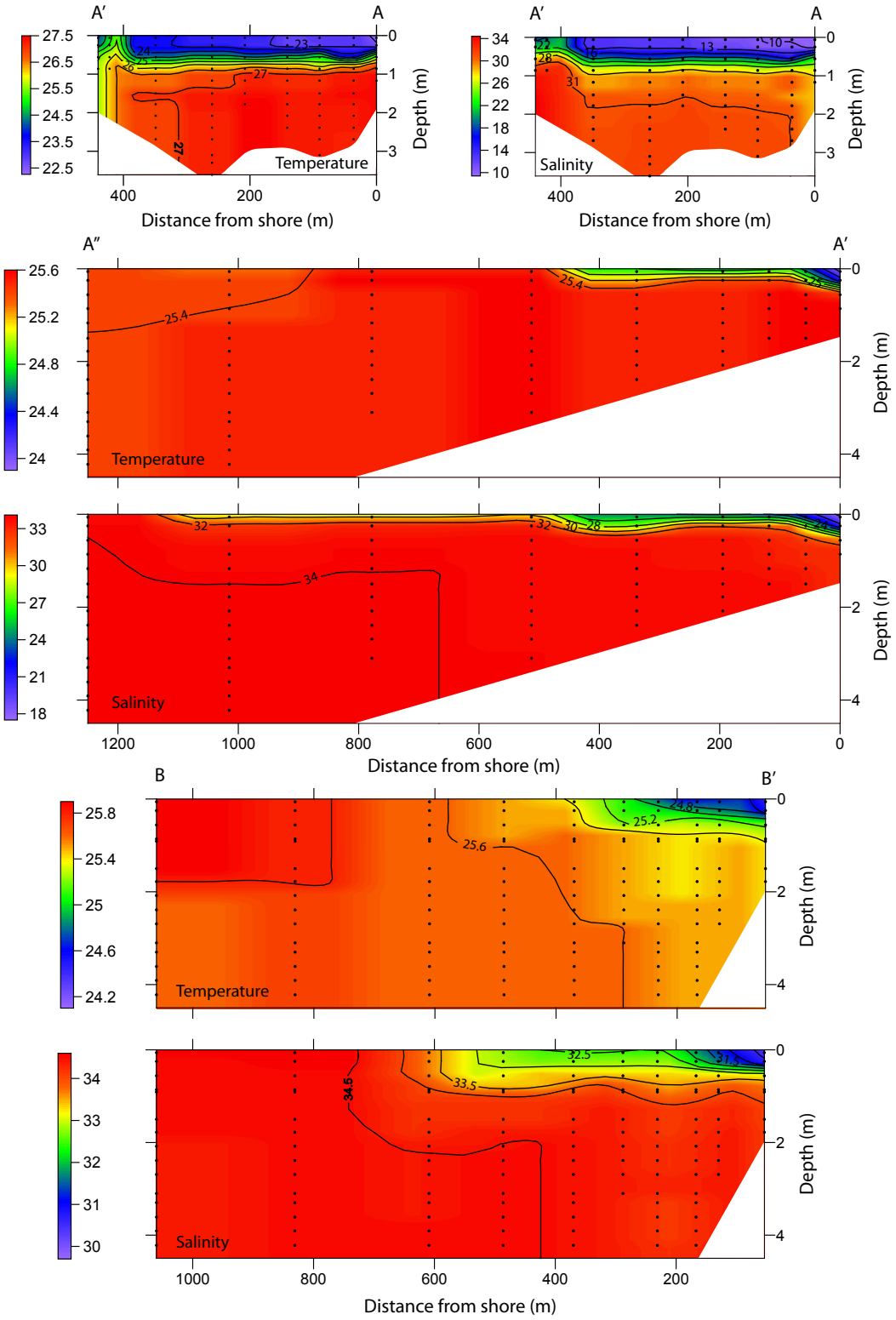

Figure 6. May 2007 water column temperature (oC) and salinity profile transects in Kiholo and Kailua Bays where x-axes are distance (m) from shoreline and y-axes are depth (m) below surface: Kiholo lagoon (A-A') Kiholo Bay plume (A'-A"), Kailua plume (B-B').

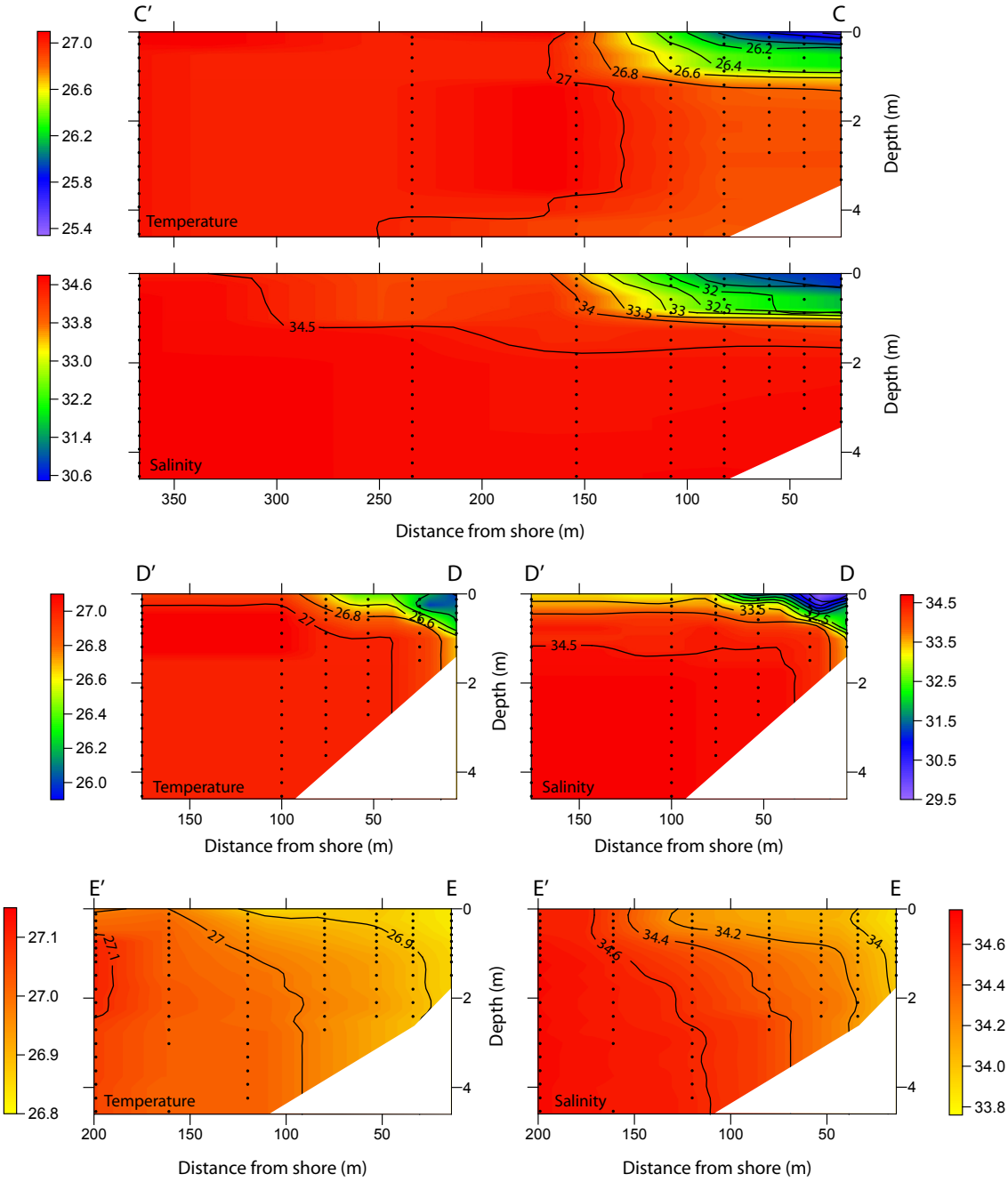

Figure 7. August 2006 water column temperature (oC) and salinity profiles in three discharge plumes in Kealakekua Bay, where x-axes are distance (m) from shoreline and y-axes are depth (m) below surface: Queen's Bath plume (C-C'), Manini Beach plume (D-D'), Kahauloa Bay plume (E-E').

Regional Nutrient Characteristics

Nutrient concentrations as a function of salinity for all sites sampled are shown in Fig. 8. Fresh and brackish terrestrial groundwaters had the highest concentrations of nutrients while ambient coastal marine waters for the region are nutrient-poor. For each plot, we place a conservative mixing line (dashed black line) between the average nutrient concentrations in freshwater wells and nutrient concentrations in ambient ocean surface waters for the region.

In *freshwater wells* (mean salinity = 0.2), DISi, DIN, and DIP concentrations average 767.5, 72.6 and 4.9 μmol L^{-1}, respectively. In nearly all *brackish wells* (mean salinity = 5.6), both DISi and DIN concentrations lie above the conservative mixing line due to inputs of these two nutrients to groundwater as it flowed toward the coastline. DIN concentrations from brackish wells average 142.0 μmol L^{-1}, but were spatially variable between study sites, ranging from 72.3 -203.8 μmol L^{-1}. The highest DIN concentrations were measured in brackish stone-lined, wide-diameter wells and pits near Manini Beach and Kahauloa Bay, whose concentrations may be related to an abundance of nitrogen-fixing biota in the area, such as *kiawe* trees (Kay et al. 1977), or to contributions from cesspools. In contrast to DISi and DIN, DIP concentrations in brackish wells average 4.3 μmol L^{-1} and plot along the conservative mixing line for the region.

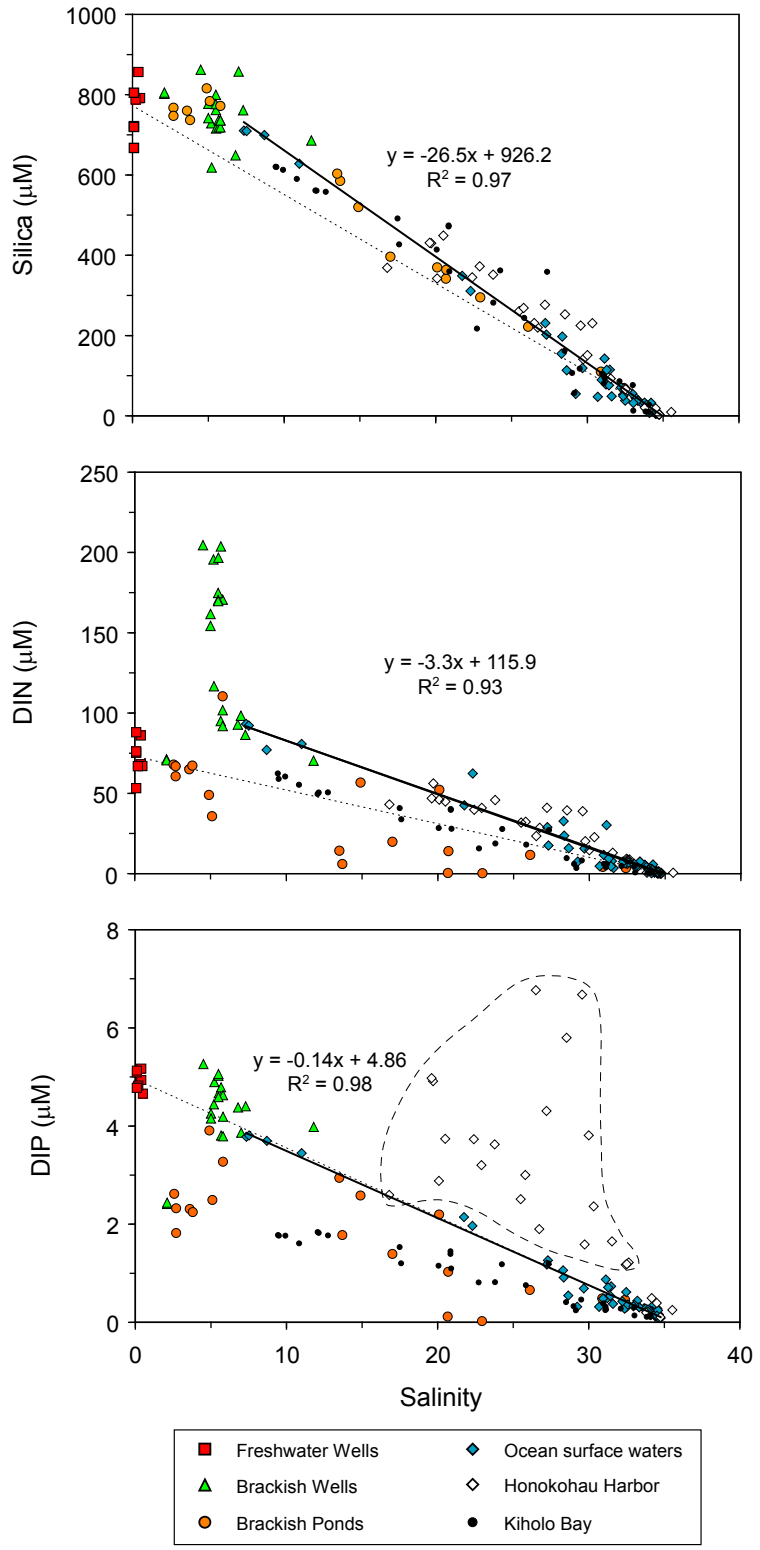

Figure 8. Nutrient concentrations measured in groundwaters and ocean surface waters for the region . Dashed lines represent conservative mixing lines between freshwater wells and ambient ocean surface water. Solid lines and equations represent the correlation for ocean surface and Honokohau Harbor waters; DIP correlation excludes Honokohau Harbor (dashed outline; See chapter 2 and Appendix D).

Owing to varying distances and degrees of hydraulic communication to the coastal ocean, salinities in *brackish ponds* range from 2.5 to 32.4. Accordingly, nutrient concentrations from ponds are also variable and DIN and DIP concentrations fall predominantly below conservative mixing trends. These brackish (anchialine) ponds are generally small (< 100 m^2 surface area), shallow (< 1 m deep), calm bodies of water, that typically host a unique variety of phytoplankton and aquatic flora (Maciolek and Brock 1974), so there is likely biological uptake of both DIN and DIP in many of them. DSi concentrations from the brackish ponds plot along the conservative mixing line.

In ocean surface waters, nutrients concentrations are highest along the shoreline at points of groundwater discharge, then progressively decrease offshore. At Queens Bath, where cold, brackish water was visibly flowing out of a crevice in the basalt shoreline, DISi, DIN, and DIP concentrations were measured to be 710.4, 93.2, and 3.8 μmol L^{-1}, respectively. At distances greater than 1 km away from the coast, DISi decrease to 2.5 μmol L^{-1}, and DIN and DIP both decreased to <0.1 μmol L^{-1}. Due to net inputs of DISi and DIN to brackish groundwaters, concentrations of these nutrients in ocean surface waters generally plot above the conservative mixing lines between pristine freshwater wells and waters offshore. Except for Honokohau Harbor, DIP concentrations in ocean surface waters correlate well with conservative mixing for the region. Of the five SGD sites we sampled in the study region, however, both DISi and DIN are negatively correlated with salinity in coastal marine surface waters at all sites, while DIP at all but one (Honokohau Harbor, see chapter 2; appendix D). The linear correlation between nutrient concentrations and salinity suggests conservative mixing of nutrient-rich

groundwater discharges in coastal ocean with little net biological uptake of DISi, DIN, or DIP.

Exceptions to these regional trends are the DIN and DIP concentrations in Kiholo Bay surface waters, which fall below our estimated conservative mixing lines. Sampling of brackish wells and ponds immediately inland from the bay, although limited in number (n=6), also have low concentrations compared to other sites. This discrepancy may simply be due to Kiholo Bay bordering a different groundwater aquifer system than other regions sampled to the south (Mink and Lau 1993). With the recent lava flows inland and bordering the bay, the newly developed soils in the area may be nutrient-poor due to limited weathering of silica and phosphorus from the area's rocks and comparatively less fixation of nitrogen from the atmosphere since plants are relatively sparse (Vitousek 2004). The catchment basin inland from Kiholo Bay is less densely-populated compared to sites further south, and may thus represent a more pristine setting with fewer inputs of anthropogenic nutrients. As with other locals, however, nutrient concentrations in Kiholo Bay linearly decrease seaward with increasing salinity.

Groundwater Discharge Fluxes

Continuous tracer measurements at each SGD site clearly indicate that groundwater inputs are dominantly regulated by tides (Peterson et al. 2007; 2008). Maximum groundwater inputs occurred during ebb/low tide when the hydraulic gradient between coastal aquifer water levels and the ocean was greatest. With increases in tidal height, SGD rates decreased, typically reaching a minimum at high tide. Average daily

SGD flux estimates for the six sites studied here ranged from 1,100 to 12,000 m^3 and were, on average, 60% freshwater by volume (Table 2).

Table 2. Total SGD fluxes for six point-source groundwater discharges determined by Peterson et al. (submitted) and their plume areas as measured in the TIR imagery.

Site	Total SGD Flux (m^3 d^{-1})	Plume Area (m^2)
Kiholo Bay (30 Apr 07)	7,100	362,000
Kiholo Bay (1 May 07)	7,100	252,000
Honokohau Harbor (16 Aug 05)	12,000	95,000
Honokohau Harbor (1 May 07)	12,000	102,000
Kailua Bay (30 Apr 07)	8,700	100,000
Kailua Bay (1 May 07)	8,700	89,000
Queen's Bath (16 Aug 05)	3,500	18,000
Manini Beach (16 Aug 05)	5,100	64,800
Kahauloa Bay (16 Aug 05)	1,350*	20,300

* SGD flux for Kahauloa Bay is the average of the fluxes measured in August 2005 and February 2006

Up-scaling Groundwater Fluxes

To gauge the relative magnitude of all identified groundwater discharges from west Hawaii, we measured the surface water area extent of each plume in the TIR survey maps (Table 1). Obviously, a plume's area will depend on how its boundary is defined. Here, we quantitatively define each plume's boundary as occurring where there is the greatest change in temperature, relative to distance, just prior to the plume's temperature being indistinguishable from ambient ocean temperature (Fig. 9). Instead of selecting a single temperature to mark all plume boundaries, we do this in order to account for slight

differences in ambient ocean temperature across the study region and between survey periods, and because the precision of the TIR imagery (0.1^{o}C) is better than its accuracy (~0.5^{o}C). Using this methodology, the boundaries for most of the plumes are well-defined, ranging in temperatures between 27.2^{o}C - 27.8^{o}C for the August 2005 survey, and between 24.3 ^{o}C -24.9^{o}C for the May 2007 survey. Plume areas for our six main SGD sites range from 18,000 m^2 for Queen's Bath in Kealakekua Bay to over 300,000 m^2 for Kiholo Bay (Table 2). Of the 58 point-source SGD plumes we mapped throughout the survey region, 31 SGD inputs have a plume area >13,000m^2 (Fig. 1 inset). As noted above, the poor quality of the 2007 TIR data for the region south of Kailua Bay does not allow for accurate determination of plume size (refer to Appendix B).

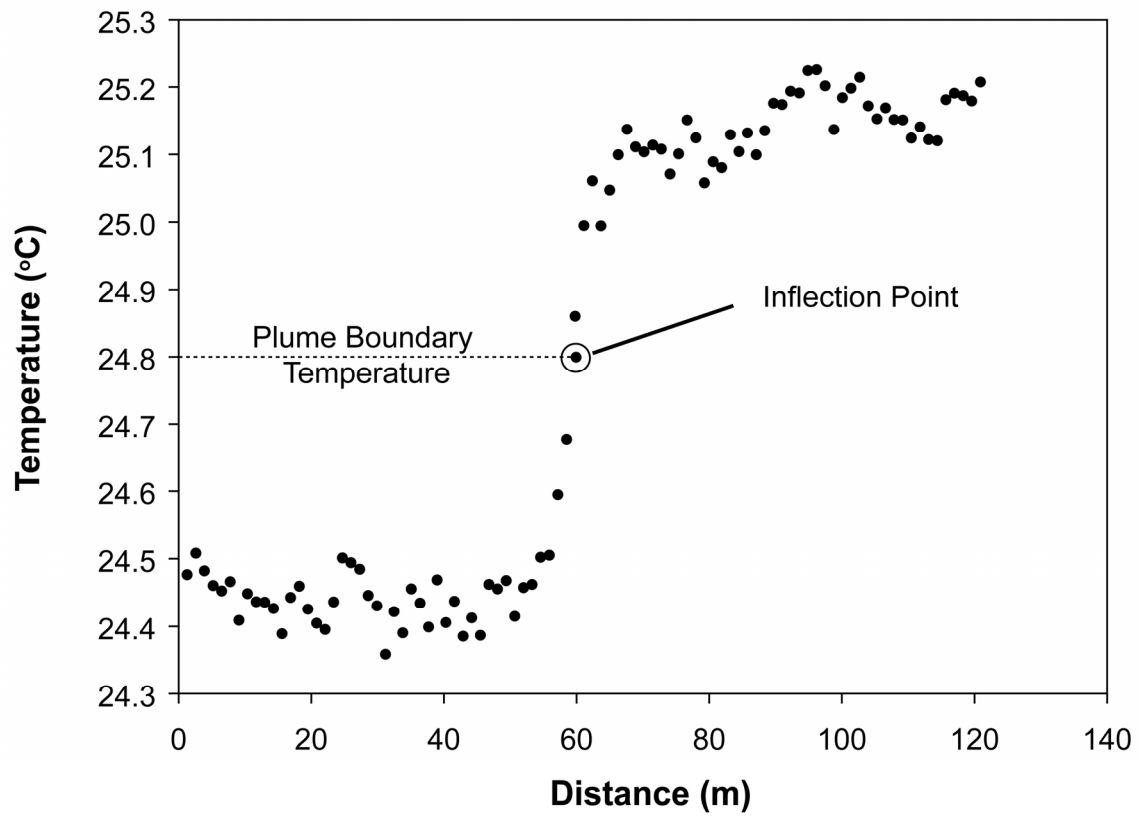

Figure 9. Example of a transect plot of surface water TIR temperature vs. distance in the Kailua Bay plume. The transect was drawn from an arbitrary point within the plume to a point outside the plume where ambient ocean water temperatures were detected. In this particular transect, at distance of about 60m, the plume temperature abruptly increases from ~24.5°C to 25.2°C. We use the inflection point (~24.8°C) of this temperature change as being the boundary of the Kailua plume. For each plume we identified in the TIR surveys, at least three transects were drawn for each plume to determine its mean boundary temperature.

A comparison of the plume area to their estimated SGD flux rate for our six main sites verifies that a plume's surface area extent is proportional to SGD flux (Table 2; Fig. 10). Kiholo Bay was excluded from this correlation because we did not obtain a total

SGD flux for of the second significant coldwater input (Fig. 3, Point "BP") that contributes to total plume area. Note that Kailua Bay and Manini Beach plume areas are slightly below the correlation line; this is probably due to additional groundwater discharge inputs not accounted for by our groundwater tracers time-series measurement platform. Using the relationship in Fig. 10 as a reasonable correlation, we thus estimated first-order approximations of the total SGD rate for each of the groundwater inputs to west Hawaii as based on their individual plume area (Table 1).

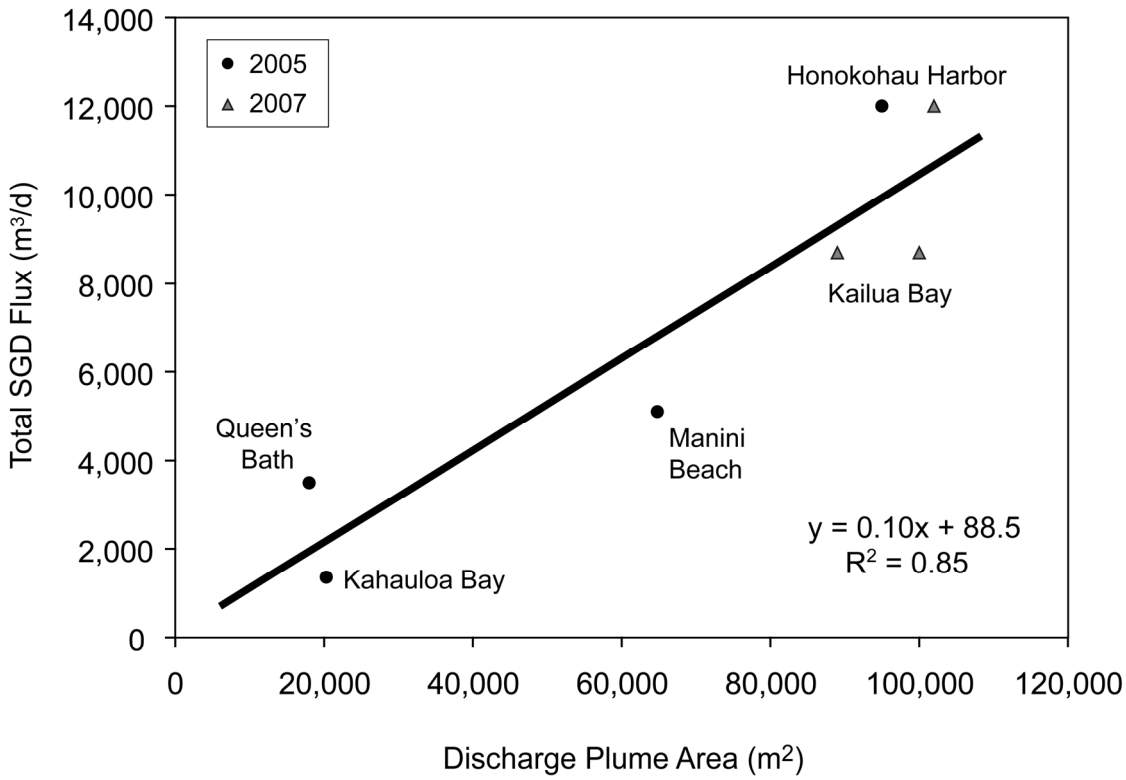

Figure 10. Correlation between groundwater discharge plume area and total SGD flux for five of the six ground-truthed sites. Kailua Bay was mapped both days of the May 2007 survey. Honokohau Harbor was mapped in August 2005 and May 2007.

For the 42 point-source plumes between Kawaihae and Kailua Bay we estimate a cumulative total SGD flux of about 260,000 m^3 d^{-1}, 75% of which (195,000 m^3 d^{-1}) occurs between Kawaihae and Kiholo Bay. In comparison, a previous land-based hydrogeologic water budget for this same area (Kay et al. 1977) estimated a fresh groundwater discharge rate of 200,000 – 725,000 m^3 d^{-1}. Since we report total discharge (freshwater + recirculated seawater), our total flux estimates are lower, but are of the same order of magnitude since ~60% of our computed discharge is fresh. For the entire catchment region between Kiholo Bay and the southern tip of the island, Oki (1999) used a numerical simulation model of fresh groundwater flow to arrive at an estimated average fresh groundwater discharge rate of about 11,300 m^3 d^{-1} per km of coastline. Between Kiholo Bay and Kailua Bay we estimate a total SGD rate of ~1,900 m^3 d^{-1} per km of coastline (65,000 m^3 d^{-1} for 35 km of coastline) and which is about six times lower than Oki's estimated freshwater discharge rate. The large difference in estimates may be due, in part, to the relatively low rainfall and high evaporation rates in this particular region compared to areas south of Kailua Bay.

In any setting, it is important to recognize that there are numerous other factors besides the rate of groundwater input that will affect a plume's area, such as spatial differences in physical mixing dynamics and surface currents across the region, as well as the temporal variability of SGD itself. To gauge the stability of the SGD plumes are, we compared the area of the plumes that were surveyed more than once. In Kiholo Bay, for example, the area of the large plume was ~30% different between the two days it was surveyed in 2007, which may be due to variable surface currents affecting the dispersion of the plume. On the other hand, the plume in Kailua Bay, which was also mapped on

both days of the 2007 survey, had very similar areas (~10% difference) both days. Honokohau Harbor, which was mapped in 2005 and 2007, had nearly identical areas between the two survey years. The locations, shapes and relative sizes of the plumes also appear to be consistent with qualitative infrared video imagery that was collected over the region during the early 1990's (Wilkins unpublished). Thus, although our surveys were conducted over multiple days and years, all TIR data was collected under similar conditions: during low tide, over a period of a few hours early in the morning, and with minimal winds and cloud coverage.

Nutrient Flux Estimates

Nutrient fluxes for our six main sites were estimated by multiplying the average SGD flux rate by nutrient concentrations in brackish groundwater samples immediately inland (within 100 m) from each discharge site (Table 3). For these six sites, we estimate respective total combined dissolved inorganic nutrient inputs to coastal waters of 26,000, 3,800 and 160 moles of Si, N, and P each day. The Wailuku River, on the windward side of the island, delivers an average of 6.7×10^5 m^3 d^{-1} (USGS gauging data) of freshwater to Hilo Bay, and thus 27 times more *freshwater* than our six SGD sites combined (2.5×10^4 m^3 d^{-1}). Despite the large disparity in fresh water flow rates, our estimates for SGD nutrient fluxes are remarkably revealing. As based on our estimates, the dissolved load supplied by total SGD at our six sites alone contribute approximately three times as much DIN than does that of the State of Hawaii's largest river (1,200 moles per day; T. Wiegner, pers. comm.) Compared to SGD-derived nutrient inputs in other regions (Table 3), the cumulative nutrient loads for our six plumes are similar.

In order to compare our nutrient fluxes with previous estimates in west Hawaii, we must scale our flux units relative to shoreline distance (moles d^{-1} m^{-1}). To do this, we divided our nutrient flux estimates at each site by the plume widths determined by our TIR imagery and used in the SGD flux estimate calculations of (Peterson et al. 2008). As shown in Table 4, the resulting nutrient fluxes are generally higher than previous estimates (Dollar and Atkinson 1992; Street et al. 2008) for other bays in the region, although our DIN fluxes are similar in magnitude to estimates that used similar tracer-based methods (Paytan et al. 2006). We suspect the wide range in estimates is attributable to the differences in scaling factors used in formulating the flux estimates, more so than the actual variability amongst the different sites of the region.

Table 3. Comparison of groundwater discharge nutrient inputs to different regions. Nutrient fluxes for this study are the cumulative inputs from six intensively studied groundwater discharge sites in Kiholo Bay, Honokohau Harbor, Kailua Bay and Kealakekua Bay.

Region	**Total SGD (m^3 d^{-1})**	**DISi flux (moles Si d^{-1})**	**DIN flux (moles N d^{-1})**	**DIP flux (moles P d^{-1})**	**Reference**
Waquiot Bay, Mass.	$3.7x10^4$	-	$2.1x10^3$	-	Charette et al. (2001)
Town Cove, Mass.	$4.3x10^4$	-	$2.5x10^3$	-	Giblin and Gaines (1990)
Northwest Florida	?	-	$1.4x10^6$	$8.2x10^4$	Santos et al. (2008)
Yeoja Bay, Korea	$2.6x10^7$	$2.8x10^6$	$2.8x10^6$	$1.2x10^4$	Hwang et al. (2005a)
West Jeju Island, Korea	$7.3x10^9$	$3.2x10^6$	$8.2x10^5$	$3.7x10^4$	Kim et al. (2003)
East Jeju Island, Korea	$9.2x10^9$	$4.1x10^6$	$8.8x10^5$	$4.8x10^4$	Kim et al. (2003)
Bangdu Bay, Jeju Island	$3.5x10^5$	$3.7x10^4$	$1.7x10^4$	$1.3x10^2$	Hwang et al. (2005b)
Gulf of Aqaba, Israel	$1.4x10^3$	-	$3.8x10^1$	$5.2x10^{-1}$	Shellenbarger and Monismith (2006)
Patos-Mirim Lagoon, Brazil	$8.5x10^7$	$5.9x10^6$	$2.4x10^6$	$5.2x10^5$	Niencheski et al. (2007)
Kahana Bay, Oahu, Hawaii	$9.0x10^4$	$1.6x10^3$	$2.7x10^3$	$1.4x10^2$	Garrison et al. (2003)
West Hawaii (six sites)	**$3.8x10^4$**	**$2.6x10^4$**	**$3.8x10^3$**	**$1.6x10^2$**	**this study**
Wailuku River (Hilo, HI)*	$6.7x10^5$	-	$1.2x10^3$	-	(T. Wiegner, pers. comm.)

*The riverine discharge from the Wailuku River is listed in the Total SGD column

Table 4. Comparison of independent estimates of groundwater nutrient input to west Hawaii. Average nutrient concentrations used in flux estimates are listed. For this study, nutrient fluxes were calculated by multiplying average nutrient concentrations in coastal wells by total SGD flux ($m^3 d^{-1}$) divided by width of discharge plume at Rn-platform (see Peterson et al., submitted Table 3)

Location	Avg DISi (µM)	Avg DIN (µM)	Avg DIP (µM)	Total SGD ($m^3 d^{-1}$)	Shoreline Length (m)	Total SGD ($m^3 d^{-1} m^{-1}$)	DISi flux (moles Si $d^{-1} m^{-1}$)	DIN flux (moles N $d^{-1} m^{-1}$)	DIP flux (moles P $d^{-1} m^{-1}$)	Reference
Kiholo Bay	804	71	2.4	7,100	82	86.6	69.6	6.1	0.21	this study
Honokohau Harbor	497	54	5.4	12,000	375	32.0	15.9	1.7	0.17	this study
Kailua Bay*	743	142	4.5	8,700	86	101.2	75.2	14.4	0.45	this study
Queen's Bath	736	94	3.8	3,500	40	87.5	64.4	8.2	0.33	this study
Manini Beach	764	164	4.6	5,100	100	51.0	39.0	8.4	0.24	this study
Kahauloa Bay**	736	188	4.5	1,350	40	33.8	24.9	6.4	0.15	this study
Other west Hawaii studies										
Keahou Bay	769	75	4.0	18,000	800	22.5	17.3	1.7	0.09	Dollar and Atkinson, (1992)
Waikoloa	906	83	1.6	10,000	800	12.5	11.3	1.0	0.02	Dollar and Atkinson, (1992)
Puako	-	126	-	50 -66	1	50.0 - 65.5	-	6.3 - 8.3	-	Paytan et al. (2006)
Kaloko	-	44	-	99 - 109	1	98.9 - 109.5	-	4.35 - 4.82	-	Paytan et al. (2006)
Spencer Beach	798	47	1.2	912	70	13.0	10.4	0.6	0.02	Street et al. (2008)***
Puako	27	7	1	2 - 3.5	50	0.04 - 0.07	0.0011 - 0.0019	0.0003 - 0.0005	<0.0001	Street et al. (2008)
Kaloko Pond (t = 1.56 d)	498	45	2.7	434 -644	50	8.7 - 12.9	4.3 - 6.4	0.4 -0.6	0.02 -0.03	Street et al. (2008)
Kaloko Pond (t = 0.7 d)	498	45	2.7	22,820 -25,900	50	456.4 -518.0	227.3 - 258.0	20.4 - 23.2	1.23 -1.4	Street et al. (2008)
Honokohau Beach (high-ebb tide)	502	48	2.4	138 -316	15	9.2 - 21.1	4.6 - 10.6	0.4 - 1.1	0.02 -0.05	Street et al. (2008)
Honokohau Beach (low tide)	502	49	2.5	536 -894	15	35.8 - 59.6	17.9 - 29.9	1.8 - 2.9	0.09 - 0.15	Street et al. (2008)
Honokohau Beach (flood-high tide)	502	60	2.7	151 -275	15	10.1 -18.3	5.1 -9.2	0.6 - 1.1	0.03 - 0.05	Street et al. (2008)
Keahou Bay	316	171	4.0	1,802 - 2,438	75	24.0 - 32.5	7.6 - 10.3	4.1 - 5.7	0.10 - 0.13	Street et al. (2008)
Kealakeakua Bay	308	40	0.1	0.75 - 2.75	25	0.03 - 0.11	0.01 - 0.03	0.001 - 0.004	<0.0001	Street et al. (2008)
Honaunau	596	19	2.9	165 - 218	15	11.0 - 14.5	6.6 - 8.6	0.21 - 0.25	0.03 - 0.04	Street et al. (2008)

*No coastal well sample was collected for Kailua Bay; average concentrations for region were used in flux estimates

**For Kahauloa Bay, the SGD flux was averaged between two seasonal estimates

***Street et al. (2008) nutrient concentrations have been back-calculated from Table 3a in Street et al. (2008).

Our data clearly shows that the loads of nutrient from SGD represent a major source of new Si, N, and P to the nutrient-poor coastal waters of the region since stream runoff is limited and rainfall is minimal. While nutrient-rich groundwater is entering the ocean in the region via SGD, the linear seaward decrease of its nutrient load with increasing salinity indicates conservative mixing and dilution with ambient seawater. Our simple cross-plots (Fig. 8), by themselves, provide no evidence for biologic nutrient drawdown in surface waters, despite the large delivery of nutrients to this setting. A decoupling between direct nutrient input and an observable phytoplankton response was thus previously suggested by Dollar and Atkinson (1992). These workers concluded nutrient utilization by phytoplankton was incomplete in coastal Hawaiian surface waters and attributed this phenomena to "rapid mixing of buoyant plumes." In the case of Honokohau Harbor, it was suggested that the substantial groundwater inputs facilitates the flushing of nutrients out of the harbor's waters (Gallagher 1980). In light of the data available, this seems a plausible explanation and we would hypothesize that if true this is because the offshore-directed surface water flow jets are too rapid to permit local establishment of high standing stock primary productivity (i.e. short residence time). Another control may, of course, be related to the low salinity of the nutrient-rich surface waters. Still, to our knowledge the only true estimates of phytoplankton primary productivity in the region are those of Bienfang (1983), who, using radiolabeled ^{14}C-bicarbonate measurements of chlorophyll-a mass in Honokohau Harbor, showed a clear spatial increase in surface water primary productivity with increasing nutrient supply towards the harbor's back basin. Further, Parsons et al. (2008) observed positive correlations between nutrients and stressed/dead coral in west Hawaii, and heeds caution

to how chronic nutrient inputs can diminish long-term coral ecosystem health and hinder recovery from other disturbances. Clearly then, one of the major unresolved tasks that lies ahead is accurate quantification of how and where the copious quantities of SGD nutrient supply to this region might impact the ecology of its coastal waters.

1.4 Conclusions

We have demonstrated the application of aerial TIR surveying by mapping dozens of distinct groundwater discharge plumes along coastal west Hawaii. SGD for the region is spatially variable and dominantly occurs as point-source inputs from the shoreline and usually from embayments. Groundwater discharge plumes are thin (<1 m), buoyant, brackish, and cold surface lenses that mix with relatively warm seawater. With minor exceptions, all SGD plumes we have measured are enriched in naturally-derived nutrients. Six of these discharges cumulatively deliver ~ 26,000, 3,800 and 160 moles of DISi, DIN, and DIP each day, respectively. As based on our estimates, the dissolved load supplied by total SGD at our six sites alone contribute approximately 3 times as much DIN than does that of the State of Hawaii's largest river (1,200 moles DIN per day; Weigner submitted). While these nutrient loads exhibit conservative mixing trends in near-shore ocean surface waters, they are the dominant source of new nutrients to the coastal ocean and may play an important role in influencing coastal biology.

The detailed SST imagery from aerial infrared surveys complements ground-truthing efforts by mapping precise input locations and dispersal patterns, and by depicting the dimensions of the discharge plumes, thus helping reduce uncertainties in generating groundwater discharge and nutrient flux estimates. Since the SST imagery

essentially provides a snap-shot of SGD for the entire region, it illustrates the relative magnitudes of groundwater discharges. We therefore utilized our SST maps as a medium for up-scaling localized ground-based SGD estimates from specific sites to regional scales. For the 42 point-source plumes between Kawaihae and Kailua Bay we estimate a cumulative total SGD flux of ~260,000 m^3 d^{-1}.

CHAPTER 2. AERIAL INFRARED IMAGING REVEALS LARGE NUTRIENT-RICH GROUNDWATER INPUTS TO THE OCEAN

Adam G. Johnson[1], Craig R. Glenn[1], William C. Burnett[2], Richard N. Peterson[2] & Paul G. Lucey[3]

[1]*Dept. of Geology and Geophysics, School of Ocean and Earth Science and Technology, University of Hawaii, Honolulu, HI 96822, USA;*
[2]*Dept. of Oceanography, Florida State University, Tallahassee, FL 32306, USA*
[3]*Hawaii Institute of Geophysics and Planetology, School of Ocean and Earth Science and Technology, University of Hawaii, Honolulu, HI 96822, USA*

Submitted to Geophysical Research Letters

Abstract

Regional high-resolution (0.1^{o}C, 0.5 m) low-altitude thermal infrared imagery (TIR) reveals the exact input locations and fine-scale mixing structure of massive, cool groundwaters that discharge into the coastal zone as both diffuse flows and as >30 large point-sourced nutrient-rich plumes along the dry western half of the large volcanic island of Hawaii. These inputs are the sole source of new nutrient delivery to coastal waters in this oligotrophic setting. Water column profiling and nutrient sampling show that the plumes are cold, buoyant, nutrient-rich brackish mixtures of groundwater and seawater. By way of example, we illustrate in detail one of the larger plumes, which discharges ca. 13,000 m^3 d^{-1} (ca. 8,600 m^3 d^{-1} freshwater), rates comparable in volume to high-flux groundwater outputs in better-known tropical karst terrains. We further show how nutrient mixing trends may be integrated into TIR sea surface temperatures to produce surface water nutrient maps of regional extent.

2.1 Introduction

Evidence now suggests that while the total freshwater input to the world's oceans from submarine groundwater discharge (SGD) represents only a few percent of that delivered by rivers, the input of nutrients to coastal environments via SGD is disproportionately large due to its elevated nutrient load (Burnett et al. 2006). Groundwaters typically bear high concentrations of dissolved chemical components, including biolimiting species of N and P, making SGD a particularly important pathway in coastal ocean biogeochemical and ecological systems (Miller and Ullman 2004; Slomp and Van Cappellen 2004). The discharge of nutrient-rich groundwater to coastal waters

has been a key factor for causing disordered growths of marine phytoplankton and macroalgae, which have consequently lead to changes in aquatic habitats and species compositions (Valiela et al. 1990; Paerl 1997), effects which may produce a cascade of changes throughout associated ecologies (Bowen et al. 2007). In several regions, large-scale harmful algal blooms have, in part, been directly linked to groundwater-bourne nutrients (Laroche et al. 1997; Hu et al. 2006; Lee and Kim 2007b). In areas with contaminated aquifers, groundwater is also a potential source of pollutants and bacteria to the ocean (Boehm et al. 2004). Thus, as human populations continue to develop within an aquifer's reach of the coastal zone, the impact of groundwater-borne nutrients and other dissolved species to the nearshore ocean will simultaneously expand. In regions where stream flow is limited, subterranean inputs become an especially important component of linkages between land and sea.

The recognition that SGD is an important pathway for nutrients, contaminants, and other components requires that we develop the necessary tools to up-scale assessments to regional bases. While progress has been made, it remains difficult to evaluate and resolve spatial variations in subterranean discharges over scales of more than a few kilometers. Recognizing this need, we initiated a study to evaluate the use of aerial thermal infrared (TIR) imagery to quantify SGD. We selected the dry, western side of the island of Hawaii as a prime study area since SGD from large islands appears to be volumetrically more important than that found in continental areas (Zekster 2000; Kim et al. 2003; Lee and Kim 2007a), and because the groundwater at this site is the only significant source of freshwater to the coastal ocean (Oki 1999).

The aerial TIR surveying method is applicable wherever there are temperature and density differences between coastal marine waters and discharging terrestrial groundwater. It has been locally utilized at high latitudes where groundwaters are warm relative to seawater (Roxburgh 1985; Banks et al. 1996; Miller and Ullman 2004), and at lower latitudes where groundwaters are cool (Shaban et al. 2005; Duarte et al. 2006). Average groundwater temperatures in coastal aquifers along Hawaii's west coast (~20°C) contrast with ambient coastal ocean temperatures (typically 24-28°C), making temperature an important SGD tracer. Because the groundwater is less saline than coastal seawater, it forms buoyant cool water "plumes" and more diffuse discharges that can be mapped and quantified using aerial sea surface thermal imaging. Cold water anomalies along the shoreline due to vertical mixing perturbations appear minor in our study region since cold water seeps are coincident with other groundwater tracers (radon, salinity, nutrients).

We surveyed surface water temperatures along west Hawaii using an airborne spectrometer with an accuracy of ~0.5^{o}C and a spatial resolution of 0.5 m. This high-resolution TIR imagery captured detailed temperature variations within and spatial extents of groundwater flowing into and mixing with the ocean in exquisite detail. With it, we identified 31 point-source groundwater discharge plumes with a surface area extent >13,000 m^2 (Fig. 11) along ~100 km of coastline and have conducted detailed ground-based measurements and flux rate studies on seven of these. In this paper, we illustrate the aerial TIR character, surface water nutrient chemistry, water column structure, and measured discharge rates of these plumes, using the groundwater outflow from a small boat harbor as an example of the utility of our approach and significance of our findings.

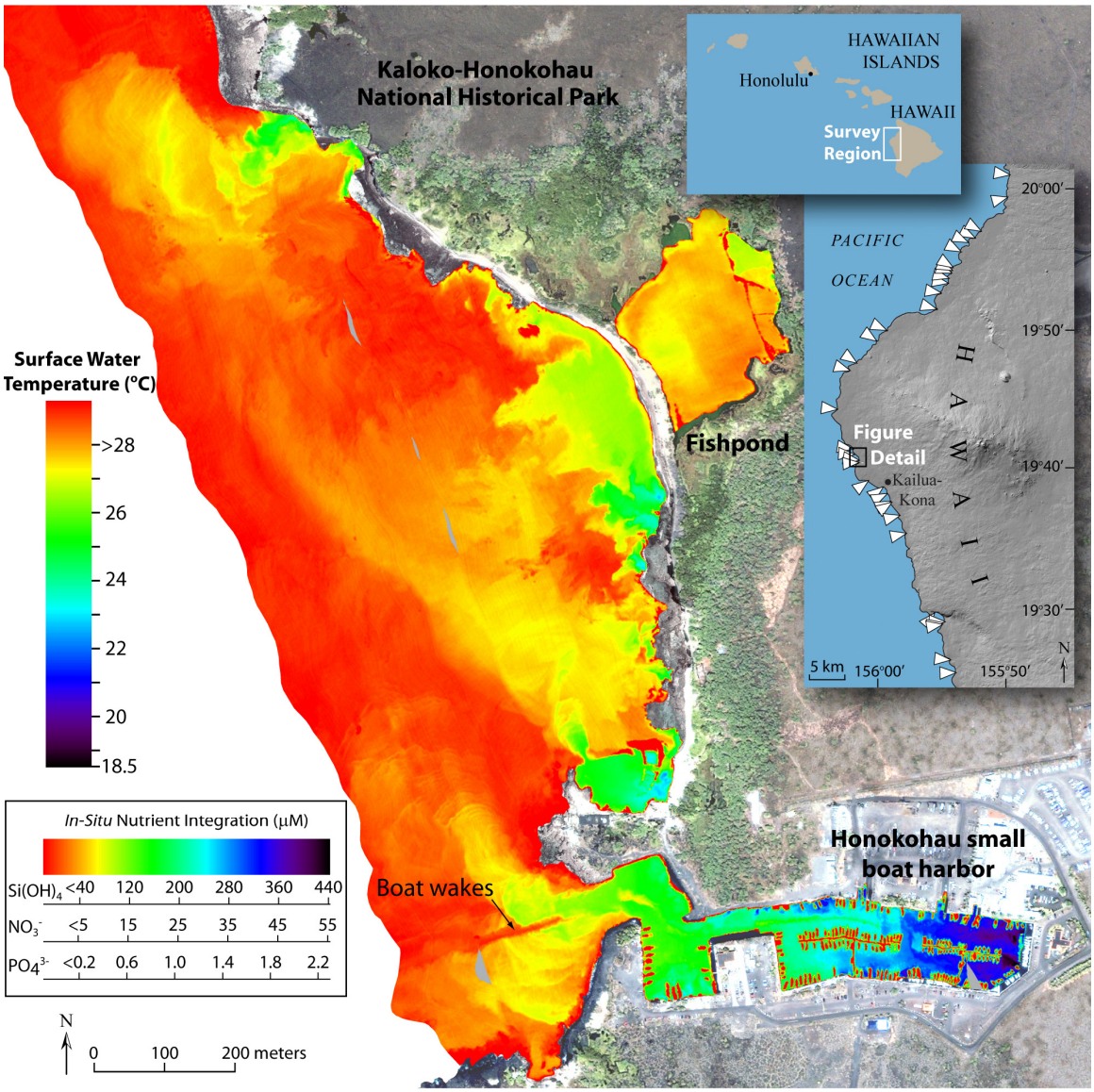

Figure 11. Sea surface temperature (SST) map produced from August 2005 aerial TIR survey over coastal waters in the vicinity of Kaloko-Honokohau National Historical Park, located on the west coast of Island of Hawaii. The SST image is a temperature-corrected, georectified mosaic of 135-m wide swath images with a spatial resolution of 0.5 m. White triangles in the inset indicate the positions of 31 major (surface area >13,000 m^2) point-sourced SGD plumes identified by TIR imagery. See text for discussion of integrating surface water nutrient concentrations into the TIR image.

2.2 Methods

Aerial TIR Surveys

Initial TIR surveys were conducted in August 2005 over Kaloko-Honokohau National Historical Park and Kealakekua Bay areas. Subsequent TIR mapping in May 2007 surveyed the entire region depicted in the Figure 11 inset. Surveys were conducted at an altitude of 1100 m using a TIR spectrometer (sensitivity of 0.1^{o}C) mounted in an aircraft's fuselage that produced TIR images for each flight line. After the aerial surveys, each flight line image was spectrally calibrated to the onboard blackbody measurements made between each flight line. All bands between 8.1 and 11.0 μm in the calibrated line images were then averaged to single band and subsequently converted to temperature by inverting the Planck equation (Pieters and Englert 1993). The temperature-converted images were georeferenced using the aircraft's navigational parameters, referenced to regional aerial photographs using tie points, and then mosaicked to form high-resolution surface water temperature maps. The temperatures in the mosaicked images were then calibrated to twelve *in situ* thermistors (Onset HOBO®, accuracy = 0.5^{o}C); this process removes atmospheric interferences (mainly due to water vapor and aerosols) between the ocean's surface and the airborne sensor. Full details of the TIR surveys can be found in Appendices A and B.

Temperature and Salinity Profiles and Nutrients

Vertical water column profiles of temperature and salinity were measured at SGD sites within several hours of low tide in order to coincide with maximum groundwater discharge. *In situ* temperature/salinity measurements were made using a calibrated multi-

parameter YSI probe accurate to ± 0.15°C and ±1% for salinity. Water samples were collected between August 2005 and May 2007 throughout west Hawaii to determine regional nutrient characteristics. Samples were collected in pristine freshwater wells, brackish wells and ponds along the coastline, nearshore coastal waters, and offshore marine water. Seawater samples were taken within 0.15 m of the ocean's surface. Samples were filtered (0.45-µm GF/C) and refrigerated until analyzed at the University of Washington using spectrophotometric segmented flow nutrient analysis. Respective standard errors (n=10) for $Si(OH)_4$, NO_3^-, and PO_4^{3-} were 1.1%, 2.5%, and 3.4% of the measured concentration.

Groundwater Discharge Fluxes

Groundwater discharge fluxes were estimated using two natural groundwater tracers, ^{222}Rn (enriched in groundwater) and salinity (depleted in groundwater), which were continuously measured at discharge locations for several tidal cycles. Inventories of ^{222}Rn and salinity were used in a non-steady-state mass balance model that accounts for inputs and outputs of these two tracers at discharge sites, in which the tidal and SGD water fluxes are the unknown factors. Coincident mass balance equations for ^{222}Rn, salinity, and tidal water volumes were solved (Peterson et al. 2007) to calculate both freshwater and total (freshwater + recirculated seawater) groundwater discharge. Our procedures and calculations are detailed in the Appendix C.

2.3 Results and Discussion

Our TIR imagery indicates that SGD for the surveyed region occurs as more than 50 point-source discharges (distinct SGD portals at the shoreline) and ~12 diffuse discharges (seepage disseminating from more extensive segments of coastline), both of which primarily occur in embayments. This is expected as groundwater table heights follow surface topography, and subsurface flow is hydraulically directed towards sea level. Thus, groundwater flow lines are directed toward and converge at coastal embayments. As those embayments are naturally or artificially enlarged, they proportionally intersect larger areas of the groundwater table and discharge larger volumes of SGD flow.

At Honokohau Harbor, as elsewhere along the coast, temperature-salinity profiles show that its cool seaward-flowing brackish surface plume is less than a few meters thick and overrides warmer and denser seawater that flows landward beneath it (Fig. 12). As the brackish water surface plume flows seaward, it mixes with and entrains the warm incoming seawater below (Bienfang 1980). Propellers from boats moving through the plume pull warm water up into the cool, brackish surface water lens (Fig. 11). Combining ground-based measurements from several areas along the west coast of Hawaii, we determined that a statistically robust linear correlation exists between temperature and salinity in marine waters throughout the region (Fig. 13a).

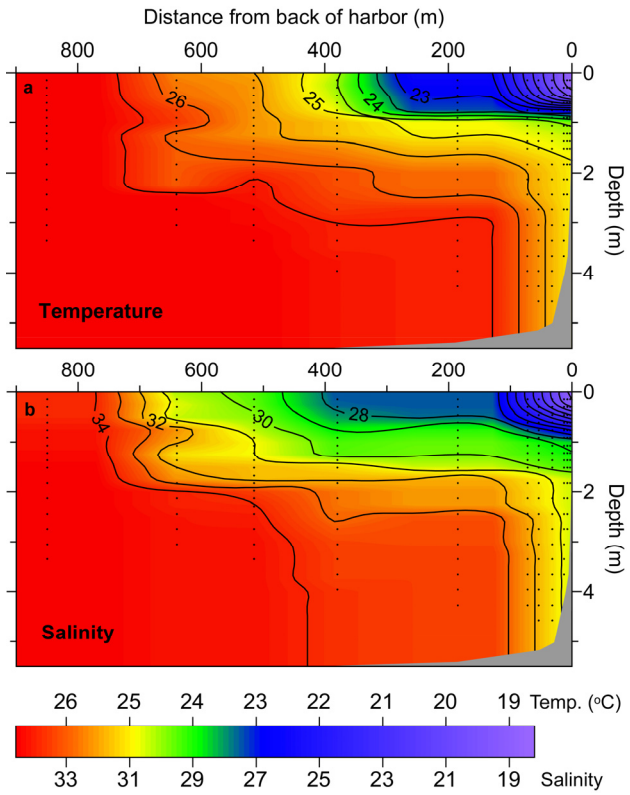

Figure 12. Water column temperature (a) and salinity (b) profiles for Honokohau Harbor, August 2006. Location and depth of individual measurements are shown by black dots. The relatively cool, brackish, nutrient-rich plume flows seaward above warm, dense seawater flowing landward (Bienfang 1980).

Based on mass balances of ^{222}Rn, salinity, and water fluxes for Honokohau Harbor (details in auxiliary material), we estimate the total groundwater flux to be 12,000 m^3/day, with an average salinity of 15.2 and a ^{222}Rn activity of 25,500 dpm/m^3. The corresponding flux for the terrestrial freshwater component of this discharge is 8,600 m^3/day, as based on a salinity of 0 and a ^{222}Rn activity of 39,100 dpm/m^3. Compared to the freshwater output of massive artesian springs in tropical karst, both our modeled total SGD and freshwater fluxes are moderately large in terms of flow rate, being classified (Rosenau et al. 1977) as Magnitude-3 Springs (~2,400 to ~24,000 m^3/day). For arid west

Hawaii, however, these water and associated nutrient fluxes are substantial. Calculated on a basis of unit width of shoreline, our estimated freshwater flow from the harbor's 80-m wide mouth is equivalent to ~107,000 m^3 d^{-1} km^{-1}. A regional water budget (Kay et al. 1977) estimated an average freshwater discharge of ~15,000 m^3 d^{-1} km^{-1} for a ~26-km length of shoreline north of our study area. More locally, using a numerical groundwater flow model developed for the regional aquifer in west Hawaii, Oki et al. (1999) calculated a freshwater coastal discharge within adjacent Kaloko-Honokohau National Historical Park of ~7,000 m^3 d^{-1} km^{-1}. These comparisons show that the point-source freshwater outputs documented by our TIR mapping are focused and amplified several times over background non-point-source regional SGD.

Regional SGD nutrient characteristics are illustrated by plots of silica, nitrate, and phosphate concentrations relative to salinity (Fig. 13b-d). Linear regressions of these data for ocean surface waters of the region (salinities 7-35) show clear linear seaward decreases of all nutrients with increasing salinity, indicating conservative mixing and dilution with ambient seawater (the one exception being anthropogenic additions of phosphate to Honokohau Harbor – see auxiliary material). These linear trends show no *net* apparent biological nutrient draw-down in ocean surface waters, despite the substantial nutrient loading from SGD (a phenomena previously observed by Dollar and Atkinson (1992), although our regional observations of nutrient loading and seaward mixing do not preclude biological utilization. If there is biological uptake of these nutrients (as one might expect), it is masked by the very high rates of nutrient supply.

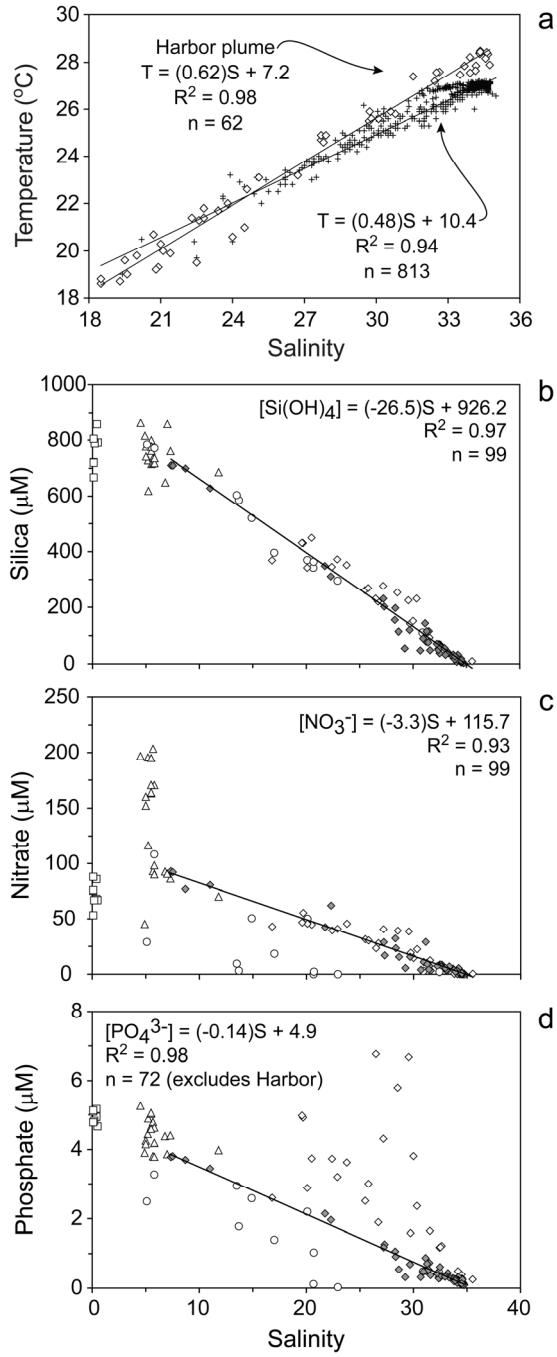

Figure 13. (a) In-situ measurements (cross symbols) from transects in Honokohau Harbor and Kealakekua Bay (Fig. 11 inset) indicate a strong linear correlation between temperature (T) and salinity (S) for coastal ocean waters in the west Hawaii region. Open diamonds represent temperature and salinity measurements in the upper 0.5 m of the Honokohau Harbor plume. (b-d) Dissolved silica, nitrate, and phosphate concentrations in pristine freshwater wells (open squares), brackish wells (open triangles), brackish ponds (open circles), and ocean surface waters (open and closed diamonds) from samples collected in Honokohau Harbor, Kealakekua Bay and Kailua Bay. Linear regressions are for ocean samples only; phosphate regression excludes Honokohau Harbor (open diamonds). Data tables included in Appendix E.

With the possible exception of phosphate, Y-intercepts of the nutrient mixing trends fail to intersect the zero-salinity nutrient concentrations measured in pristine freshwater aquifers (Fig. 13). Although brackish coastal ponds and coastal well waters are spatially located between the marine SGD nutrient plumes and pristine high-elevation freshwater aquifers, they show significant deviation from the well-defined ocean mixing trends. Nitrate in coastal wells, in particular, shows marked enrichments relative to both the marine mixing regression and the freshwater aquifers. Natural leaching from the variety of west Hawaiian soils with differing plant covers (cf. Vitousek (2004)), and local anthropogenic contributions from fertilizers and septic systems likely all contribute to these variations. Moreover, the coastal (anchialine) ponds are small, shallow, and often support a unique assemblage of invertebrate and algal species (Maciolek and Brock 1974), and thus internally modify their own micro-environmental chemistry. All these deviations illustrate that the nutrient compositions of the Hawaiian groundwaters undergo modification during their transit from inland recharge areas toward their coastline exit portals, a phenomena well documented in many groundwater systems (Slomp and Van Cappellen 2004; Bowen et al. 2007; Santos et al. 2008). However, despite all these modifications, what is most important with regards to nutrient dynamics in west Hawaii is that the region's aquifers are naturally enriched in Si-N-P, and that the discharge of groundwater into the ocean must be the only source of new nutrients to the oligotrophic waters of the region.

TIR mapping can provide a framework for integration of a variety of ancillary data sets, so long as those data are coherently related to temperature. The relatively constant temperature, salinity and nutrient trends in the marine surface waters of west Hawaii, for

example, allow our TIR imagery to be used as an approximation of surface water nutrient distributions. This can be accomplished by combining linear temperature-salinity variations with linear nutrient-salinity trends. Since we lack a statistically robust temperature-salinity data set solely for the period of the initial TIR flight (August 2005), we take advantage of persistent temperature-salinity relationships within the Honokohau Harbor plume (Fig. 13a), which are dominated by the high rates of SGD inflow and are sheltered from inter-seasonal open ocean temperature extremes. Solving this localized linear temperature-salinity correlation for salinity (Fig. 13a), and substituting the resulting function into each regional nutrient-salinity trend (Fig. 13b-d) yields co-linear correlations relating nutrient concentrations to surface water temperature. The resultant *in situ* nutrient-to-TIR temperature integrations are illustrated in the boxed inset of Figure 11. We caution that such up-scaling integrations depend on critical consideration of the variables involved, including surface water nutrient drawdown by biota, coastal ocean mixing dynamics, anthropogenic nutrients, and localized runoff effects on temperature, salinity and nutrients.

2.4 Conclusions

This work demonstrates that aerial infrared surveying is an efficient method for mapping SGD on a large-scale basis and, when combined with ground-based studies, forms a powerful tool for regional SGD analysis. The anomalous temperatures of the SGD plumes are coincide with its other defining properties (salinity, nutrients, radon). High-resolution aerial imagery along coastal west Hawaii details spatial inputs and seaward mixing of cool, brackish, nutrient-rich groundwaters discharging as both point-

source plumes and diffuse flow. On west Hawaii, these nutrient inputs represent the sole source of new nutrient delivery to the coastal ocean. Estimates indicate point-source discharge rates for this region are amplified over background SGD and are comparable in magnitude to large springs in continental coastal regions. High groundwater fluxes and rapid oceanic mixing produce conservative temperature, salinity, and nutrient relationships, allowing SST to be used as a semi-quantitative estimate of spatial sea-surface nutrient concentrations in this region. Most importantly, however, is the principal strength of TIR surveying in the coastal ocean, which is the ability to differentiate and map inputs of water masses with differing SST, and up-scaling quantitative discharge estimates. The TIR technique for recognizing SGD is not limited to tropical regions, but can be applied in a variety of other environments wherever temperature contrasts exist, such as where stream flow to the ocean has a different temperature than groundwater, or in temperate latitudes where warm groundwaters intrude colder seawater.

APPENDIX A

August 2005 Aerial Thermal Infrared Survey

Overview

This appendix contains a more thorough explanation of the August 2005 aerial TIR survey and data processing procedures than was presented in chapters 1 and 2. The first section of this appendix contains details of the survey. The second section discusses data processing done after the survey; this includes thermal image temperature conversions, spatial corrections of the imagery, and ground-truthing temperature calibrations.

Survey Details

The aerial survey was conducted on 16 August 2005 over Kealakekua Bay and Kaloko-Honokohau National Historical Park (KAHO) areas of the western half of the Big Island. Kealakekua Bay was surveyed between 06:10h and 07:50h, and the KAHO area was surveyed between 08:00h and 10:10h Hawaiian Standard Time (HST). Low tide (-0.1 ft) occurred at 07:00h with subsequent high tide (+2.5 ft) at 15:00h HST. Weather conditions were excellent with minimal winds and no visible cloud coverage.

Surface water temperatures were determined using University of Hawaii's Airborne Hyperspectral Imager (AHI) mounted in the fuselage of a Twin Piper Navajo aircraft. The AHI measures 256 bands in the thermal infrared spectral range of 7.5 – 11.7 microns at a sensitivity of 0.1^{o}C. The AHI is a pushbroom scanner that continuously collects sequential lines of TIR imagery as the plane flies over the survey area. All flight lines were flown in a northwest trending direction at an altitude of 3,600 feet. For each

flight line, the AHI captured ~135-m wide swath images with a spatial resolution of 0.5 m. In between data collection for each flight line, the AHI measured the radiance of an onboard blackbody adjusted to four to six temperatures between 15 - 45°C for use in calibrating the thermal images during post-flight processing. Fifteen and eleven overlapping (~30%) flight lines were flown over Kealakekua Bay and KAHO areas, respectively. Table A1 contains the times of the flight lines.

Flight Line	Time	Notes
1	6:21	
2	6:10	
3	6:30	
4	6:39	
5	6:45	
6	6:54	
7	7:02	no data
7b	7:08	
8	7:14	no data
9	7:20	
10	7:25	
11	7:31	
12	7:38	
13	7:45	
14	7:51	
15	8:04	
16	8:09	
17	8:16	
18	8:22	
19	8:30	
20	8:35	
21	8:41	
22	8:46	
23	8:52	
24	8:58	
25	9:03	

Table A1. Times of flight lines for August 16, 2005 aerial TIR survey. Lines 1-14 were flown over Kealakekua Bay, Lines 15-25 were flown over KAHO/Honokohau Harbor area.

Post-flight image processing

Initial temperature calibrations

After the survey, each "raw" flight line image was spectrally calibrated to the onboard blackbody measurements. This mitigates temperature errors caused by changes in the AHI's sensitivity during the survey. Next, all bands between 8.1 and 11.0 microns in the calibrated image were averaged to single band. The averaged image data, in units of spectral radiance, were then converted to temperature by inverting the Planck equation (Pieters and Englert 1993) as shown below.

$$T = \frac{c_2}{\lambda}\left[\ln\left(\frac{c_1}{L\lambda^5}\right)+1\right]$$

Where $\boldsymbol{c_1}$ = 1.191066*10^{-8} W/m^2/sr/cm^{-4}, $\boldsymbol{c_2}$ = 1.438833 cm.K, $\boldsymbol{L}$ = radiance (W/m^2/sr/μm), $\boldsymbol{\lambda}$ = 10.0 μm, and $\boldsymbol{T}$ = temperature (K).

Image spatial corrections

Due to technical errors during the survey, most of the flight lines images had missing sections data, where no imagery was collected for 25 to 250 meters. These data gaps, when not corrected for, caused significant spatial errors in the imagery and required extensive processing. Since the AHI records lines of data sequentially, the blank data sections were not included in the flight line images, and thus were not obvious at first. After the flight line images were initially georeferenced, however, there were obvious

amounts of warping and spatial distortions within each flight line, and poor alignment of features between adjacent flight lines images. Upon close inspection, the missing sections of data were apparent when two features, located several hundred meters apart in reality, erroneously appeared only a few meters apart in a flight line image. In contrast, the navigation data for the imagery appeared to be complete with no missing data. Thus, the spatial errors and distortions in the imagery were due to a *complete* navigational data being used to georeference *incomplete* image data.

In order to mitigate the spatial distortion errors, the missing data sections were patched into each flight line. Determining exactly when and how long each recording error occurred, however, was difficult. Since the navigational information was continuously recorded without any errors, it was not possible to calculate the duration of the recording errors and the consequent length of the blank data gaps. Instead, the length of each data gap, which varied between flight lines, had to be visually approximated. When the data gaps occurred over land, the length could be estimated using identifiable features as reference points, and the corresponding number of blank data lines could be patched into the gap. When the data gaps occurred over water, blank data lines of various lengths were added by trial and error until the spatial distortion of recognizable land features was visually reduced. This process of patching in blank data lines removed much of the spatial distortion, but since it is not an exact method, some distortion remains in the imagery. Details of the spatial correction "patching" procedures are discussed below. All corrections were done using ENVI and IDL software.

Patching procedure

First, each flight line image was split into two separate images at the data gap. Based on the approximated distance of each data gap, the corresponding number of blank lines (lines having no data values) were placed between the two separated images. The two separated images and blank data lines were then combined into a single "patched" flight line image. Next, each patched flight line image was scaled back to its original length. For example, if a flight line image was 9,000 lines long and 300 lines were patched into the data gap, the patched flight line image would be scaled lengthwise from 9,300 pixels to 9,000 pixels. During this procedure, samples 1-5 and 248-256 for each flight line image were also cropped off since these are the edges of the flight line images and contain no data.

The patched flight line images were then individually georeferenced using the plane's navigational characteristics; these included time, plane velocity and heading, latitude, longitude, altitude, pitch, yaw, and roll that were recorded by the AHI system during the survey. This navigational information was converted into an '.igm' file in IDL, which was subsequently utilized in ENVI's standard georeferencing procedure.

Prior to mosaicking all the georeferenced thermal flight line images into a single composite image, "cutlines" were drawn for each image. Cutlines essentially allow one to define where the edges of each flight line image are and remove the blank data from the edges of each image. Using the cutlines, all thermal flight line image images were then mosaicked into a single composite SST image in ENVI.

Ground-truthing temperature calibrations

Due to atmospheric interference between the ocean surface and airborne AHI sensor (mainly absorption by water vapor and aerosols), temperatures determined from the aerial survey were recalibrated to temperatures measured by thermistors stationed in the surface water. Twelve GPS-located thermistors (Onset Corp. accuracy = 0.5^{o}C) within the survey area simultaneously recorded surface water temperatures as the survey was being conducted. A linear correlation between temperatures measured by in-situ thermistors and the corresponding temperatures in the georeferenced imagery was used to recalibrate the surface water temperature map (Fig. A1). Finally, the recalibrated SST maps were converted from gray-scale to color and placed onto satellite images of the region for geographic reference.

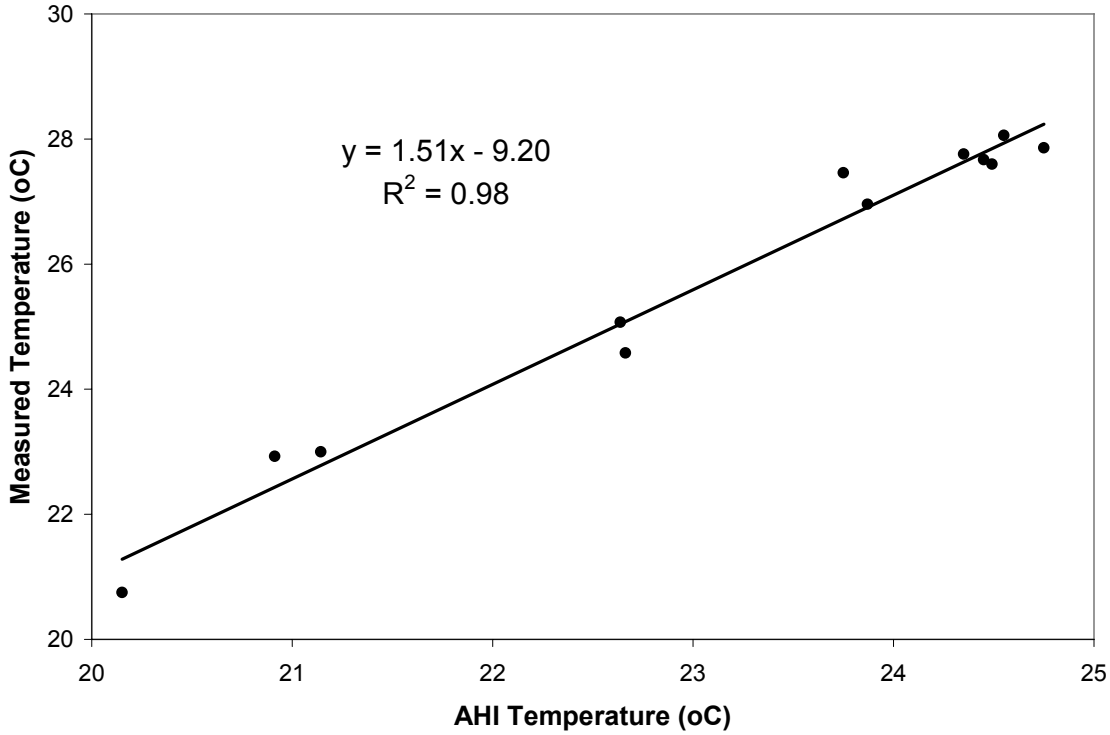

Figure A1. Relationship between water temperatures determined from AHI instrument (x-axis) and water temperatures measured by *in-situ* thermistors (y-axis). The linear equation was used to recalibrate temperatures in the thermal infrared imagery to *in-situ* surface water temperatures.

APPENDIX B

April/May 2007 Aerial Thermal Infrared Survey: Kawaihae to Hookena

Overview

This appendix contains a more thorough explanation of the April/May 2007 aerial TIR survey and data processing procedures than was presented in chapters 1 and 2. The first section of this appendix contains details of the survey. The second section discusses data processing done after the survey; this includes thermal image temperature conversions, spatial corrections of the imagery, and ground-truthing temperature calibrations. The third section discusses other sources of temperature error that could not be corrected.

Survey Details

The second aerial TIR survey covered >100 km of the western half of the Big Island from Kawaihae to Hookena. It was conducted over a period of two days: 06:55-10:15h April 30, 2007 (day 1) and 07:53-10:30h HST, May 1, 2007 (day 2). On April 30, low tide (-0.2 ft) was at 08:15h and the subsequent high tide (+2.0 ft) was at 15:15h HST. On May 1, low tide (-0.2 ft) was at 08:30h and the subsequent high tide (+2.1 ft) was at 15:45h HST. Cloud coverage was minimal early in the day, then became scattered and patchy along the coastline at about 09:00h both days.

The second aerial survey measured surface water temperatures using a Merlin infrared camera. Similar to the AHI, Merlin is a highly sensitive (0.1^{o}C) framing imager that collects surface water temperature swath images for each flight line. Merlin's 22°

instantaneous field of view lens, compared to AHI's 7°, allowed us to survey a much larger area with less flight lines. Along each flight line track, 320 x 240-pixel infrared images were captured at a rate (60 Hz) where there was 90% overlap in coverage between sequential images in a flight line.

Forty flight lines were flown at an altitude of 3,500 feet with each flight line surveying an area ~ 414m wide at a spatial resolution of 1.3m. For each segment of coastline, two to three parallel and overlapping (~30%) flight lines were flown. Due to sporadic cloud cover, flight lines were not flown in sequential order, and some lines were repeated. On day 2, after all 3,500-ft elevation flight lines were completed, six additional flight lines were flown at altitude of 10,000-ft. These high elevation flight lines surveyed approximately the same extent of coastline as the 3,500-ft elevation flight lines. Flight line locations are shown in Figures B1 and B2. The dates, times, and notes for all flight lines are shown in Tables B1 and B2.

During the survey, onboard calibrations to a variable temperature flat-panel blackbody were taken sparingly due to power supply problems on the aircraft. On day 1, blackbody calibrations were made only prior to surveying the first flight line. On day 2, blackbody calibrations were made before and after all the 3,500 feet elevation flight lines, and then after the 10,000 feet elevation flight lines.

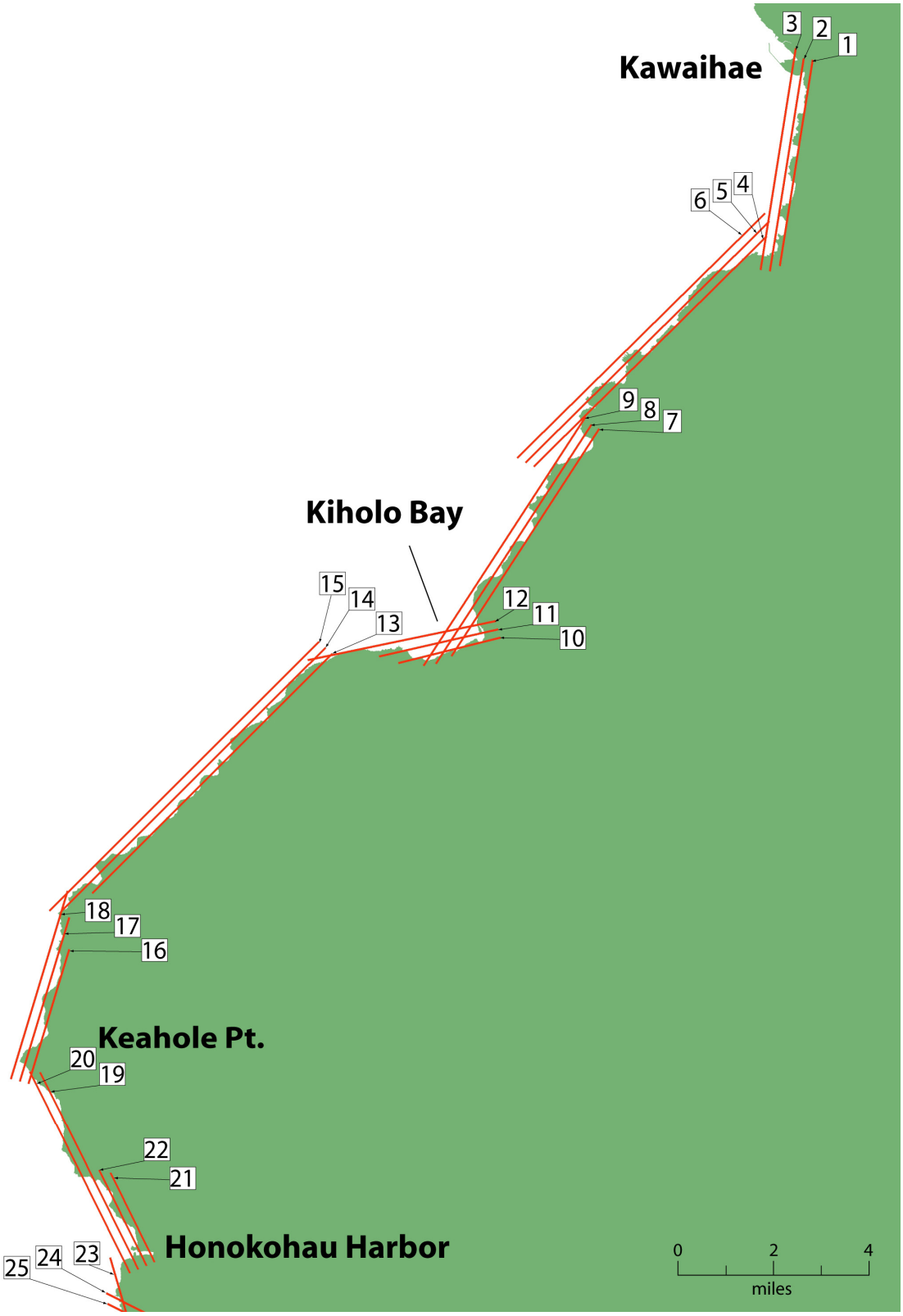

Figure B1. Flight line locations in northern section of survey region.

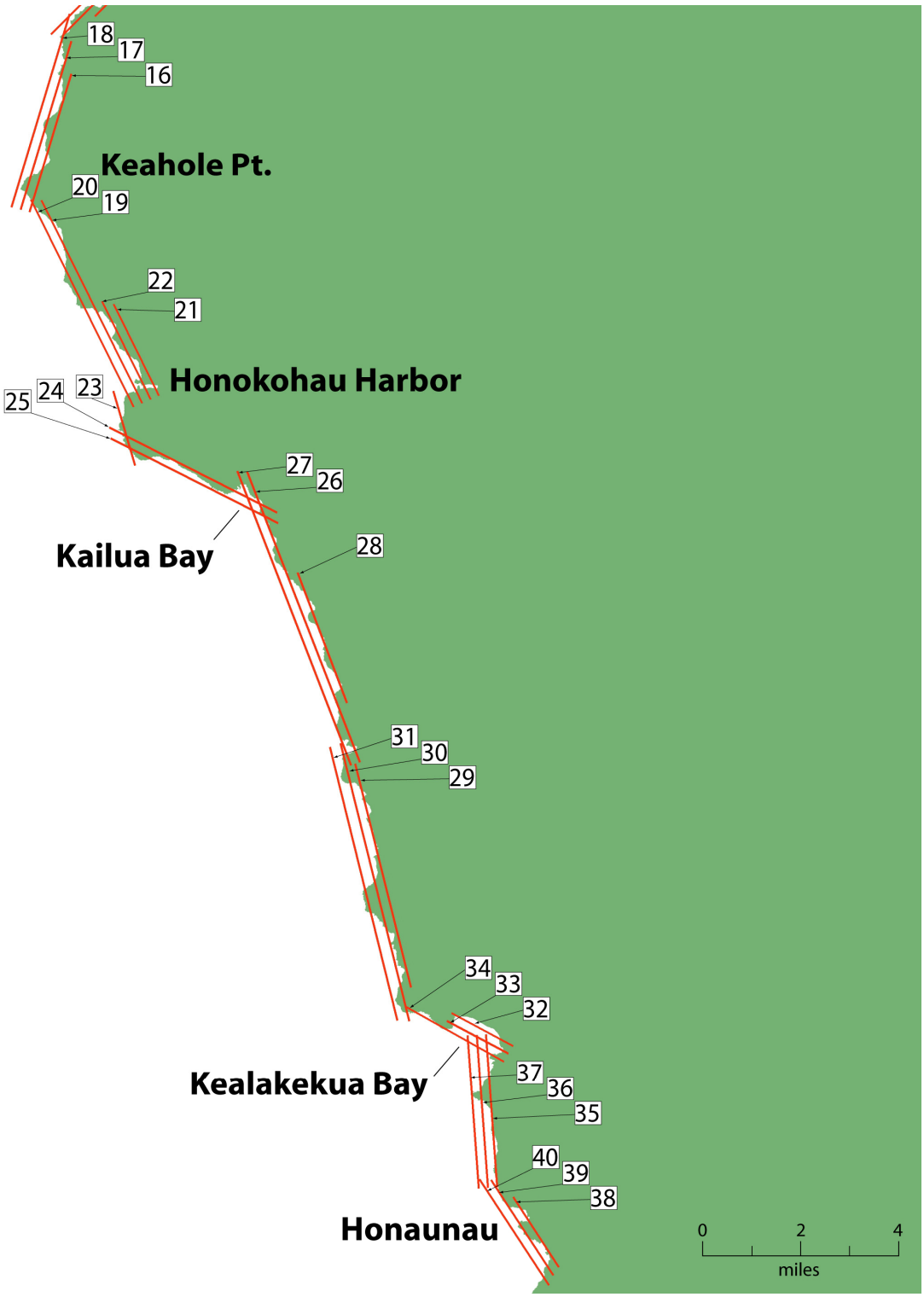

Figure B2. Flight line locations in southern section of 2007 aerial TIR survey region.

DAY1 Flight Line	Time	Heading	Notes
calibrate	6:38	-	15, 25, 30°C
1	6:55	S	turbulent ride, data warped
2	7:00	N	turbulent ride, data warped
3	7:08	S	turbulent ride, data warped
4	7:18	S	
5	7:23	N	
6	7:31	S	
7	7:37	N	
8	7:47	S	
9	7:57	N	
10	8:05	S	
11	8:10	N	
12	8:15	S	
26	10:04	N	H
27	8:30	N	Cloudy
27b	8:42	N	redo of 27
27c	10:11	S	H
28	8:38	S	
29	8:56	S	
30	9:02	N	H
31	9:08	S	H
32	9:15	S	H
33	9:19	S	H
34	9:22	S	H
35	9:29	S	H
36	9:35	N	H
37	9:39	S	H
38	9:46	N	Disk full error
38b	9:50	N	H, sunglint
39	9:55	S	H, sunglint
40	10:00	N	H, sunglint

Table B1. Flight line times, heading, and notes for April 30, 2007. "H" indicates images with erroneous heating artifacts as discussed in the "other sources of temperature error" section of this appendix.

DAY2 Flight Line	Time	Heading	Notes
calibrate	7:13	-	25, 30°C
calibrate	7:25	-	25°C
calibrate	7:26	-	25, 30°C
calibrate	?	-	23, 25, 30°C
10B	7:53	S	day 2 of Kiholo
11B	7:58	N	day 2 of Kiholo
12B	8:03	S	day 2 of Kiholo
13	8:09	S	
14	8:16	N	
15	8:23	S	sunglint
16	8:33	S	
17	8:38	N	
18	8:45	S	
19	8:52	S	out of focus
20	8:59	N	
19B	9:05	S	redo of 19
21	9:06	S	
22	9:11	N	no data (Honokohau Harbor)
23	9:16	S	
24	9:02	S	
25	9:26	S	H
calibrate	9:30	-	23, 30°C
41	9:47	N	10,000-ft elevation
42	9:57	N	10,000-ft elevation
43	10:08	N	10,000-ft elevation
44	10:11	N	10,000-ft elevation
45	10:22	N	10,000-ft elevation
46	?	N	10,000-ft elevation
calibrate	10:25	-	20, 25, 30°C

Table B2. Flight line times, heading, and notes for May 1, 2007. "H" indicates images with erroneous heating artifacts as discussed in the "other sources of temperature error" section of this appendix.

Post-flight image processing

Overview

Similar to AHI, there were several steps involved in processing the "raw" survey data. Individual thermal images for each flight line were first converted to temperature using onboard blackbody measurements and then mosaicked together into a composite thermal flight line image. Next, each flight line image was georeferenced to a base map. After georeferencing the flight line images, corrections were made for three sources of temperature error: 1) drift in the camera's sensitivity during the survey 2) atmospheric interferences between the airborne sensor and the ocean 3) surface water skin layer effects 4) assumption that water has an emissivity of one. Finally, all georeferenced, temperature-calibrated flight line images were mosaicked into composite SST maps.

Initial temperature calibration

Each thermal image collected during the survey was first converted to temperature (^{o}C) using onboard blackbody measurements. Based on image digital numbers (DN) measured by the camera when it was aimed at a blackbody, DN were converted to temperature. Due to slight differences in Merlin's sensitivity across its field of view, DN were converted to temperature on a pixel-by-pixel basis. For each pixel in the image, we determined a DN that corresponds to 15°C and a DN that corresponds 30°C. Assuming a linear relationship between temperature and DN in between these two

temperatures, we formulated a linear equation that relates the DN of each pixel in all the images to temperature. Ideally, onboard blackbody measurements are made before and after each flight line so a unique DN to temperature correlation can be determined for each flight line. These calibration measurements would correct for drift in the spectrometer's sensitivity during the survey.

Next, temperature-converted flight line images were georeferenced. Unlike the first survey, no synchronous flight navigational information was recorded during the second survey that could be used to spatially correct the imagery. Instead, flight line images were individually georeferenced to basemaps by selecting ground control points such as rock outcrops, unique lava flow features, road/trail intersections, and other distinctive features at ground level near the shoreline that could be identified in both the TIR imagery and basemaps. Basemaps were ortho-rectified, aerial photograph composites collected in 2000 at 0.85 m resolution with NAD83/UTM Zone4 datum (available at http://www.soest.hawaii.edu/coasts/data/hawaii/pdcimagery.html).

Correcting sensor drift

Drift in the spectrometer's sensitivity was evident in slight (0.2 – 3°C) temperature differences between adjacent flight line images. Sensor drift can be caused by air temperature changes in the airplane, vibrations, and other stresses. Normally, sensor drift can be corrected for by taking frequent blackbody calibration measurements during data collection, preferably before and after each flight line. Unfortunately, due to power problems on the aircraft, it was only possible to take calibration measurements prior to collecting the first line and after collecting the last line each survey day. Instead,

temperature errors caused by sensor drift were corrected by comparing water temperatures at specific locations where two adjacent images overlap. As exemplified in Fig. B3, a correlation relating the temperatures between two images can be used to adjust the temperatures in one image so they are coherent with the temperatures in the adjacent image. This was done for each set of parallel overlapping flight line images. Although frequent onboard blackbody calibrations would eliminate sensor drift more exactly, our method does yield a consistent set of overlapping thermal images for each segment of coastline.

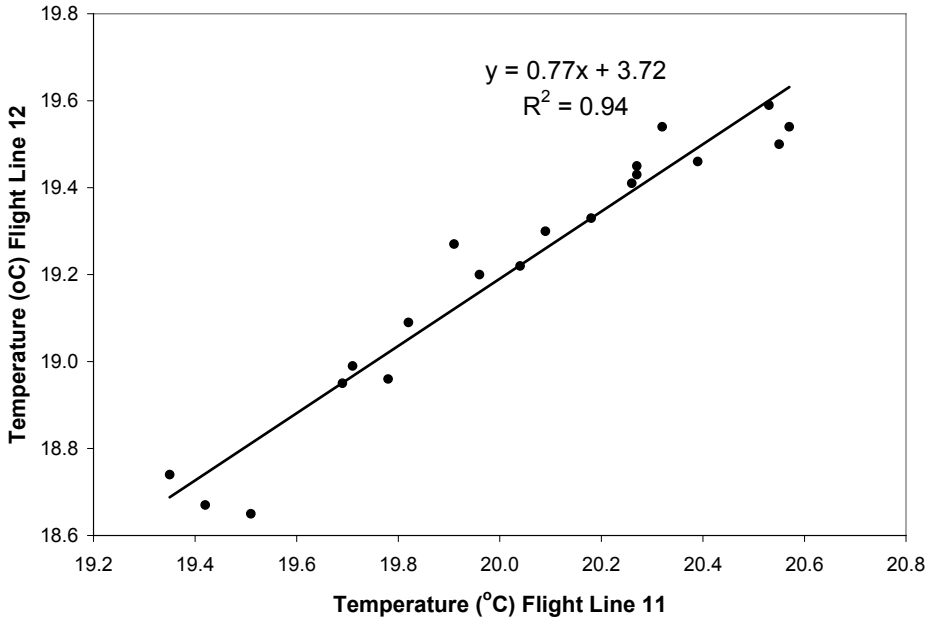

Figure B3. Correlation between water temperatures in overlapping areas between two adjacent flight lines. The linear equation was used to calibrate temperatures in one flight line image to another, thus removing slight changes in Merlin's sensitivity that occurred between the two adjacent flight line images. In this example, flight line image 11 is calibrated to flight line image 12.

In several of the longer flight lines that were flown near the shoreline there was obvious sensor drift within the flight line images. The sensor drift within a flight line

image was most apparent between two stretches of mainly water that were separated by a stretch of land several hundred meters long. Thus, it appears that the sensitivity of the Merlin changed when it was only viewing land (and no water) for several hundred meters between two sections of mainly viewing water. Therefore, many of the longer flight line images were split into small sections that were then calibrated separately.

Atmospheric and skin-layer corrections

Atmospheric scattering, emission, and attenuation of radiance between ocean's surface and airborne sensor can also cause temperature errors in the TIR imagery (Pieters and Englert 1993). For our surveys, radiance emitted from the ocean's surface was likely absorbed by water vapor and aerosols from human and volcanic activity on the island. As a result, radiance reaching the airborne sensor is reduced, leading to calculated temperatures being too low. Additionally, the TIR sensor measures the radiance emitted from the upper 1mm ("skin") of the ocean's surface, which can be up to 0.3^{o}C cooler that the "bulk" temperature immediately beneath the skin (Schluessel et al. 1990). Both atmospheric interferences and skin layer effects can, however, be corrected to *in-situ* temperature measurements made during the survey (Cracknell and Hayes 1991). We thus recalibrated our TIR images to 12 thermistors (Onset HOBO® pendant, accurate to 0.5^{o}C) stationed throughout survey area and to direct ground-truthing temperature measurements in Kailua Bay and Honokohau Harbor. Figure B4 is an example of a linear correlation between temperatures determined by the Merlin camera and ground-truthing measurements in Kailua Bay used to calibrate one of the images is Kailua Bay. Confident absolute temperature corrections were made to the imagery of Honokohau Harbor and in

Kailua Bay where we had the highest concentration of ground-truthing measurements. Ground-truthing temperature corrections to the other flight lines was done in the same manner as removing sensor drift; temperatures in each coastline segment set of images were correlated to temperatures in the imagery of the adjacent coastline segment image set where overlaps occurred.

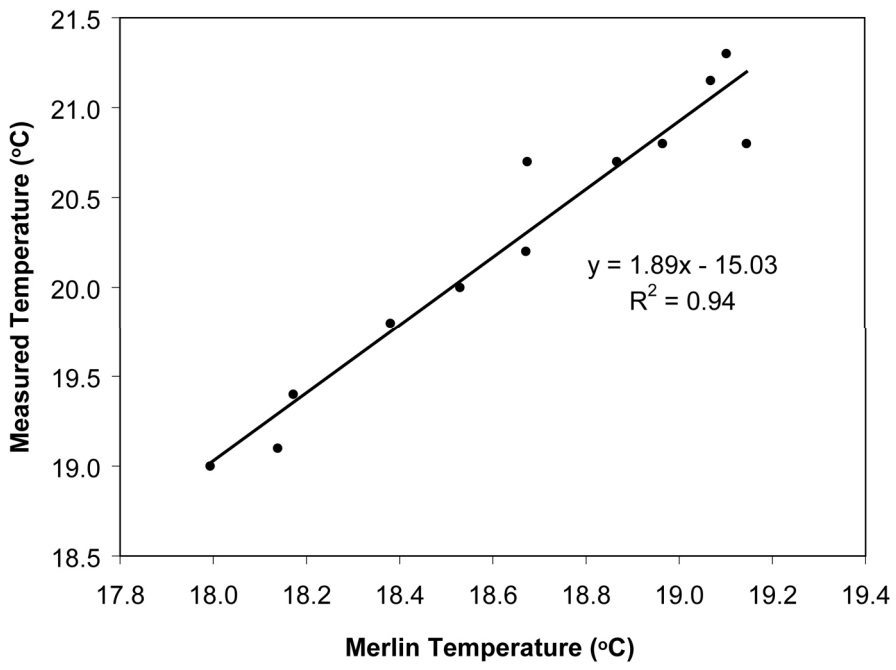

Figure B4. Correlation between surface water temperatures determined by the airborne Merlin camera (x-axis) and ground-truthing measurements (y-axis). The linear equation was used to recalibrate temperatures in the thermal infrared imagery to remove atmospheric interferences.

Other sources of temperature error

Sunglint and edge effects

Some of the images contain noticeable brightness artifacts along their edges. These artifacts are caused by longer atmospheric path lengths at the image ends and

consequently, increased amounts of atmospheric interferences (Brown et al. 2005). Other erroneously bright areas in the imagery may have been caused by sunglint, which is the reflection of sunlight off ocean surface into the view of the sensor. While both of these artifacts occur in the imagery, their overall effect on the data quality is minimal.

Heating artifacts and reduced water temperature contrast

The flight line images collected after ~0900h exhibit comparably less contrast in surface water temperature than images collected to further north. The dampened contrast was most obvious in parts of the images where sections of water were adjacent to land. My hypothesis is that later in the morning when the land became considerably warmer than the ocean, the spectrometer was saturated by the land's thermal radiance, and consequently, the sensor's ability to resolve differences in water temperatures was considerably dampened. On the other hand, earlier in the morning when the land-ocean thermal contrast was minimal, the sensor was able to resolve temperatures differences as expected. Figure B5 llustrates the erroneous warming artifacts in the water for flight lines that were flown later in the morning. While these warming artifacts could be due to surface heating of the water itself, the coincident alignment of these warm water areas with sections of land in imagery and apparent abrupt cooling of water in parts of the image with no land, seems to refute this possibility. Moreover, sections of flight line images that were flown furthest from the shoreline and contain no land image, display more contrast than adjacent flight lines images further inland with sections of warm land.

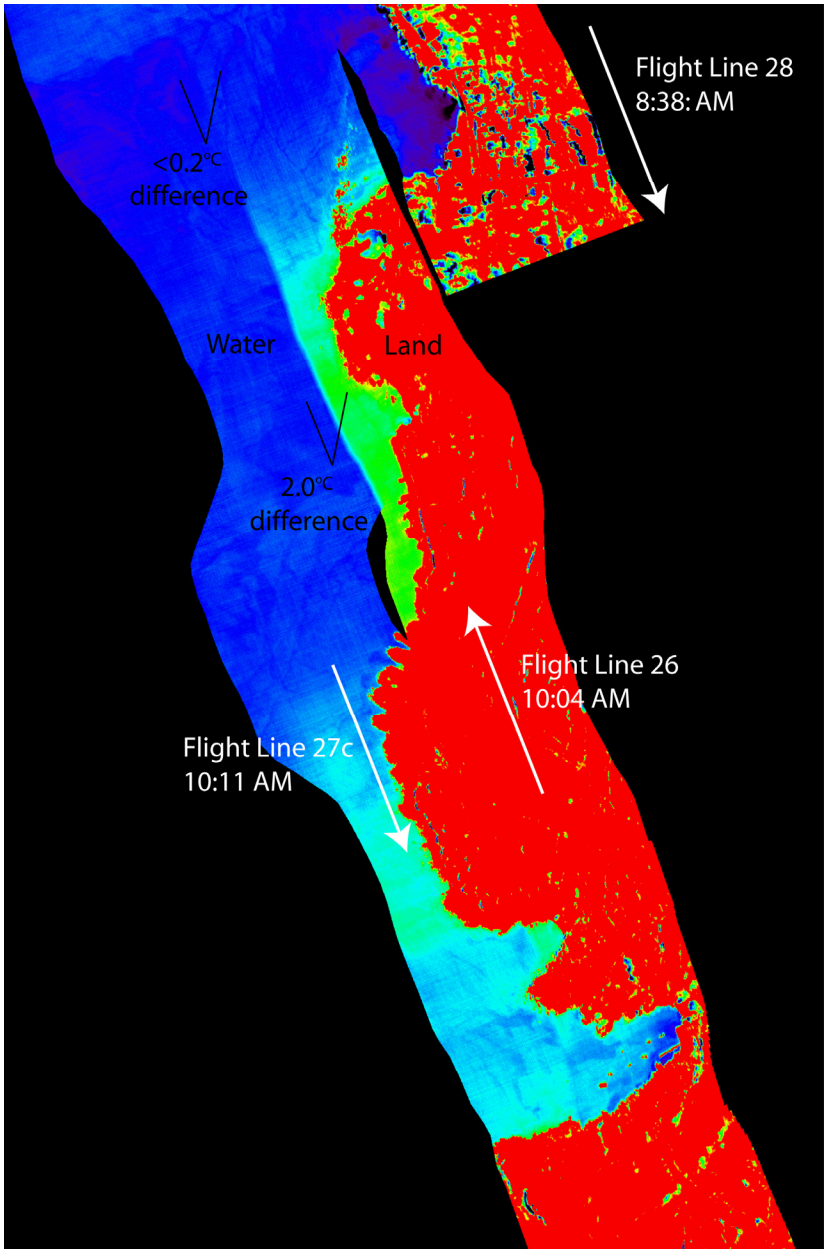

Figure B5. Erroneous warm surface water areas with limited temperature contrast in sections of the flight line images adjacent to the coastline. Notice the 2.0°C temperature difference between lines 26 and 27c where near land, whereas the temperature difference between these two lines is less than 0.2°C where there is no land in either image.

Unfortunately, all flight line images south of Kailua Bay were collected after 0900h (flight lines 28-40) and exhibit these warming artifacts along the coastline with

very little temperature contrast in the water. While some of these images still show weak cold groundwater seeps at the shoreline, the validity of the data is questionable, and therefore they were not used in the our up-scaling flux estimates. Also, all the 10,000 ft elevation flight lines (41-46), which were flown after 0945h, show very little contrast in surface water temperatures.

This problem is exemplified by Kealakekua Bay, where in the August 2005 TIR survey, there were brilliant cold, groundwater discharge plumes debouching from the shoreline into the bay. In the 2007 TIR survey imagery of the bay, there are only very minor cold patches at the discharge sites, but no overall temperature contrast in the imagery. For comparison, the bay was surveyed between 0610-0751h, (0-2 hours after sunrise) in 2005, and between 0930-0922h (3.5 hours after sunrise) in 2007. While the drastic difference could potentially be due to decreased amounts of groundwater discharge into the bay, it seems more likely that the airborne sensor was saturated by the thermally warmer land surrounding the bay, and was not able to resolve to cold surface water plumes in the bay. Qualitative TIR imagery of Kealakekua Bay collected by George Wilkins in the early 1990's shows nearly identical coldwater plumes to those in our August 2005 survey image. This implies a consistent source of groundwater flow into the bay. It should also be noted that an M 6.7 earthquake occurred offshore of Kiholo Bay in October 2006. According to accounts of local residents in the Kealakekua Bay area, tremors from the earthquake were strong enough to dislodge numerous boulder-size rocks from the cliff bordering the bay. Therefore it may be possible that groundwater conduits and flow were altered in the area after the earthquake.

APPENDIX C

Mass Balance Model to Quantify SGD

We use a modified version of a LOICZ-style box model approach (Gordon et al., 1996) to derive SGD rates from the point-source discharge plumes. This model was originally presented by Peterson et al. (2007), but our current version contains some slight modifications from that original form.

The non-steady-state mass balance box model employed here (Figure C1) uses the relatively high radon, low salinity nature of discharging groundwater, and the relatively low radon, high salinity characteristics of open ocean water to determine the flux of groundwater/seawater into and out of a specified control volume, which in our case, is described as a 'plume.' Water inputs to the plume are considered from open ocean intrusion (Q_{IN}) and SGD (Q_{SGD}). These fluxes are balanced by plume water loss to the open ocean (Q_{OUT}). By convention, we consider fluxes directed offshore from the plume to be positive (Q_{SGD} and Q_{OUT}), whereas landward fluxes are negative (Q_{IN}). We ignore any meteorological water fluxes that should be negligible compared to the other fluxes over these short time scales (hours to days). Constant values are assigned to the radon and salinity end-members for groundwater (Rn_{SGD} and S_{SGD}, respectively) and for the open ocean (Rn_O and S_O, respectively). Continuously monitoring the coastal plume radon (Rn_C) and salt (S_C) concentrations allows us to examine how the groundwater flux changes over time. Reference to the measured radon activity here implies "excess" radon, meaning the total radon activity minus that activity supported by its parent, ^{226}Ra. Water densities (ρ_{SGD}, ρ_O, and ρ_C) are included to convert salinity to absolute salt mass.

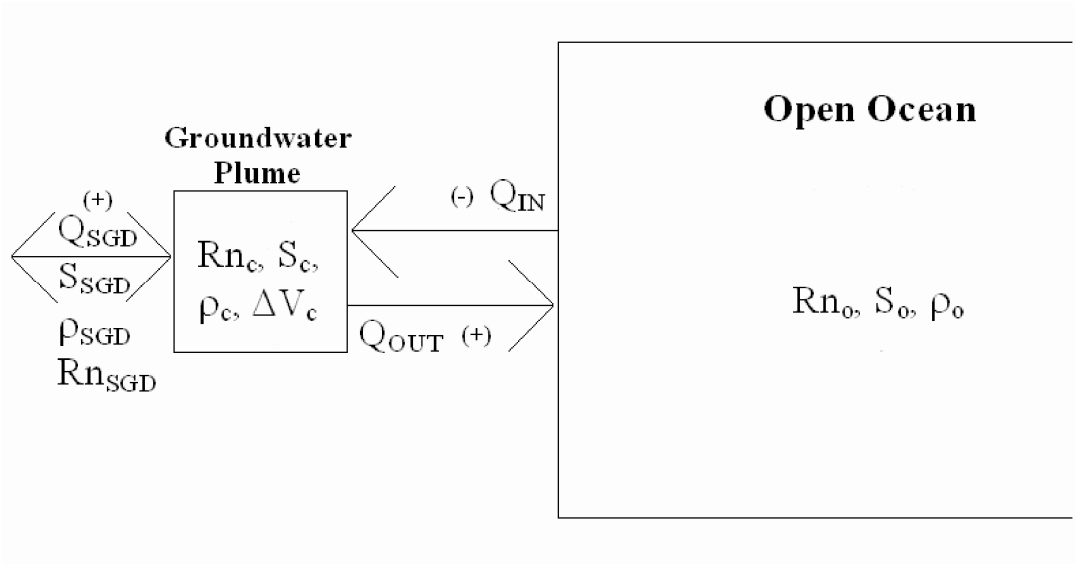

Figure C1. Diagram of model variables and their interactions used to simulate the changing water fluxes into and out of the control volume, defined here as the 'groundwater plume.'

Other parameters required by the model include the length, width, and depth of the groundwater plume. We take the length term (l) to be the distance between the SGD source location at the shoreline and the site where the radon and salinity are continuously monitored. For Honokohau Harbor, the plume described in this paper, this distance is 10 m. The width (w) is taken as the length of shoreline where the discharge is thought to occur. At Honokohau Harbor, we estimate, based on field observations, that the effected shoreline length is 375 m, covering the back section of the harbor. Our measured water depths throughout the course of the time-series measurement are taken as the vertical dimension. We thus estimate the plume volume as V=lwd.

The model is developed using simultaneous mass balance equations for water, salt, and radon. We first parameterize the model using average values over an entire tidal cycle (24-hours in this case) using the following equations for water balance:

$$\frac{\Delta V_C}{\Delta t} = Q_{OUT} - Q_{IN} - Q_{SGD}$$

(1)

for salt balance:

$$\frac{lw\left(S_{C(t+1)}\rho_{C(t+1)}d_{C(t+1)} - S_{C(t)}\rho_{C(t)}d_{C(t)}\right)}{\Delta t} = S_C\rho_C Q_{OUT} - S_O\rho_O Q_{IN} - S_{SGD}\rho_{SGD}Q_{SGD}$$

(2)

and for radon balance:

$$\frac{lw\left(Rn_{C(t+1)}d_{C(t+1)} - Rn_{C(t)}d_{C(t)}\right)}{\Delta t} = Rn_C Q_{OUT} - Rn_O Q_{IN} - Rn_{SGD}Q_{SGD}$$

(3)

Terms marked with subscripts (t) and (t+1) refer to consecutive measurements made throughout the time-series deployment. For the parameterization, the left sides of the equations represent the average hourly change in volume, salt mass ($\Delta S_C/\Delta t$), and radon activity ($\Delta Rn_C/\Delta t$) throughout a complete tidal cycle. The model used previously by Peterson et al. (2007) assumed steady-state conditions over the course of a tidal cycle (therefore, $\Delta V/\Delta t$, $\Delta S_C/\Delta t$, and $\Delta Rn_C/\Delta t$ were assumed to be 0), but parameterizing according to this current approach eliminates any error associated with that assumption. The right sides of the equations represent the cumulative effects of the average coastal groundwater plume fluxing offshore, the offshore water flowing into the harbor, and the

groundwater fluxing into the harbor. Solving these equations for Q_{OUT}, Q_{IN}, and Q_{SGD} establishes average water flux values over the tidal cycle.

We next examine the dynamics of these flows by using smaller time increments (as in Q + ΔQ). A few processes inherently require an inverse relationship between tracer end-member concentration and the corresponding water flux to achieve the expected response. For these processes, we expect the water flux to decrease if the end-member tracer concentration increases, so we use (Q – ΔQ). Radon input via SGD and salt input from the open ocean follow this convention. All other fluxes are represented as (Q + ΔQ).

The resulting equations are used for time-series modeling for water balance:

$$\frac{\Delta V_C}{\Delta t} = \left(Q_{OUT} + \Delta Q_{OUT}\right) - \left(Q_{IN} + \Delta Q_{IN}\right) - \left(Q_{SGD} + \Delta Q_{SGD}\right)$$

(4)

for salt balance:

$$\frac{lw\left(S_{C(t+1)}\rho_{C(t+1)}d_{C(t+1)} - S_{C(t)}\rho_{C(t)}d_{C(t)}\right)}{\Delta t} = S_C\rho_C\left(Q_{OUT} + \Delta Q_{OUT}\right) - S_O\rho_O\left(Q_{IN} - \Delta Q_{IN}\right) - S_{SGD}\rho_{SGD}\left(Q_{SGD} + \Delta Q_{SGD}\right)$$

(5)

and for radon balance:

$$\frac{lw\left(Rn_{C(t+1)}d_{C(t+1)} - Rn_{C(t)}d_{C(t)}\right)}{\Delta t} = Rn_C\left(Q_{OUT} + \Delta Q_{OUT}\right) - Rn_O\left(Q_{IN} + \Delta Q_{IN}\right) - Rn_{SGD}\left(Q_{SGD} - \Delta Q_{SGD}\right)$$

(6)

Atmospheric evasion losses of radon as well as decay losses, while minimal (often < 1% of radon inventory for the time steps used here), were accounted for by including these

loss terms into equation (6). Solving these equations for ΔQ_{OUT}, ΔQ_{IN}, and ΔQ_{SGD} allows for the calculation of the variation of the water fluxes from their average value found during the parameterization step, and ultimately for the total water flux over the entire measurement interval.

We used open ocean values for radon and salinity, 64.3 dpm/m^3 and 35.7, respectively, as constants in the model. We sampled a series of wells around the harbor location to determine the groundwater end-member values for radon and salinity. We used the average measured radon concentration and salinity from these 6 wells as the groundwater end-member values (radon = 25,500 ± 5500 dpm/m^3; salinity = 15.2 ± 6.5). Since no coastal wells containing completely freshwater were available, we determined the appropriate freshwater end-member for radon (39,100 dpm/m^3) based on extrapolating a correlation plot of radon versus salinity as measured during our time-series ($r = 0.65$; $n = 92$; $p < 0.01$) to a salinity of 0.

Our results indicate that the groundwater discharges peak at the low tides, indicating that the hydraulic gradient affected by the changing ocean level drastically influences the groundwater fluxes. The average total positive discharge is estimated to be 11,600 m^3/day in Honokohau Harbor with a freshwater component discharge of 8,600 m^3/day.

APPENDIX D

Anthropogenic phosphate in Honokohau Harbor

Despite its open connection with the ocean, dissolved phosphate concentrations in Honokohau Harbor surface waters were persistently elevated (measured 8/05, 2/06, 4/07) relative to our regional mixing line regressions (Figure 3d), attaining concentrations as high as 6.8 μM. We demonstrate here that these elevated values are largely a result of phosphate additions to local groundwaters as a component of treated wastewater effluent from the Kealakehe Wastewater Treatment Plant (6.8×10^6 m^3 d^{-1}; Hawaii Department of Health Waste Water Branch) that is injected via gravity draining into the subsurface at ~1.2 km ESE inland from the back of the harbor. Our measured phosphate concentrations at the injection point averaged 180 μM. We also measured nutrient concentrations from water samples from eight brackish wells located between the injection point and the back of the harbor, all of which were found to exhibit phosphate concentrations similar to or intermediate between the injection site and the harbor's surface water, ranging from 5.3 and 21.3 μM, with concentrations generally higher in wells closest to the injection point and progressively decreasing toward the harbor (Fig. D1). Phosphate concentrations in these wells were all elevated compared to brackish wells elsewhere in the region, which average 4.3 ± 0.8 μM (n =20).

We further compared our measured phosphate concentrations in Honokohau Harbor surface waters to previous measurements of Bienfang (1980; 1983), made prior to the construction of the Kealakekhe WWTP in 1993. Due to potential errors in making comparisons based on sample position in the harbor, we compared the samples based on

their salinity (Fig. D2). From this comparison, it is clear that phosphate concentrations within harbor surface waters have more than doubled since 1980. Based on these comparisons, the high amounts of phosphate in the treated effluent and in wells down-gradient from the injection point, we conclude that the relatively high phosphate concentrations in Honokohau Harbor are anthropogenic.

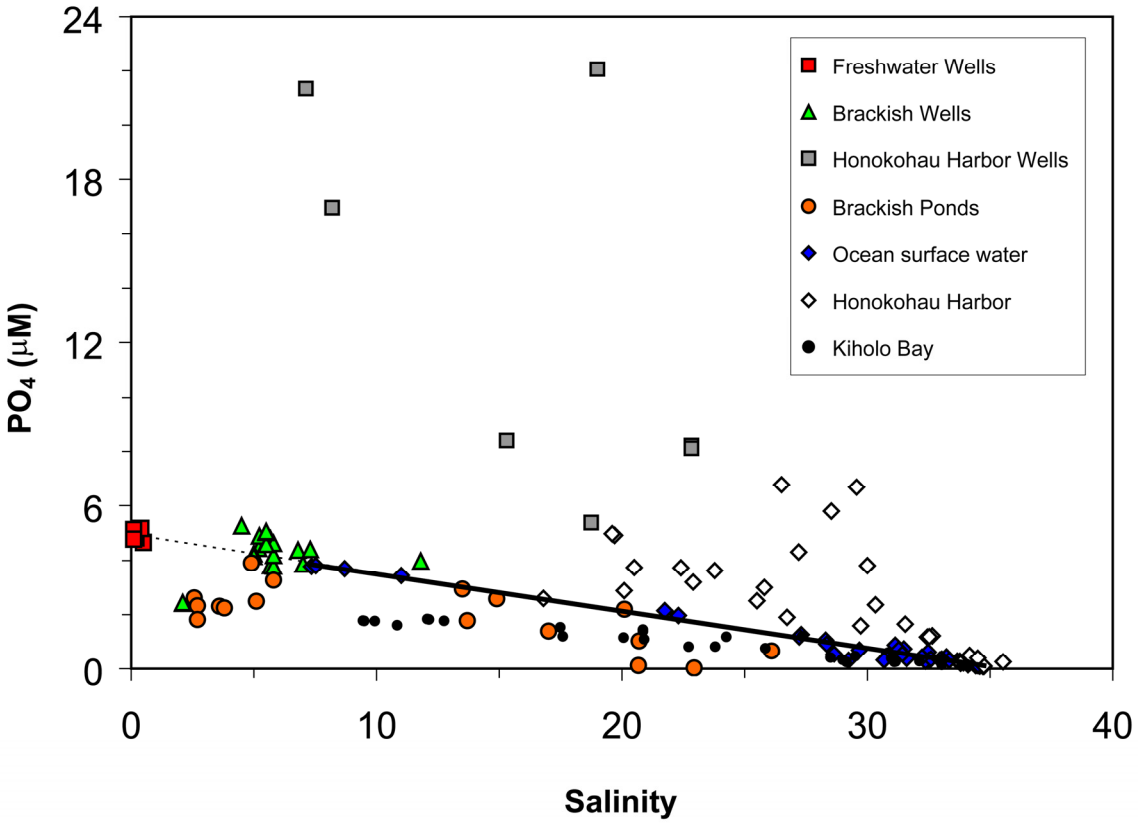

Figure D1. Dissolved phosphate concentrations for all samples collected in west Hawaii region (cf. Fig. 8 in chapter 1). Gray squares are samples collected from brackish wells between Honokohau Harbor and the WWTP disposal pit in August 2006. Dotted line represents conservative mixing line between freshwater wells and offshore ocean surface samples. Solid line is correlation line for ocean surface water samples.

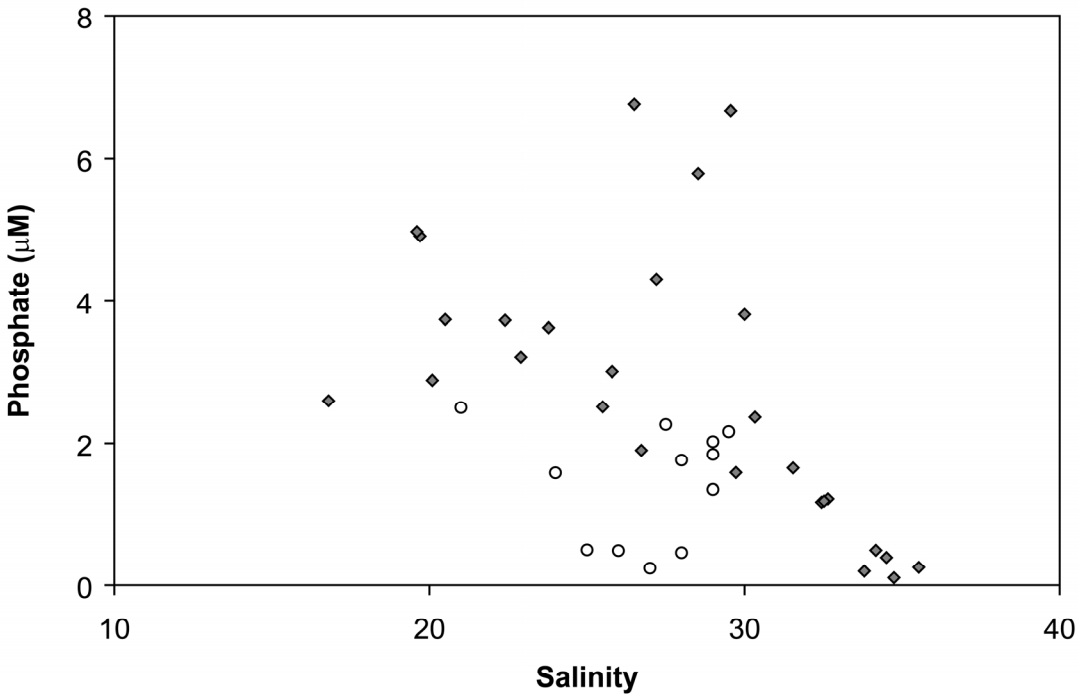

Figure D2. Comparison of phosphate concentrations in Honokohau Harbor surface waters before and after the continuous injection of treated wastewater effluent inland from the harbor, which began in 1993. Open circles represent measurements made prior to injection (Bienfang, 1980; 1983). Closed diamonds represent measurements in August 2005, February 2006, and April 2007 (this study).

APPENDIX E.

Nutrient Sample Tables

Table E1. Freshwater Well samples

DATE	WELL	LAT.	LONG.	TEMP. (^oC)	SAL.	TP	TN	CONCENTRATION (μM) PO_4^{3-}	$Si(OH)_4$	NO_3^-	NO_2^-	NH_4^-
2/13/06	Kahaluu D	19.58144	-155.94924	21.0	0.4	6.67	141.37	4.94	791.23	67.95	0.02	0.06
2/13/06	Kahaluu B	19.58174	-155.94980	20.8	0.5	6.32	147.58	4.66	791.45	66.91	0.02	0.06
2/13/06	Kahaluu C	19.58270	-155.94953	21.9	0.2	6.20	140.76	4.82	787.86	66.80	0.02	0.06
2/13/06	Kahaluu A	19.58296	-155.94980	21.0	0.4	9.41	119.78	5.17	856.47	86.03	0.03	0.00
2/13/06	Halekii	19.51811	-155.91624	21.8	0.1	10.19	117.63	5.09	721.37	75.30	0.02	0.00
2/13/06	Keei D	19.46200	-155.88031	19.8	0.1	10.03	94.64	5.13	667.27	53.18	0.02	0.01
2/14/06	Honokonau	19.68234	-155.96442	21.8	0.1	11.29	129.56	4.78	804.65	88.00	0.01	0.00
2/14/06	Hualalai Well	19.70416	-155.97397	21.1	0.1	11.70	121.15	4.78	719.64	76.08	0.01	0.00

Table E2. Brackish Well samples

DATE	AREA	LAT.	LONG.	TEMP. (^oC)	SAL.	TP	TN	CONCENTRATION (μM) PO_4^{3-}	$Si(OH)_4$	NO_3^-	NO_2^-	NH_4^-
8/14/05	Kahauloa Bay	19.46979	-155.92111	20.4	5.2	6.51	287.04	4.44	728.87	195.60	0.04	0.01
8/16/05	Kealakaua Bay	19.48277	-155.93353	22.1	5.7	5.67	133.61	3.81	736.40	93.12	0.15	1.79
8/16/05	Kahauloa Bay	19.46979	-155.92111	-	5.5	8.46	273.10	4.67	715.95	195.01	0.04	1.68
8/17/05	Kahauloa Bay	19.46979	-155.92111	-	5.7	8.02	278.94	4.79	718.30	203.49	0.03	0.26
8/17/05	Kealakaua Bay	19.48277	-155.93353	-	5.8	8.00	124.42	3.79	736.15	90.18	0.09	1.67
8/18/05	KAHO Park	19.68722	-156.02917	22.3	6.8	6.57	117.66	4.38	648.98	92.77	0.02	0.06
8/18/05	KAHO Park	19.68586	-156.02350	21.7	5.2	7.14	144.12	4.89	618.68	116.67	0.02	0.02
2/11/06	Kahauloa Bay	19.46974	-155.92111	20.6	5.8	6.40	227.97	4.19	718.65	170.49	0.06	0.13
2/14/06	KAHO Park	19.68722	-156.02917	20.9	7.3	7.43	118.32	4.40	761.10	86.43	0.06	0.00
2/14/06	KAHO Park	19.67843	-156.02217	21.5	11.8	7.09	108.45	3.98	686.03	70.19	0.10	0.00
2/14/06	KAHO Park	19.68586	-156.02350	23.8	5.8	10.66	131.72	4.63	735.87	98.35	0.06	3.36
10/25/06	Honaunau	19.41797	-155.91037	23.2	7.0	null	null	3.87	857.57	90.78	0.11	7.45
10/25/06	Manini Beach	19.47070	-155.92075	21.4	5.0	null	null	4.25	777.59	159.92	0.08	1.69
10/25/06	Manini Beach	19.47070	-155.92075	21.4	5.0	null	null	4.15	741.63	152.14	0.15	1.97
10/25/06	Kahauloa Bay	19.46979	-155.92111	21.4	5.5	null	null	4.59	799.74	170.60	0.11	4.09
10/25/06	Manini Beach	19.47110	-155.92079	21.5	5.5	null	null	5.02	761.84	163.05	0.11	7.22
10/26/06	Keahou	19.56081	155.96198	21.8	4.5	null	null	5.26	862.11	196.75	0.26	7.50
10/25/06	Manini Beach	19.47110	-155.92079	21.5	5.5	null	null	5.06	776.45	163.70	0.19	5.84
5/18/07	Kiholo	19.85399	-155.92313	22.9	2.1	3.05	70.39	2.41	802.31	71.14	0.09	0.00
5/18/07	Kiholo	19.85399	-155.92313	22.9	2.1	2.96	65.75	2.44	805.19	70.59	0.07	0.00

Table E3. WWTP and brackish wells inland from Honokohau Harbor

DATE	WELL	LAT.	LONG.	TEMP. (^oC)	SAL.	TP	TN	CONCENTRATION (μM) PO_4^{3-}	$Si(OH)_4$	NO_3^-	NO_2^-	NH_4^-
10/26/06	WWTP	19.66689	-156.01028	28.3	1.7	null	null	177.84	374.25	51.93	166.95	409.41
4/29/207	WWTP	19.66689	-156.01028	null	1.7	208.48	2585.70	182.84	149.13	208.31	78.76	365.26
5/16/07	HW17	19.66864	-156.02062	19.935	18.75	4.90	97.99	5.38	497.32	54.09	0.16	0.10
5/16/07	HW6	19.66662	-156.02362	20.74	19	22.83	63.80	22.06	455.32	43.32	0.11	0.03
5/16/07	HW9	19.66463	-156.02485	20.31	22.83	8.73	112.77	8.22	411.88	41.59	0.11	0.01
5/16/07	HW9	19.66463	-156.02485	20.31	22.83	8.27	118.13	8.12	413.72	41.57	0.13	0.01
5/16/07	HW14	19.66899	-156.01845	20.65	7.12	25.14	155.93	21.34	871.39	83.29	0.11	0.20
5/16/07	HW15	19.66855	-156.01925	20.88	8.19	18.35	151.61	16.97	866.68	81.55	0.13	0.13
5/16/07	HW16	19.66805	-156.02018	20.54	15.3	9.87	136.71	8.40	758.35	59.24	0.38	0.06

Table E4. Brackish Pond samples

DATE	AREA	LAT.	LONG.	TEMP. (°C)	SAL.	TP	TN	CONCENTRATION (μM) PO_4^{3-}	$Si(OH)_4$	NO_3^-	NO_2^-	NH_4^-
8/18/05	Kaloko Pond	19.68713	-156.03142	31.4	17.0	4.22	46.71	1.39	396.37	18.32	0.23	1.24
8/18/05	Kaloko Pond	19.68747	-156.03178	29.0	20.7	3.18	38.06	0.12	341.71	0.18	0.00	0.20
8/18/05	Kaloko Pond	19.68765	-156.03247	29.7	22.9	2.22	30.64	0.02	294.99	0.05	0.00	0.17
8/18/05	Kaloko Pond	19.68730	-156.03300	29.2	30.9	1.16	15.81	0.49	109.96	2.84	0.16	1.19
8/18/05	Kaloko Pond	19.68710	-156.03317	27.9	32.4	0.67	11.72	0.46	69.08	2.20	0.13	1.13
10/26/06	KAHO Park	19.67130	-155.02634	25.7	20.1	null	null	2.20	369.85	50.13	0.23	1.86
10/26/06	KAHO Park	19.67043	-155.02718	27.9	20.7	null	null	1.03	363.91	2.29	0.15	11.53
10/26/06	KAHO Park	19.67051	-155.02625	24.5	14.9	null	null	2.58	520.08	50.52	0.11	6.06
10/25/06	City of Refuge	19.42081	-155.91159	33.7	13.7	null	null	1.78	585.26	3.15	0.23	2.56
10/25/06	City of Refuge	19.42098	-155.91152	29.7	13.5	null	null	2.94	603.34	9.41	0.38	4.43
10/25/06	City of Refuge	19.40832	-155.90464	21.4	4.9	null	null	3.91	815.81	45.37	0.11	3.47
10/26/06	Kahaluu Beach	19.57833	-155.96746	23.4	5.8	null	null	3.27	771.92	108.34	0.11	1.95
10/26/06	Kahaluu Beach	19.57968	155.96670	23.4	5.1	null	null	2.49	783.99	28.92	1.31	5.54
5/16/07	Kiholo	19.85490	-155.92031	25.9	3.6	null	null	2.31	760.00	64.36	0.14	0.49
5/16/07	Kiholo	19.85490	-155.92031	27.7	26.1	null	null	0.66	221.82	10.93	0.14	0.59
5/17/07	Kiholo	19.85490	-155.92010	23.8	3.8	null	null	2.24	736.88	66.74	0.18	0.33
5/18/07	Kiholo	19.85490	-155.92010	24.3	2.57	null	null	2.62	null	67.55	0.16	0.14
5/20/07	Kiholo	19.85530	19.91975	25.3	2.7	null	null	2.32	767.30	66.54	0.14	0.21
5/20/07	Kiholo	19.85530	19.91975	25.3	2.7	null	null	1.82	747.14	59.80	0.16	0.66

Table E5. Kiholo Bay surface samples

DATE	TIME	LAT.	LONG.	TEMP. (°C)	SAL.	TP	TN	CONCENTRATION (μM) PO_4^{3-}	$Si(OH)_4$	NO_3^-	NO_2^-	NH_4^-
5/17/07	8:05	19.85697	-155.92064	23.9	17.49	null	null	1.53	491.58	40.31	0.07	0.41
5/17/07	8:07	19.86048	-155.92247	24.8	22.72	null	null	0.81	217.45	15.36	0.09	0.24
5/17/07	8:15	19.86042	-155.92241	25.0	27.34	null	null	1.20	358.80	26.85	0.10	0.23
5/17/07	8:30	19.86023	-155.92213	24.8	24.25	null	null	1.18	361.98	27.43	0.10	0.27
5/17/07	8:40	19.85998	-155.92205	25.5	29.50	null	null	0.46	117.57	7.95	0.10	0.18
5/17/07	8:50	19.85978	-155.9219	25.5	29.00	null	null	0.33	106.75	5.66	0.08	0.24
5/17/07	9:00	19.85977	-155.92197	25.3	29.15	null	null	0.25	57.07	3.27	0.06	0.22
5/17/07	9:15	19.85973	-155.92194	25.7	31.11	null	null	0.32	97.46	4.65	0.09	0.30
5/17/07	9:25	19.85961	-155.92172	25.5	30.98	null	null	0.38	104.75	5.85	0.06	0.13
5/17/07	9:30	19.85949	-155.92155	25.6	31.15	null	null	0.26	93.89	5.75	0.06	0.08
5/17/07	10:00	19.85923	-155.92142	25.4	34.06	null	null	0.11	10.19	0.40	0.01	0.06
5/17/07	10:15	19.85908	-155.92122	25.4	33.84	null	null	0.11	10.68	0.42	0.00	0.05
5/17/07	10:40	19.85887	-155.92112	26.0	33.03	null	null	0.14	12.75	0.65	0.01	0.11
5/17/07	10:50	19.85856	-155.92104	25.7	25.84	null	null	0.76	243.83	17.76	0.14	0.16
5/17/07	12:10	19.85841	-155.92083	25.5	20.06	null	null	1.15	414.29	27.87	0.21	0.31
5/17/07	12:21	19.85783	-155.92081	25.9	23.8	null	null	0.82	281.90	18.36	0.17	0.19
5/17/07	12:29	19.85788	-155.92082	26.0	28.5	null	null	0.41	161.88	9.05	0.13	0.43
5/17/07	12:34	19.85787	-155.92083	26.2	31.1	null	null	0.25	81.18	3.77	0.08	0.16
5/17/07	12:40	19.85786	-155.92086	26.1	33	null	null	0.31	76.43	4.48	0.06	0.12
5/17/07	12:52	19.85746	-155.92079	26.2	32.12	null	null	0.28	86.06	4.59	0.08	0.09
5/17/07	13:00	19.85718	-155.92074	26.0	34.06	null	null	0.15	27.68	1.32	0.05	0.04
5/18/07	9:18	19.85688	-155.92063	22.3	9.50	null	null	1.77	619.81	58.74	0.14	0.16
5/18/07	9:24	19.85672	-155.92052	22.9	9.45	null	null	1.78	620.41	62.04	0.15	0.16
5/18/07	9:30	19.85646	-155.92066	22.9	9.93	null	null	1.77	612.91	60.11	0.17	0.19
5/18/07	9:35	19.8561	-155.92097	22.8	10.84	null	null	1.61	590.00	54.95	0.14	0.26
5/18/07	9:41	19.8549	-155.92031	23.2	12.07	null	null	1.84	561.36	49.32	0.18	0.11
5/18/07	10:00	19.8572	-155.92158	23.2	12.14	null	null	1.82	560.67	50.16	0.19	0.14
5/18/07	10:06	19.85723	-155.92152	23.6	12.75	null	null	1.77	557.90	50.23	0.21	0.14
5/18/07	10:13	19.85717	-155.92198	25.4	20.86	null	null	1.39	474.21	39.32	0.21	0.68
5/18/07	10:13	19.85717	-155.92198	25.4	20.86	null	null	1.45	471.72	39.32	0.22	0.15
5/18/07	10:32	19.85718	-155.92255	25.5	17.59	null	null	1.20	426.96	33.38	0.23	0.24
5/18/07	11:00	19.85723	-155.9233	25.7	20.90	null	null	1.10	359.54	27.58	0.22	0.17

Table E6. Honokohau Harbor surface samples

DATE	TIME	LAT.	LONG.	TEMP. (^oC)	SAL.	TP	TN	CONCENTRATION (µM) PO_4^{3-}	$Si(OH)_4$	NO_3^-	NO_2^-	NH_4^-
8/17/05	8:58	19.66882	-156.02120	23.2	26.7	2.20	28.55	1.90	220.17	27.88	0.03	0.65
8/17/05	9:22	19.66992	-156.02628	25.9	29.7	1.72	23.28	1.59	141.05	19.24	0.48	0.48
8/17/05	9:36	19.66935	-156.02875	27.6	32.6	1.27	8.55	1.22	63.84	8.35	0.13	0.29
8/17/05	9:48	19.66850	-156.03065	27.9	34.2	0.55	9.02	0.49	18.34	2.32	0.07	0.18
8/17/05	10:48	19.66920	-156.03377	27.9	34.7	0.26	5.93	0.10	3.43	0.31	0.03	0.08
8/17/05	11:03	19.66947	-156.02793	27.4	31.5	1.70	15.92	1.65	92.87	12.41	0.13	0.47
8/17/05	15:10	19.66882	-156.02602	27.2	32.4	1.22	8.51	1.17	67.72	8.55	0.08	0.55
8/17/05	15:21	19.66972	-156.02665	27.6	32.5	1.26	12.65	1.19	66.18	8.35	0.08	0.33
2/12/06	15:44	19.66883	-156.02114	20.8	22.4	6.63	58.07	3.73	345.07	39.50	0.04	0.23
2/12/06	15:30	19.66938	-156.02137	18.4	16.8	4.69	59.61	2.60	368.77	42.93	0.03	0.11
2/15/06	11:07	19.66859	-156.02154	19.3	20.5	6.61	84.41	3.74	449.11	44.71	0.07	0.16
2/15/06	11:27	19.66835	-156.03134	24.4	35.5	0.78	9.56	0.25	9.59	0.44	0.09	0.00
2/15/06	12:00	19.66951	-156.02703	23.0	30.3	5.13	63.36	2.36	230.90	22.52	0.12	0.13
2/15/06	12:10	19.66884	-156.02586	23.0	29.6	9.26	75.79	6.68	224.91	38.52	0.17	0.20
2/15/06	12:19	19.66922	-156.02454	22.4	28.5	9.69	75.09	5.80	252.79	39.17	0.11	0.13
2/15/06	12:30	19.66891	-156.02355	22.0	27.2	7.44	68.98	4.31	276.67	40.60	0.18	0.21
2/15/06	1:05	19.66936	-156.02281	21.7	25.5	6.15	76.61	2.51	260.72	31.39	0.12	0.28
2/15/06	1:52	19.66875	-156.02203	20.4	23.8	7.56	81.84	3.63	351.60	45.60	0.10	0.13
2/15/06	2:12	19.66923	-156.02144	19.5	20.1	7.29	81.26	2.88	342.25	45.67	0.10	0.30
10/26/06	14:15	19.66876	-156.02119	18.9	19.7	null	null	4.92	430.09	55.37	0.11	0.71
4/30/07	9:56	19.66876	-156.02119	18.5	19.6	6.53	122.80	4.98	430.83	46.73	0.05	0.10
4/30/07	10:04	19.66911	-156.02200	20.1	22.9	4.62	80.82	3.20	372.47	40.82	0.05	0.07
4/30/07	10:24	19.66927	-156.02335	21.6	25.8	3.93	69.02	3.00	268.65	30.39	0.59	1.29
4/30/07	10:28	19.66918	-156.02451	22.8	26.5	8.16	93.25	6.77	230.95	23.34	0.03	0.05
4/30/07	10:34	19.66910	-156.02627	23.6	30.0	4.33	30.17	3.81	151.09	14.55	0.05	0.03
4/30/07	10:40	19.66838	-156.03133	25.4	34.5	1.12	18.62	0.39	18.53	0.93	0.01	0.02
4/30/07	10:52	19.68571	-156.03434	25.1	33.8	0.99	20.34	0.20	20.63	0.53	0.02	0.02

Table E7. Kailua Bay surface samples

DATE	TIME	LAT.	LONG.	TEMP. (°C)	SAL.	TP	TN	CONCENTRATION (μM) PO_4^{3-}	$Si(OH)_4$	NO_3^-	NO_2^-	NH_4^-
5/19/07	9:02	19.63762	-155.9953	25.1	32.4	null	null	0.31	53.05	6.22	0.12	0.27
5/19/07	9:02	19.63762	-155.9953	25.1	32.4	null	null	0.28	49.36	6.14	0.10	0.34
5/19/07	10:03	19.63873	-155.99581	25.2	32.6	null	null	0.36	59.74	6.66	0.10	0.10
5/19/07	9:17	19.63966	-155.99535	24.6	31.2	null	null	0.50	78.46	10.05	0.13	0.13
5/19/07	9:36	19.6392	-155.99504	24.1	29.7	null	null	0.69	119.05	15.54	0.14	0.04
5/19/07	9:42	19.63859	-155.99445	24.9	32.2	null	null	0.43	70.56	7.28	0.10	0.14
5/19/07	9:52	19.63812	-155.99532	24.3	28.6	null	null	0.55	113.47	15.53	0.13	0.15
5/19/07	10:13	19.63904	-155.99552	24.7	30.9	null	null	0.48	89.73	10.86	0.10	0.66
5/19/07	10:23	19.63943	-155.99586	25.5	33.8	null	null	0.28	32.69	3.73	0.06	0.35
5/19/07	10:15	19.63968	-155.99596	25.6	34.1	null	null	0.24	23.03	2.91	0.05	0.12
5/19/07	10:55	19.63578	-155.99527	25.5	33.0	null	null	0.36	32.06	3.74	0.01	0.50
5/19/07	11:10	19.63473	-155.99575	25.6	33.9	null	null	0.26	16.17	2.27	0.00	0.38
5/19/07	11:30	19.63088	-155.99749	25.6	34.6	null	null	0.24	6.00	0.56	0.00	0.13
5/19/07	12:15	19.63312	-155.99356	25.8	34.6	null	null	0.09	9.61	1.21	0.01	0.23
5/19/07	12:45	19.63612	-155.99712	25.6	34.5	null	null	0.13	12.96	0.88	0.01	0.05
5/19/07	12:51	19.63707	-155.99668	25.6	33.9	null	null	0.22	27.21	2.26	0.02	0.07
5/19/07	13:00	19.63821	-155.99696	25.1	33.0	null	null	0.33	55.74	5.58	0.06	0.48
5/19/07	13:15	19.63913	-155.99733	24.5	29.2	null	null	0.32	54.66	5.57	0.08	1.87
5/20/07	9:55	19.63929	-155.99601	24.6	30.7	null	null	0.32	47.31	3.86	0.09	0.75
5/20/07	10:30	19.63913	-155.99768	23.7	27.3	null	null	1.26	202.39	16.91	0.17	0.47
5/20/07	10:45	19.63855	-155.99714	24.8	31.5	null	null	0.73	114.66	7.35	0.14	0.34
5/20/07	10:50	19.63896	-155.99701	24.7	31.3	null	null	0.71	114.61	8.89	0.14	0.38
5/20/07	11:00	19.63905	-155.63905	24.0	31.4	null	null	0.54	76.19	4.28	0.10	0.20
5/20/07	12:00	19.63969	-155.99527	null	28.3	3.42	31.07	0.91	197.31	23.40	0.09	0.12
5/20/07	12:00	19.63969	-155.99527	null	27.2	1.84	19.73	1.18	231.06	28.80	0.09	0.01

Table E8. Kealakekua Bay surface samples

DATE	TIME	LAT.	LONG.	TEMP. (°C)	SAL.	TP	TN	CONCENTRATION (μM) PO_4^{3-}	$Si(OH)_4$	NO_3^-	NO_2^-	NH_4^-
8/16/05	13:12	19.482330	-155.932530	28.4	34.3	0.25	5.47	0.19	12.67	1.12	0.08	0.40
8/16/05	13:30	19.481380	-155.931730	28.4	34.4	0.25	9.05	0.17	9.98	0.88	0.05	0.26
8/16/05	13:48	19.480620	-155.931720	28.4	34.5	0.24	7.56	0.15	7.42	0.58	0.03	0.17
2/11/06	14:30	19.482246	-155.933180	21.0	8.7	5.11	148.88	3.70	699.39	77.01	0.06	0.00
2/11/06	13:30	19.482220	-155.932650	24.7	31.6	0.83	9.84	0.38	48.53	3.27	0.11	0.17
2/11/06	13:37	19.481284	-155.933047	24.9	34.3	0.57	7.41	0.23	14.66	0.38	0.10	0.13
2/11/06	13:45	19.480188	-155.933020	25.3	34.5	0.58	6.95	0.19	10.95	0.35	0.08	0.21
2/11/06	14:00	19.478897	-155.932946	24.5	34.5	0.54	6.58	0.13	5.20	0.06	0.06	0.00
8/16/05	14:25	19.482040	-155.932631	28.4	34.4	0.29	9.02	0.23	13.22	0.83	0.05	0.58
8/16/05	14:33	19.480910	-155.931900	28.4	34.6	0.26	5.49	0.16	7.85	0.31	0.04	0.35
8/16/05	14:41	19.479230	-155.931340	28.5	34.6	0.25	4.07	0.14	6.77	0.08	0.03	0.15
8/16/05	8:27	19.469430	-155.922300	27.8	33.7	0.28	5.42	0.28	29.18	4.92	0.18	0.29
8/16/05	8:54	19.469250	-155.923000	27.9	33.3	0.35	8.38	0.31	38.21	6.96	0.10	0.33
8/16/05	9:05	19.469130	-155.923500	27.9	34.1	0.24	4.77	0.20	17.83	2.94	0.05	0.19
8/7/06	7:30	19.48201	-155.93315	null	7.3	4.40	121.13	3.78	710.43	93.15	0.05	0.00
8/7/06	7:35	19.48202	-155.93312	null	7.5	4.14	115.82	3.81	709.37	92.16	0.04	0.00
8/7/06	7:39	19.48204	-155.93308	null	11.0	4.45	105.62	3.45	628.03	80.67	0.06	0.00
8/7/06	7:43	19.48204	-155.93303	null	21.7	2.94	75.85	2.14	348.70	42.41	0.10	0.02
8/7/06	7:50	19.48205	-155.93297	null	32.5	0.84	14.70	0.62	65.79	6.99	0.06	0.59
8/7/06	7:56	19.48205	-155.93289	null	33.2	0.55	10.12	0.44	43.41	4.10	0.06	0.52
8/7/06	8:02	19.47937	-155.93229	null	34.5	0.39	8.76	0.28	7.65	0.81	0.06	0.23
8/7/06	8:10	19.47944	-155.93157	null	34.5	0.51	8.23	0.25	6.44	0.00	0.03	0.39
8/7/06	8:15	19.47854	-155.93232	null	34.5	0.39	8.68	0.18	6.91	0.00	0.03	0.21
8/7/06	8:21	19.47838	-155.93089	null	34.5	0.36	7.93	0.17	6.92	0.11	0.03	0.21

Table E9. Kealakekua Bay surface samples (Kahauloa Inlet)

DATE	TIME	LAT.	LONG.	TEMP. (^oC)	SAL.	TP	TN	CONCENTRATION (μM) PO_4^{3-}	$Si(OH)_4$	NO_3^-	NO_2^-	NH_4^-
8/16/05	8:27	19.469430	-155.922300	27.8	33.7	0.28	5.42	0.28	29.18	4.92	0.18	0.29
8/16/05	8:54	19.469250	-155.923000	27.9	33.3	0.35	8.38	0.31	38.21	6.96	0.10	0.33
8/16/05	9:05	19.469130	-155.923500	27.9	34.1	0.24	4.77	0.20	17.83	2.94	0.05	0.19
8/16/05	9:17	19.469500	-155.924650	27.9	34.6	0.22	5.86	0.14	6.62	0.53	0.03	0.11
8/16/05	9:52	19.469780	-155.932400	28.1	34.7	0.25	3.89	0.09	4.70	0.03	0.02	0.02
8/16/05	10:21	19.469680	-155.941320	28.2	34.7	0.24	2.39	0.09	4.05	0.04	0.02	0.12
8/16/05	11:00	19.473550	-155.969750	28.6	34.8	0.27	8.12	0.09	3.28	0.03	0.03	0.07
8/16/05	12:00	19.469520	-155.923870	28.3	34.6	0.24	9.70	0.10	6.33	0.29	0.12	0.08
8/16/05	12:16	19.469250	-155.922700	28.5	34.4	0.25	7.28	0.12	9.76	1.07	0.05	0.22
8/16/05	12:27	19.469420	-155.921870	28.4	34.4	0.23	4.08	0.12	9.87	1.05	0.23	0.26
8/16/05	14:58	19.469430	-155.921330	null	34.4	0.32	5.92	0.17	12.10	0.45	0.06	0.51
8/16/05	14:59	19.469330	-155.921560	29.3	34.4	0.32	5.98	0.16	10.80	0.40	0.06	0.52
8/16/05	15:02	19.469420	-155.921840	29.2	34.4	0.27	5.23	0.14	10.79	0.36	0.06	0.56
8/16/05	15:05	19.469380	-155.922260	29.1	34.5	0.26	5.45	0.13	9.92	0.37	0.05	0.45
8/16/05	15:07	19.469220	-155.922790	29.0	34.5	0.27	4.77	0.12	8.85	0.25	0.04	0.16
8/16/05	15:09	19.469110	-155.923380	29.0	34.6	0.29	6.73	0.12	8.20	0.21	0.03	0.13
2/11/06	15:45	19.469046	-155.922390	24.4	34.1	0.58	7.48	0.15	7.35	0.18	0.07	0.09
2/11/06	15:55	19.469287	-155.921223	24.5	32.5	0.77	12.24	0.31	37.90	5.50	0.12	0.40
2/11/06	16:48	19.469443	-155.921418	25.0	31.1	2.16	40.73	0.88	142.61	28.99	0.15	1.07
2/11/06	17:25	19.469328	-155.921257	22.7	22.3	3.79	78.12	1.97	310.91	62.04	0.07	0.21
2/12/06	9:30	19.469367	-155.921620	23.5	28.3	2.14	34.42	1.06	154.92	32.21	0.10	0.34
2/12/06	9:45	19.469354	-155.922676	24.4	34.2	0.83	12.49	0.33	32.30	5.37	0.10	0.17
2/12/06	10:08	19.469358	-155.924014	24.4	34.2	0.69	9.70	0.23	14.56	1.82	0.08	0.11

APPENDIX F.

2007 Aerial TIR Survey Imagery

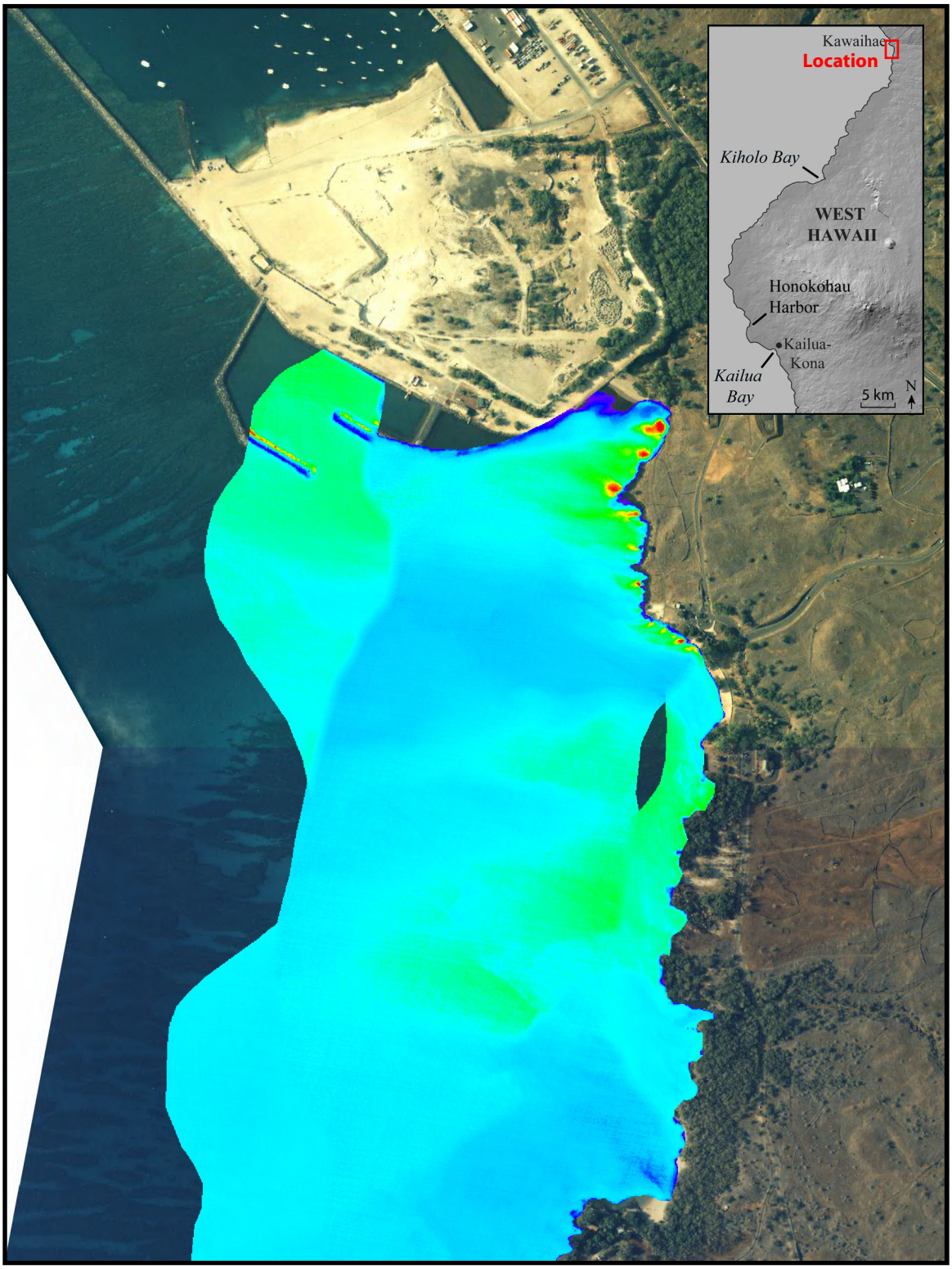

Panel 1.
Kawaihae Bay

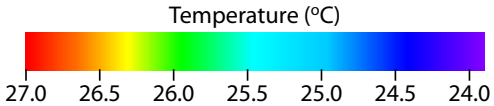

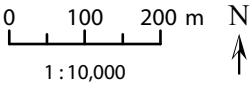

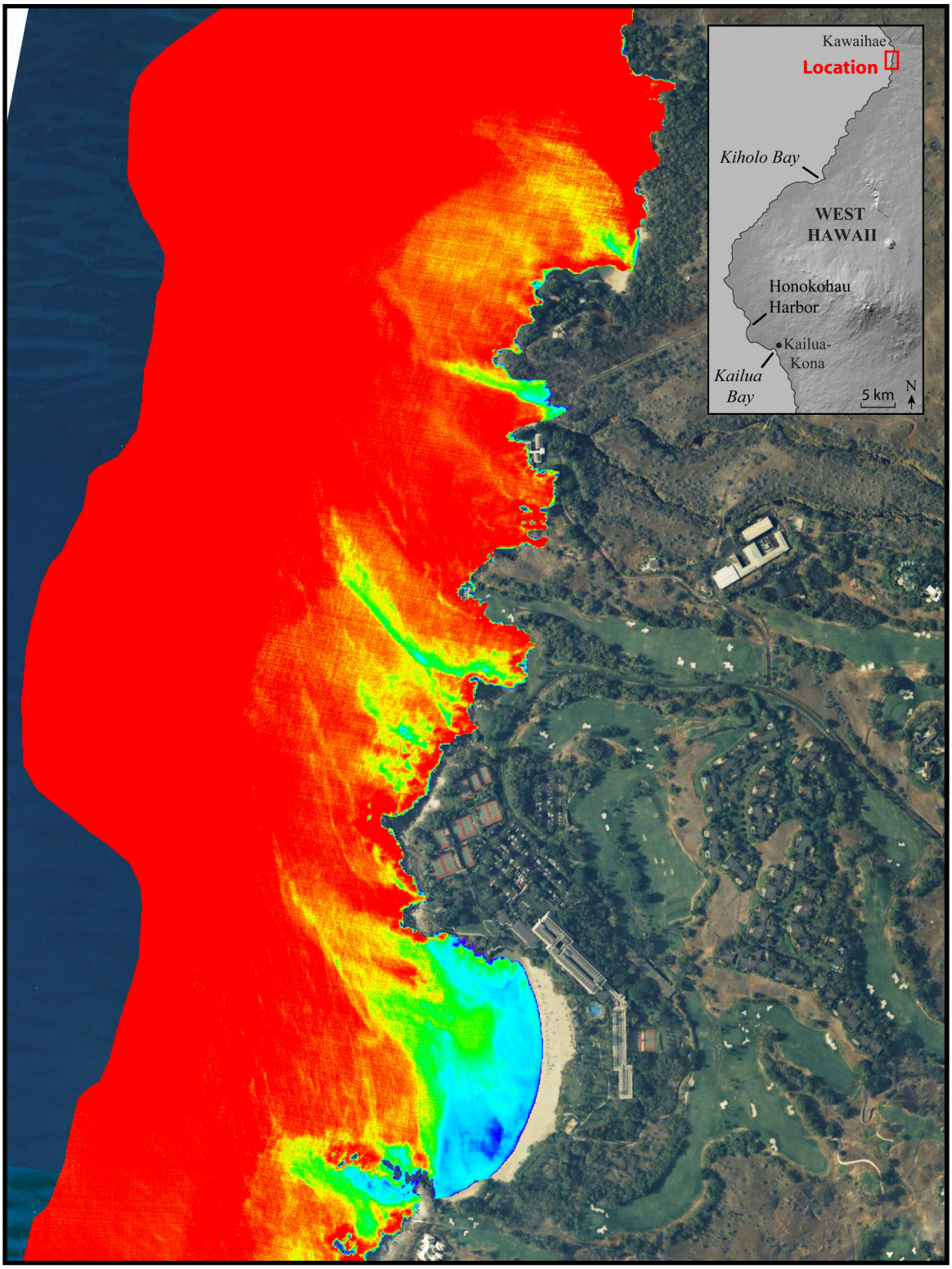

Panel 2.
Mauna Kea Beach

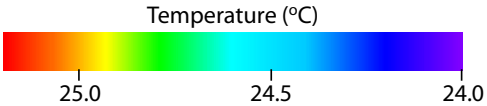

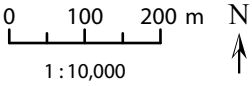

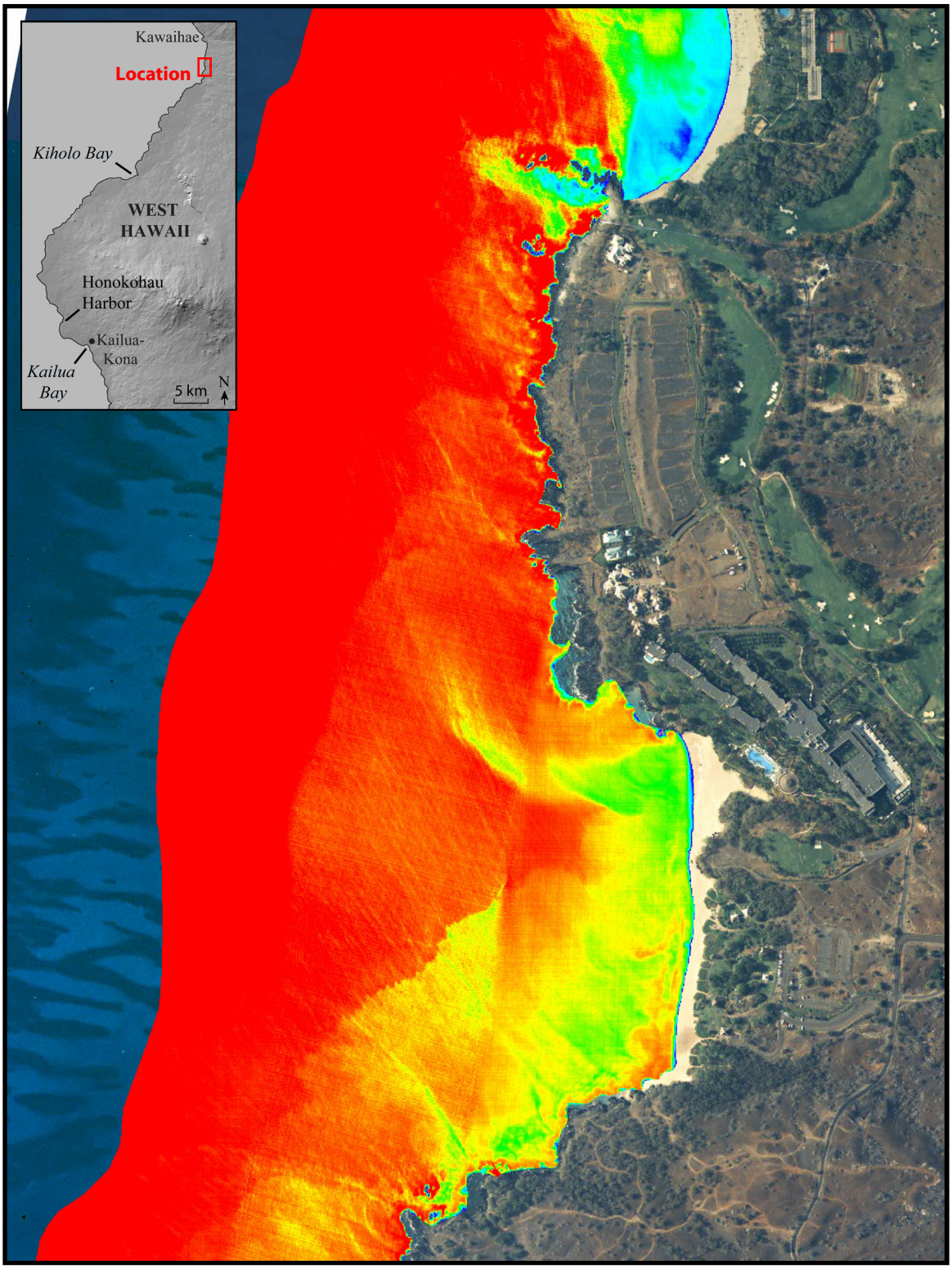

Panel 3.
Hapuna Beach

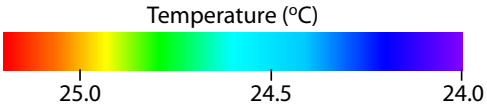

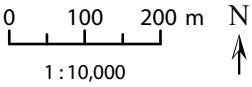

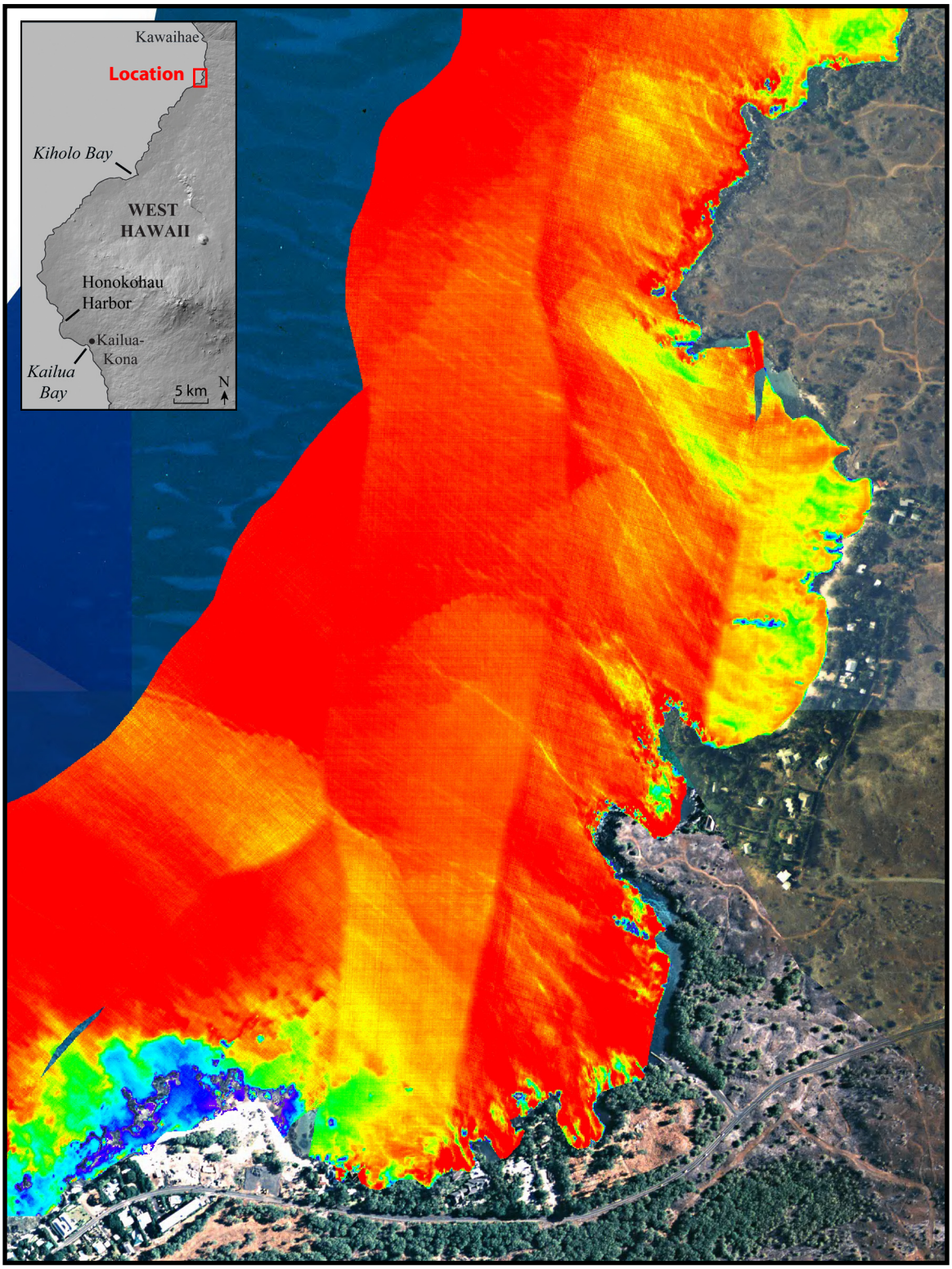

Panel 4.
Puako Bay

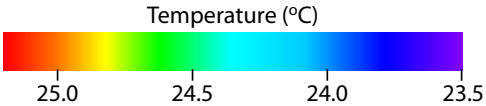

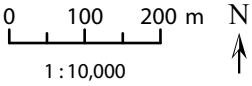

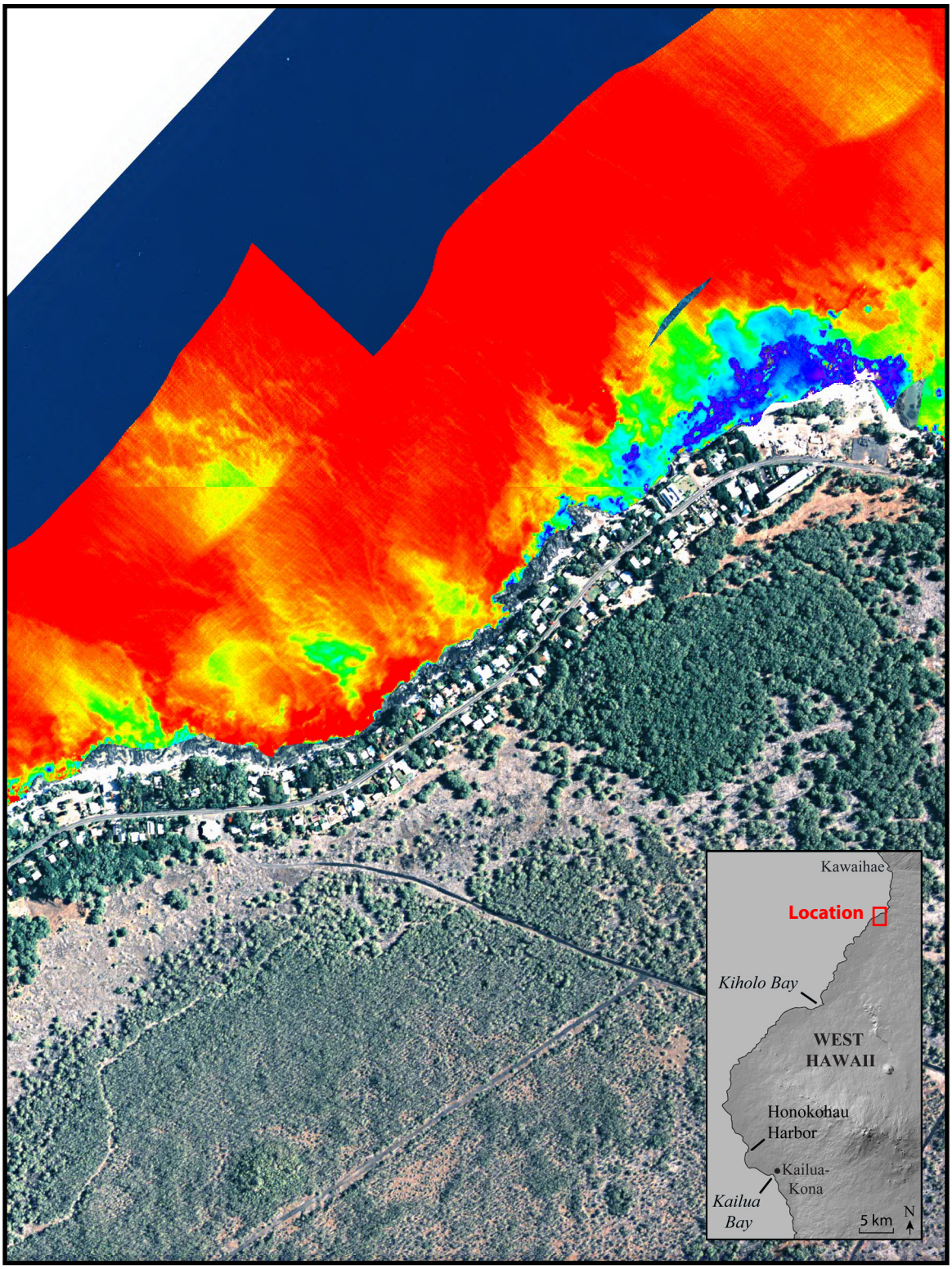

Panel 5.
Puako Pt.

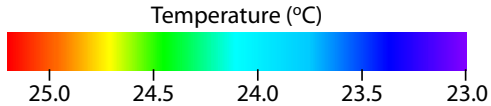

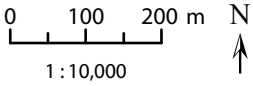

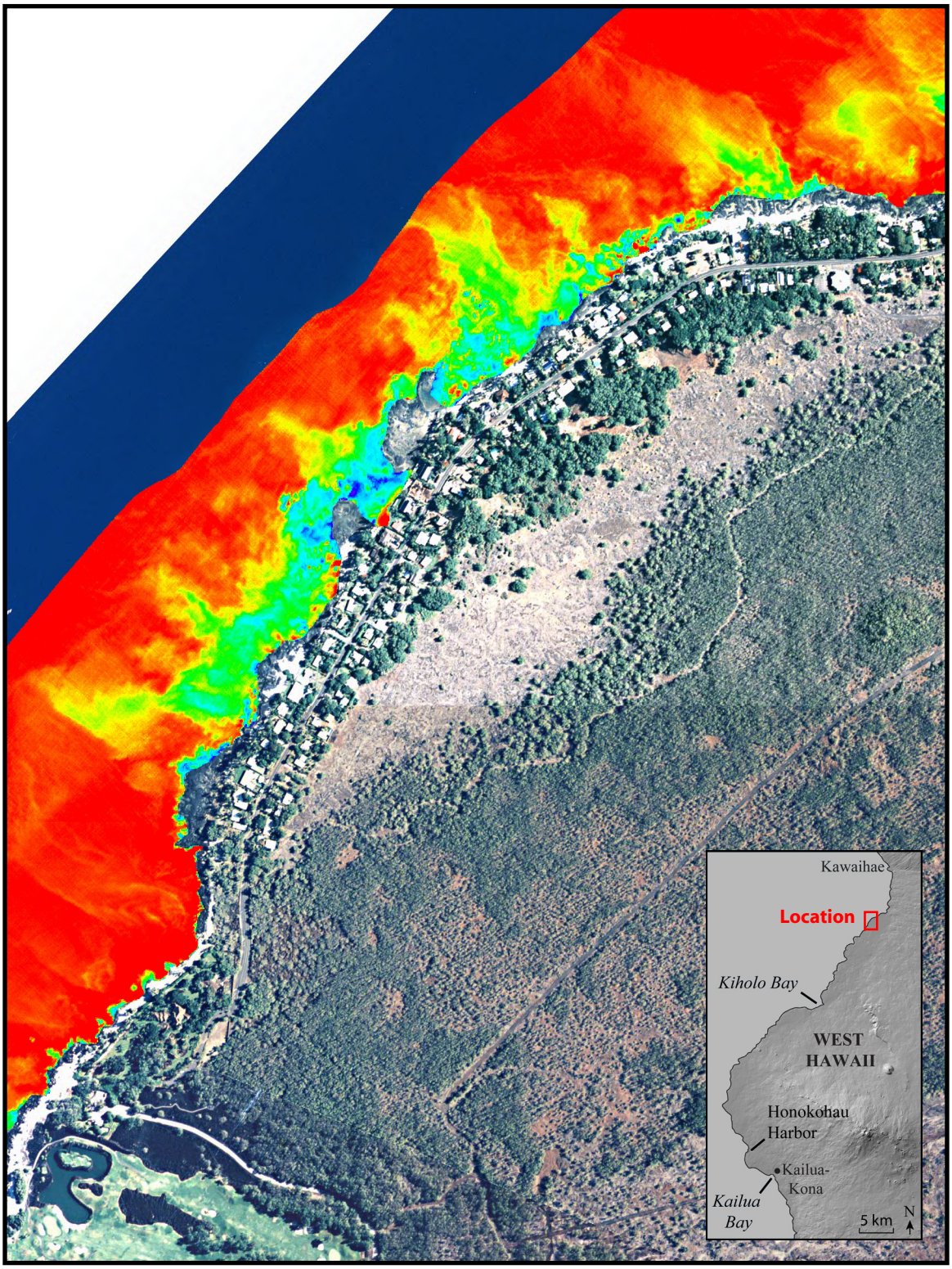

Panel 6.
Waima Pt.

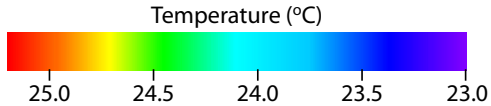

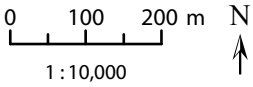

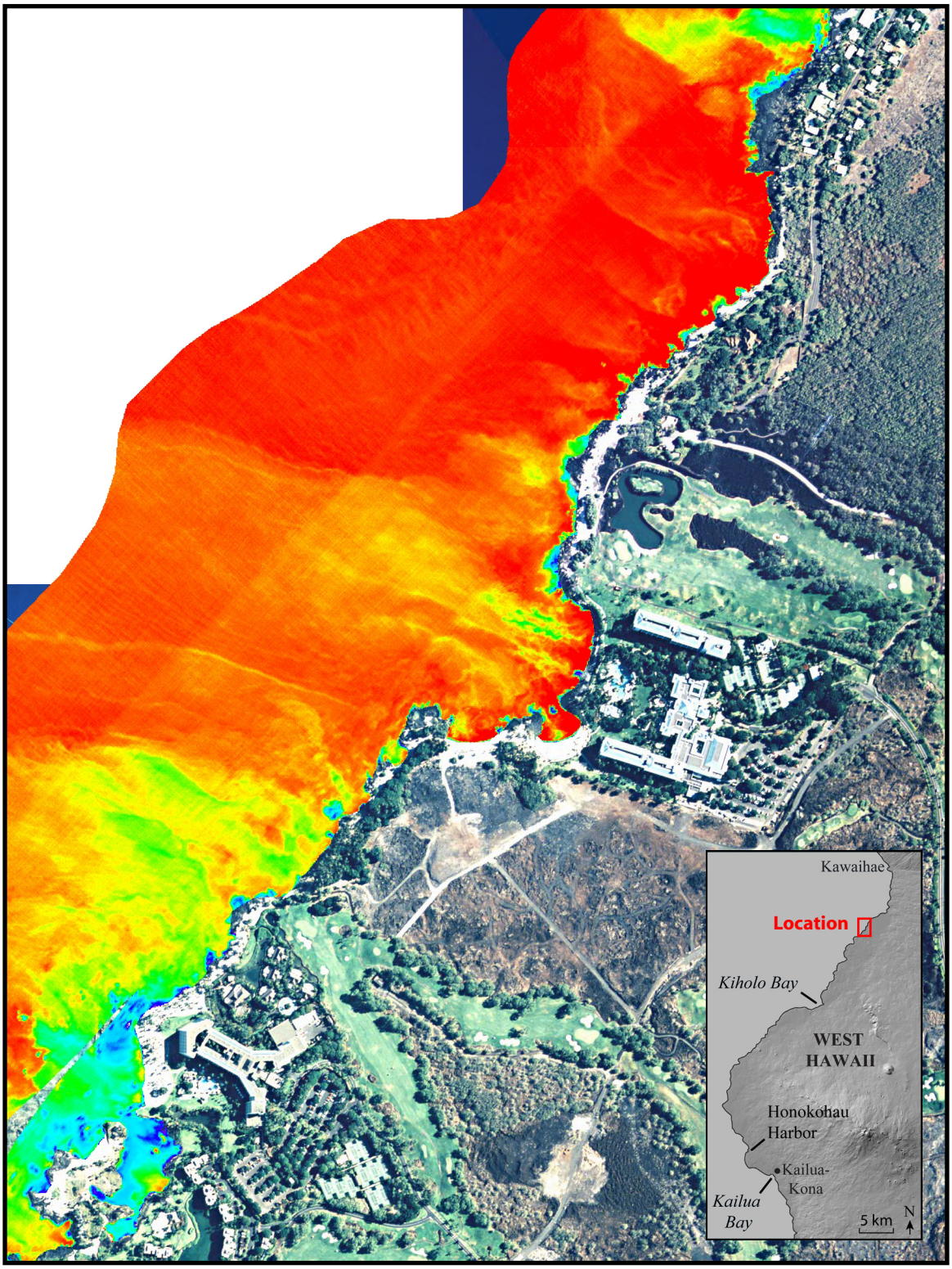

Panel 7.
Pauoa Bay

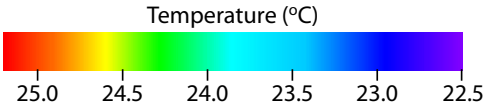

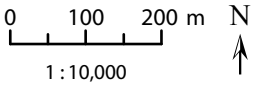

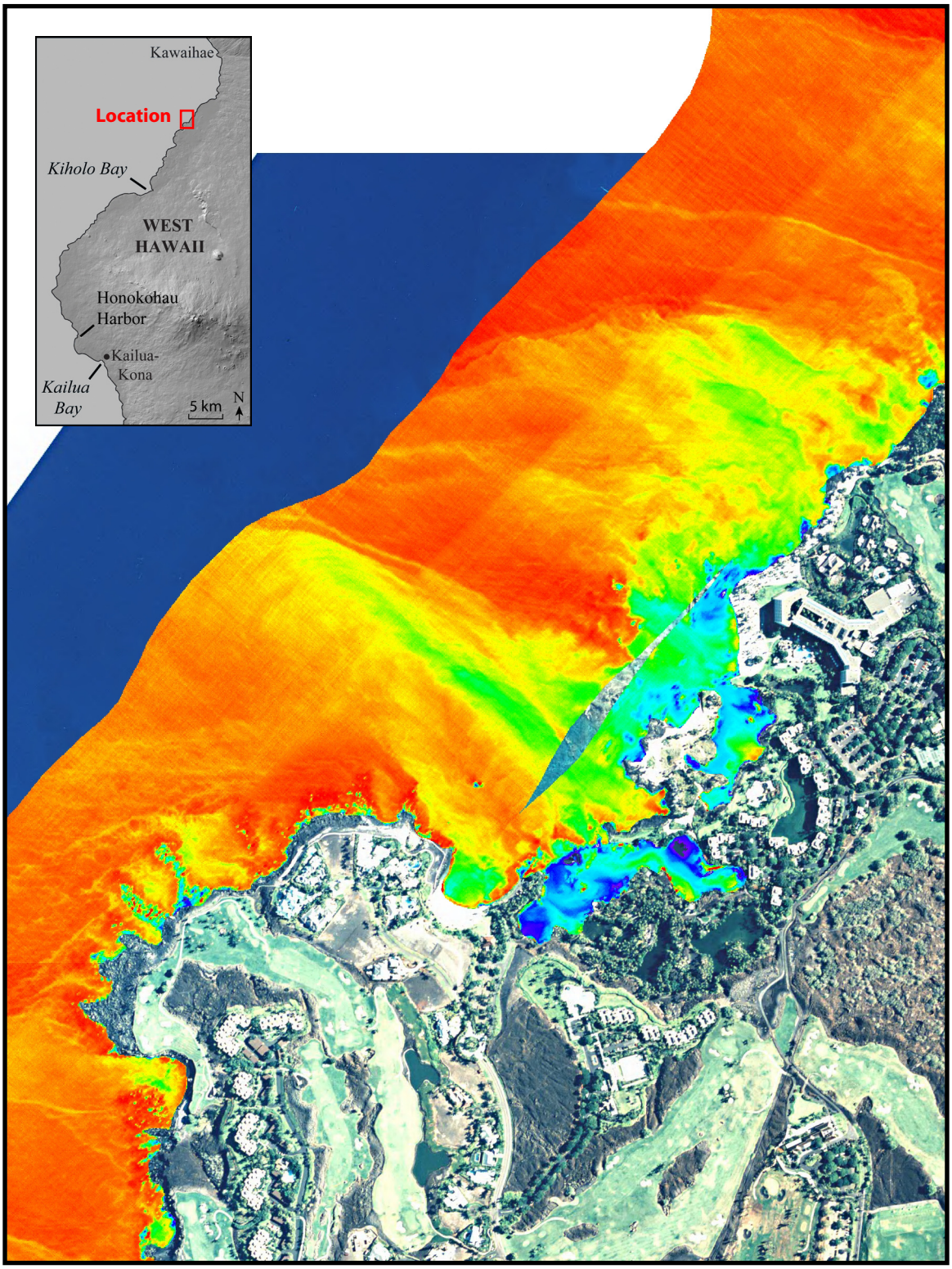

Panel 8.
Makaiwa Bay

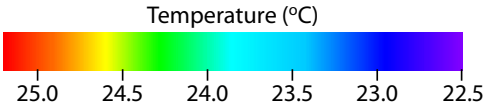

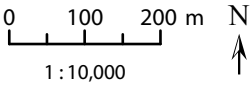

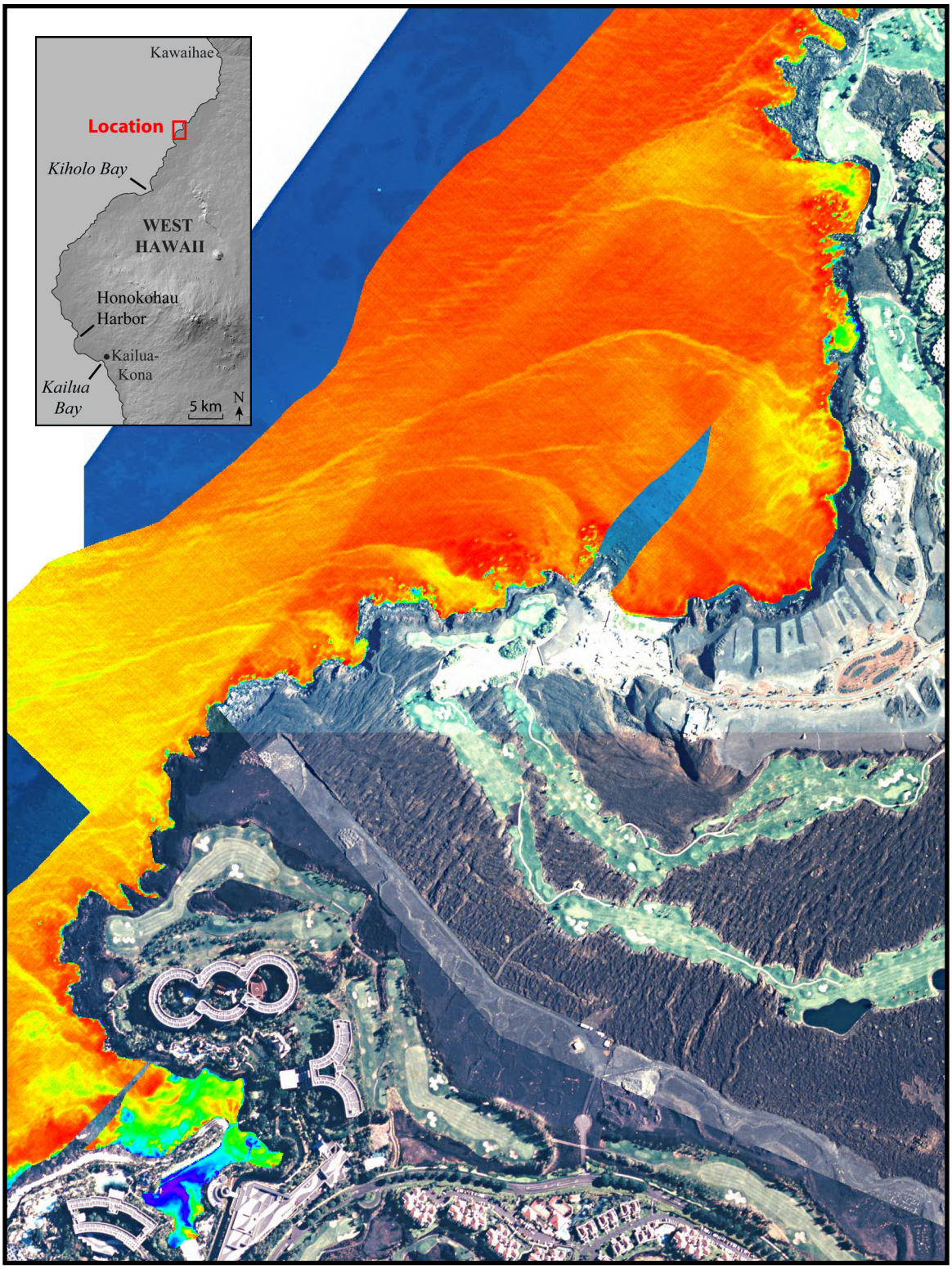

Panel 9.
Honokaope Bay

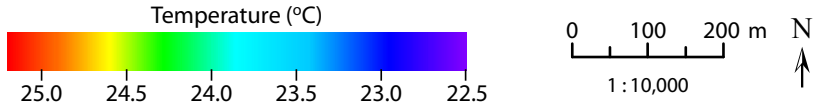

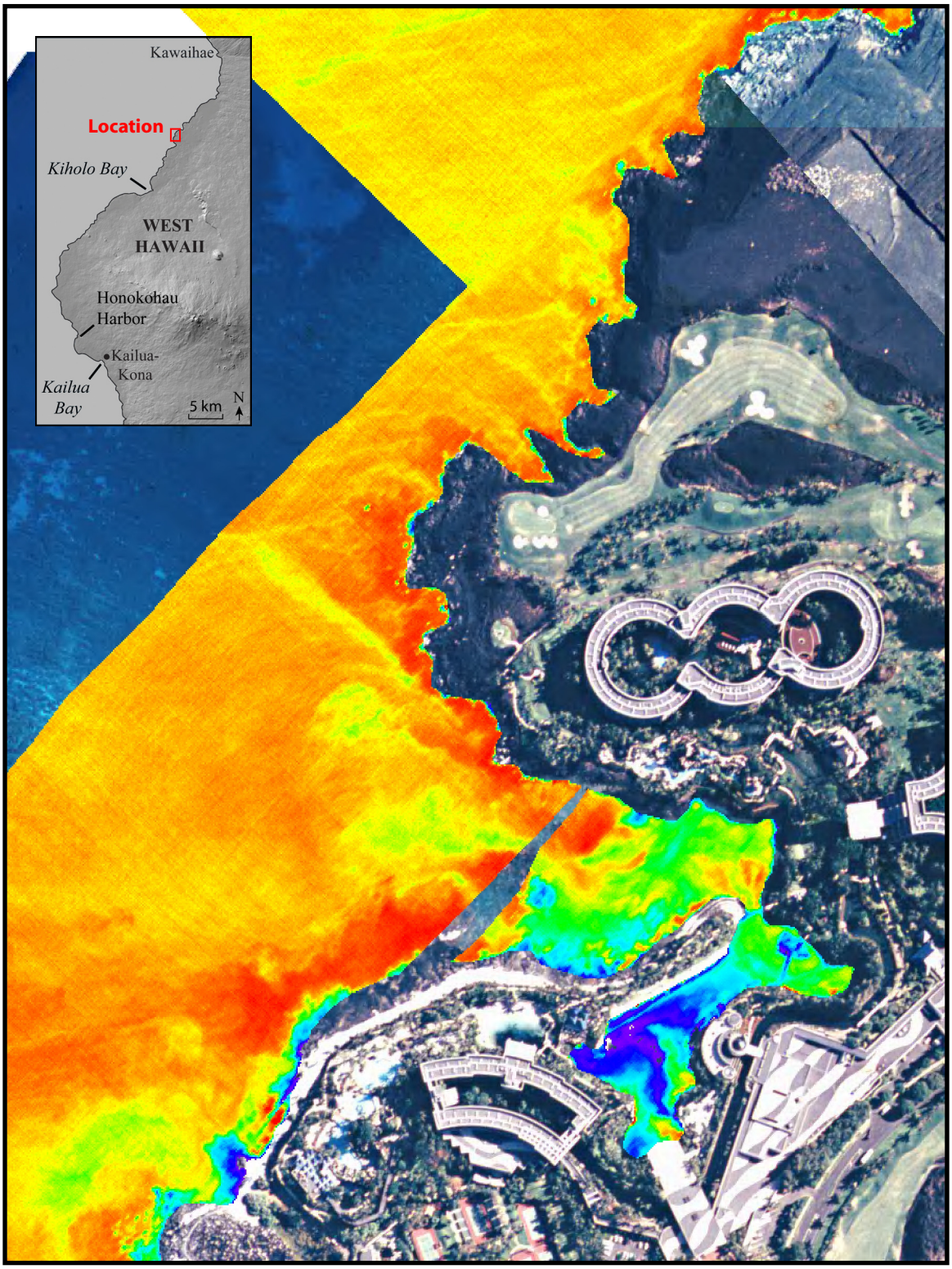

Panel 10.
Waiulua Bay

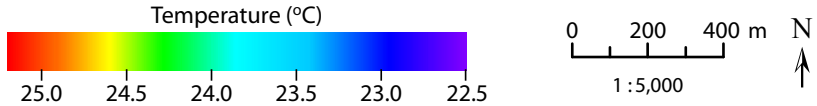

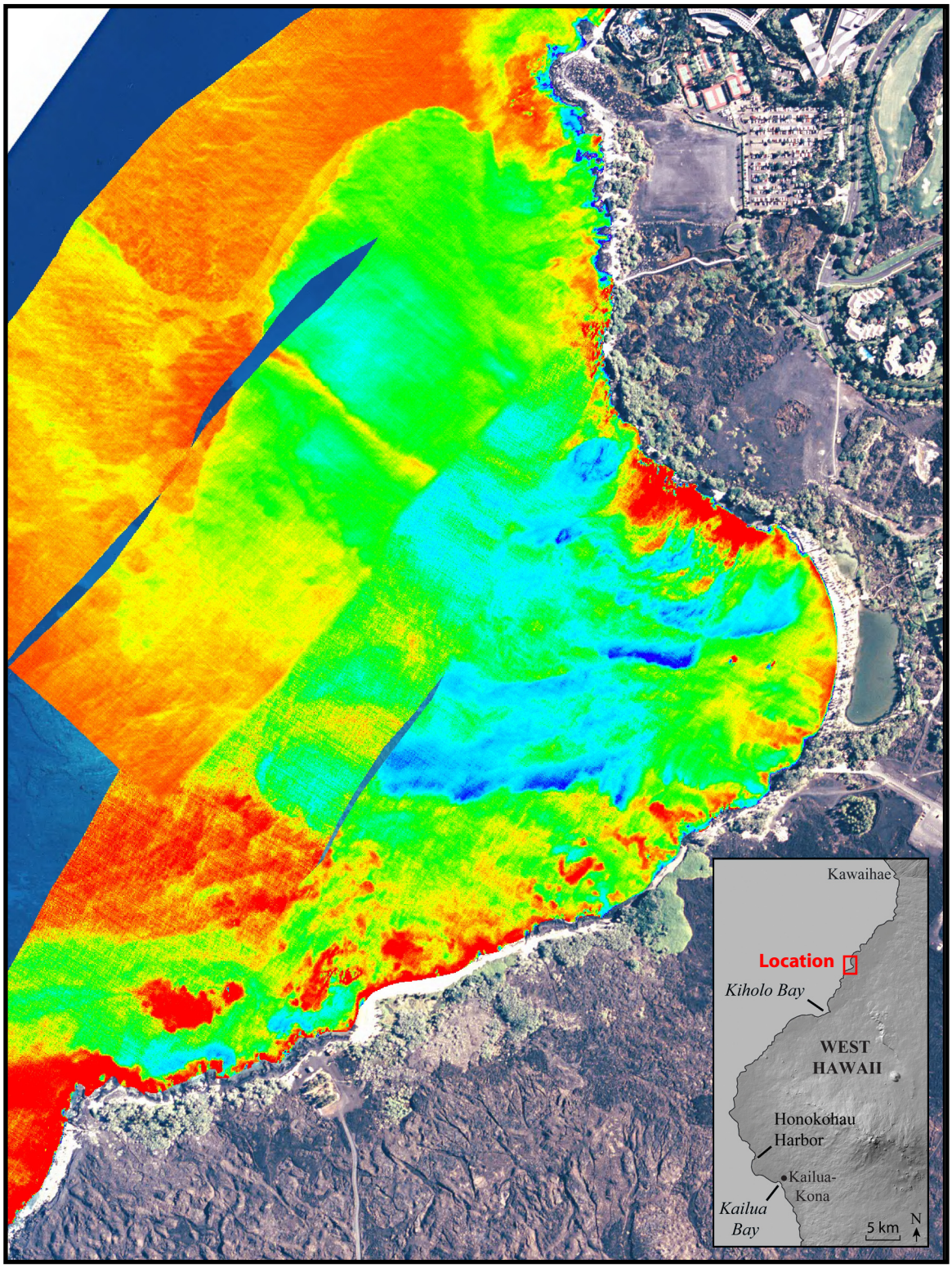

Panel 11.
Anaehoomalu Bay

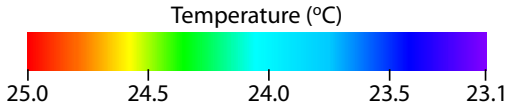

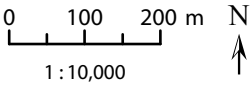

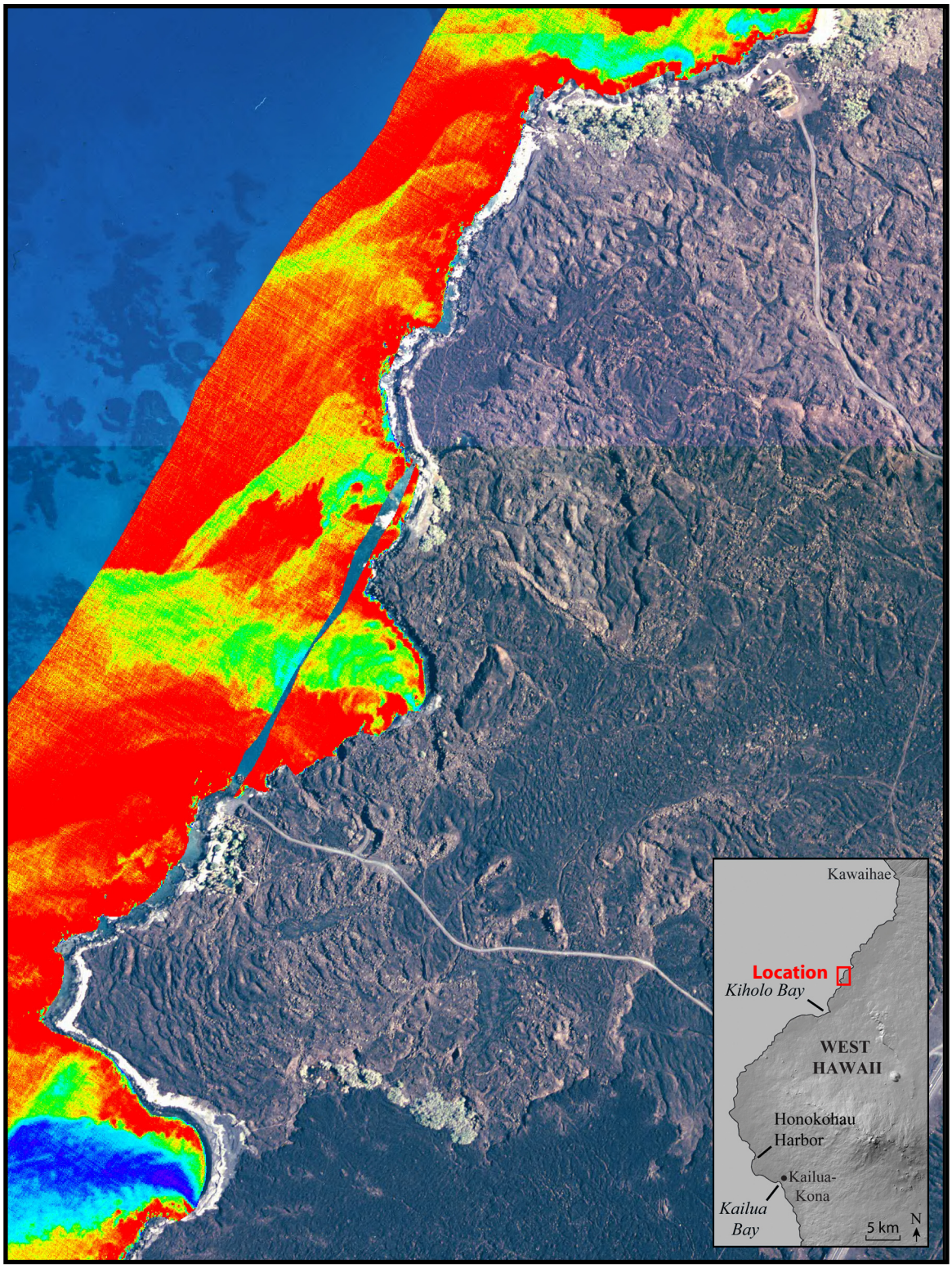

Panel 12.
Weliweli

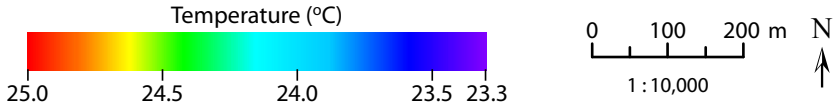

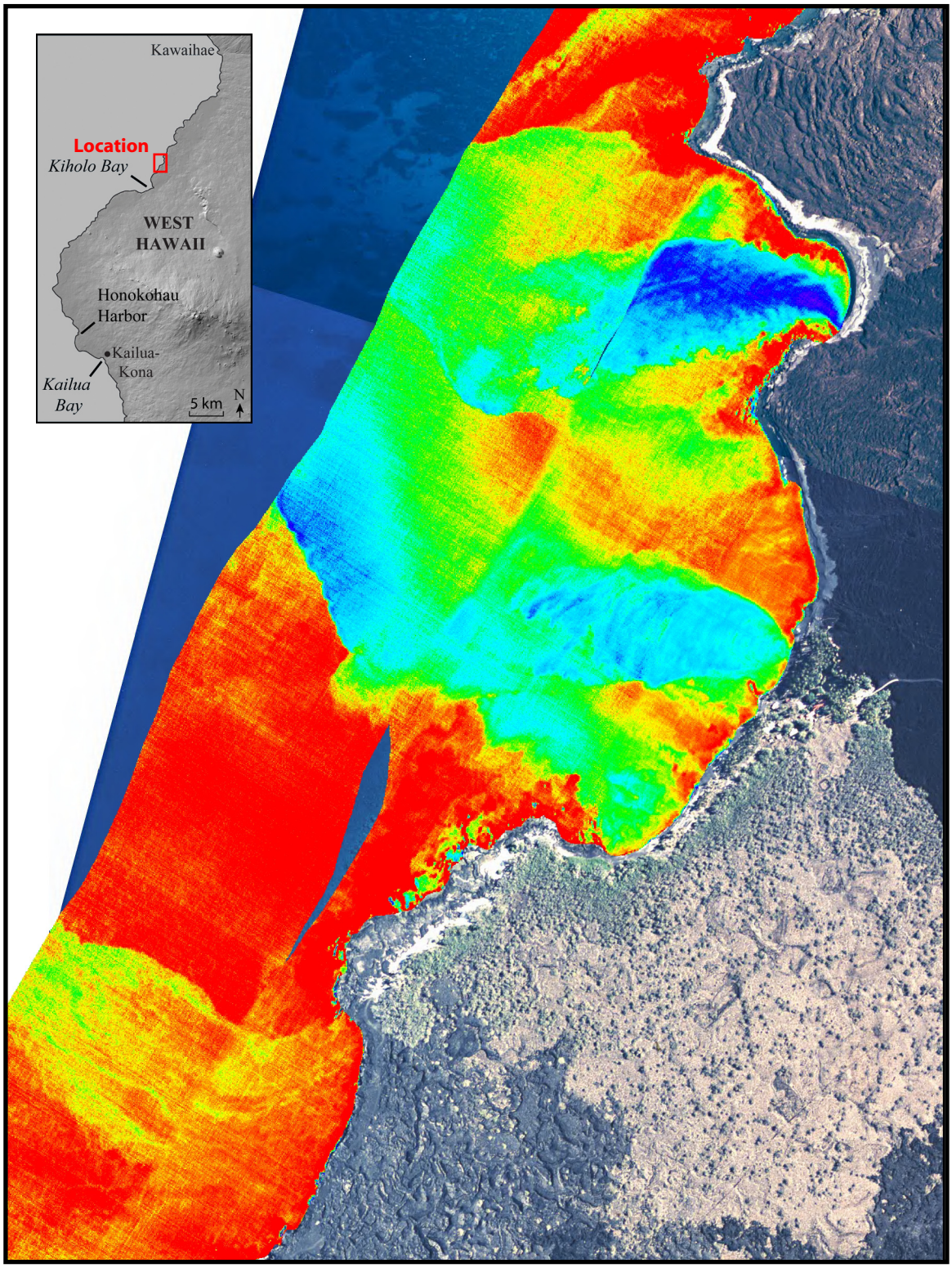

Panel 13.
Keawaiki Bay

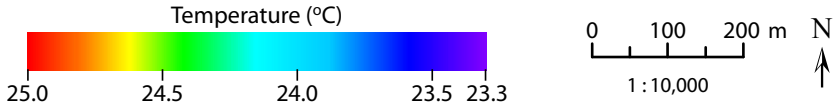

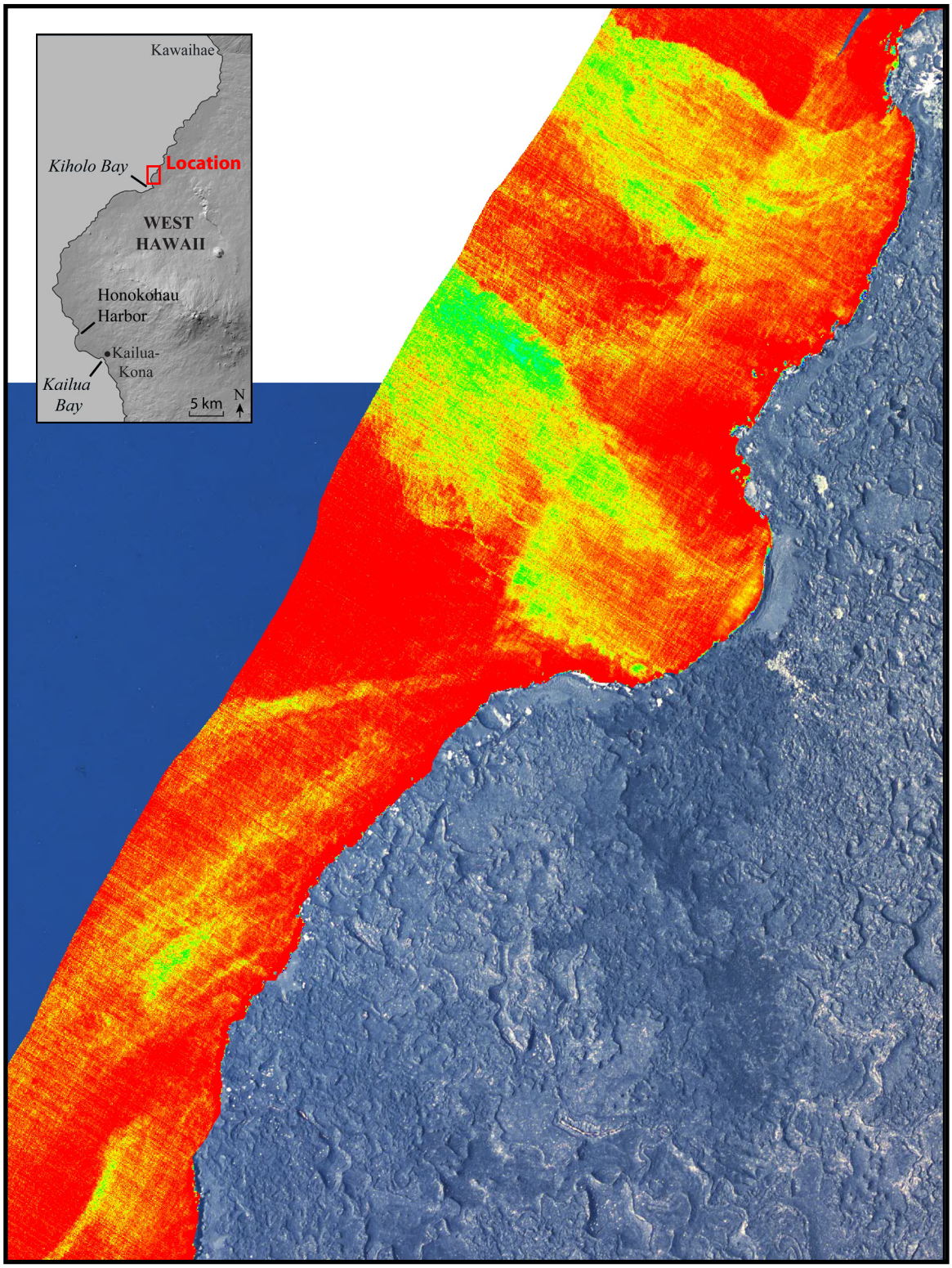

Panel 14.
Ohiki Bay

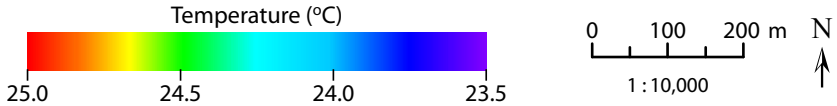

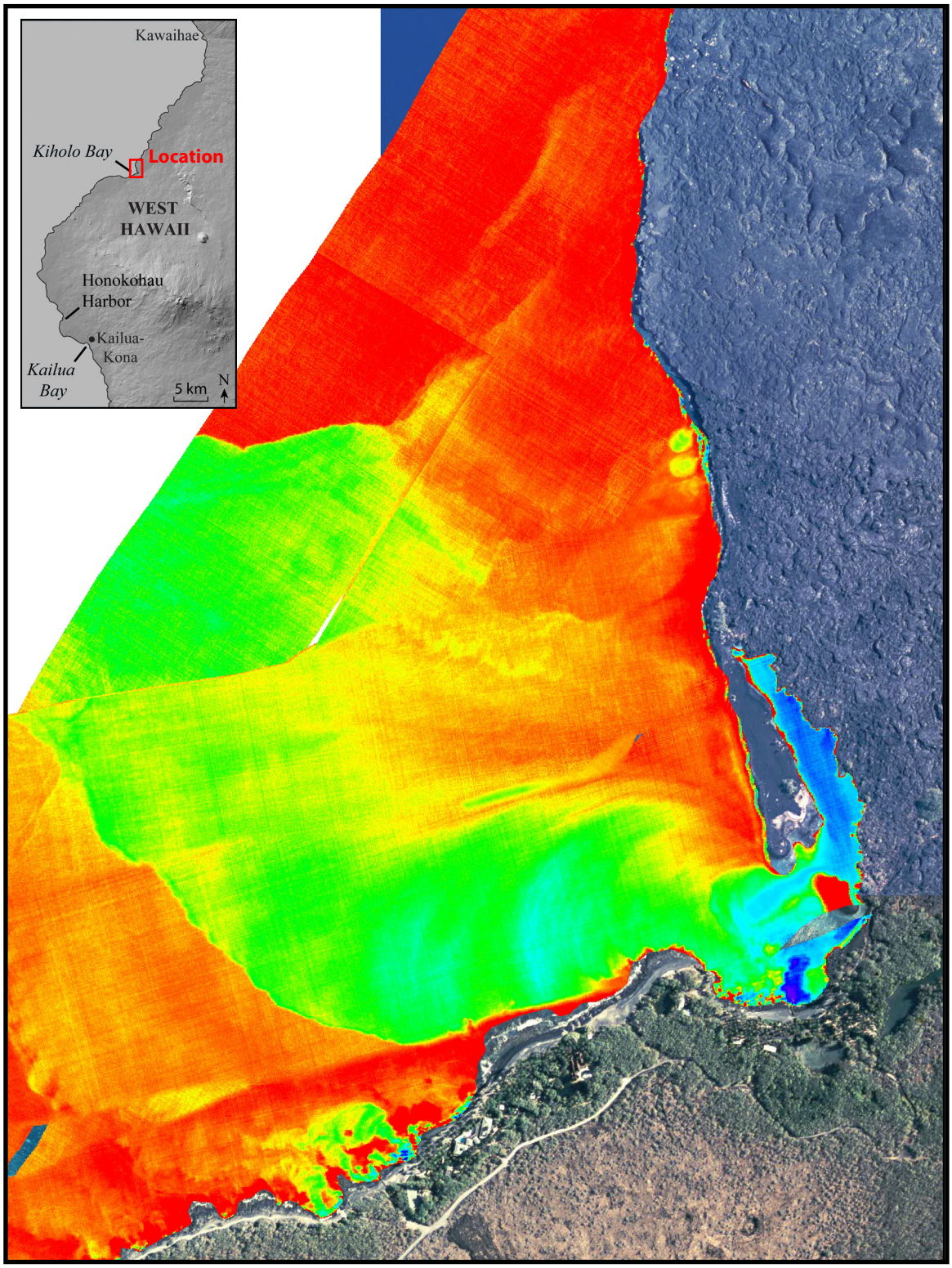

Panel 15.
NE Kiholo Bay (Apr. 30)

Temperature (°C)
25.0 24.5 24.0 23.5 23.0 22.5 22.1

0 100 200 m
1 : 10,000
N

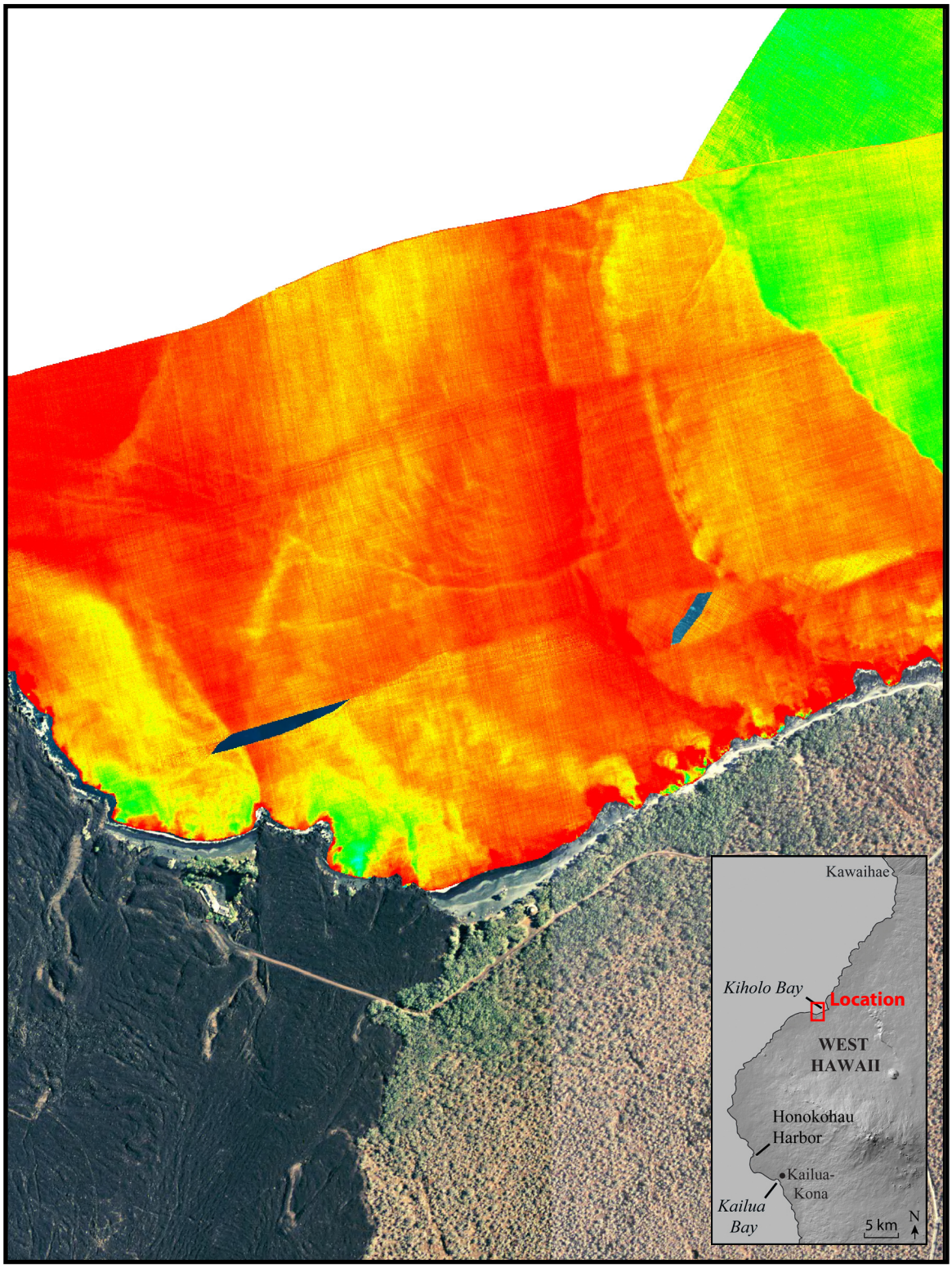

Panel 16.
SW Kiholo Bay (Apr. 30)

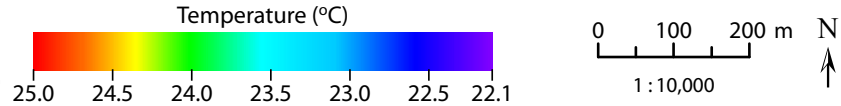

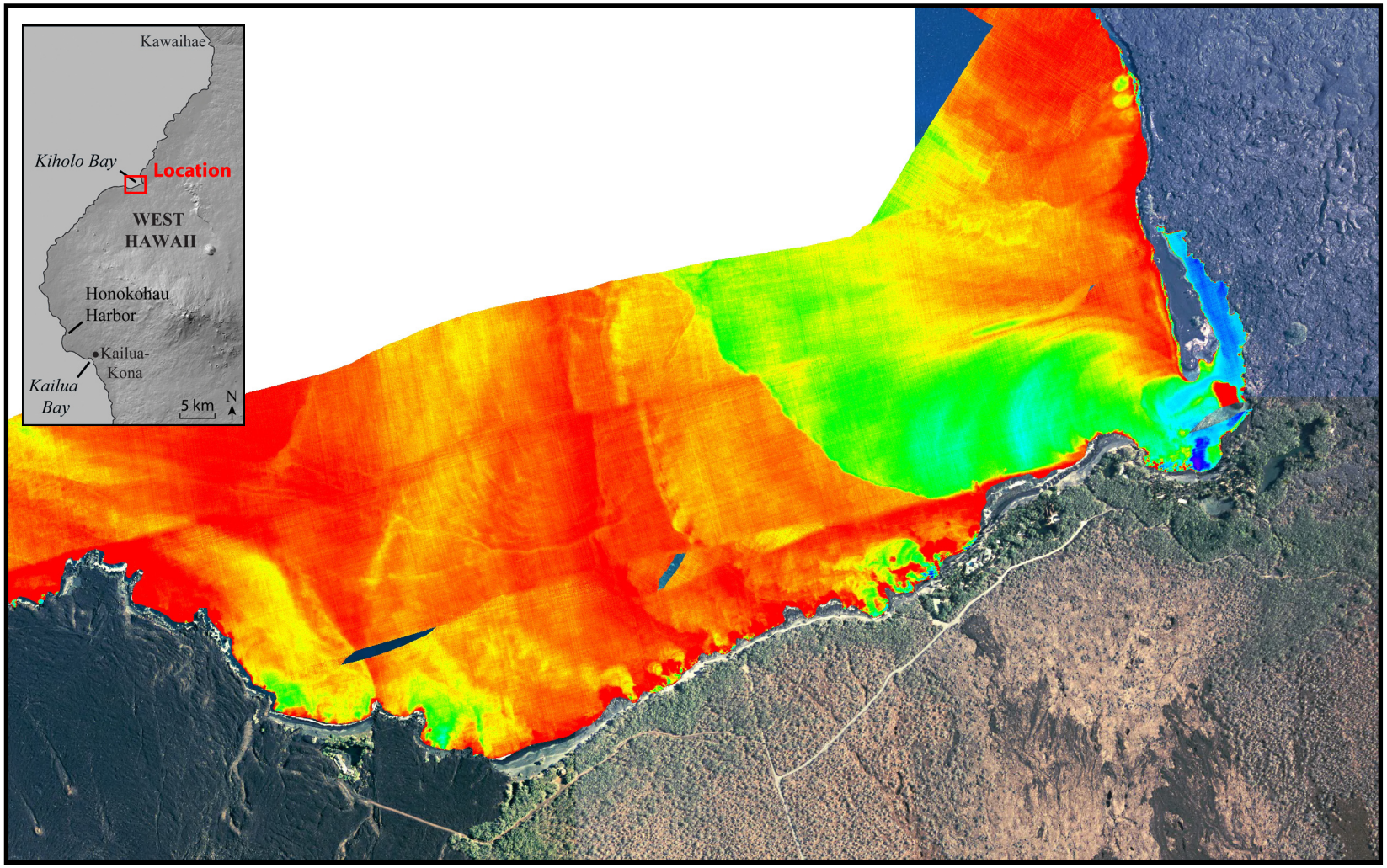

Panel 17.
Kiholo Bay (Apr. 30)

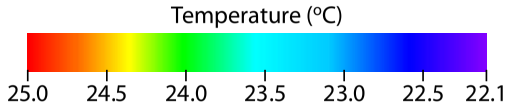

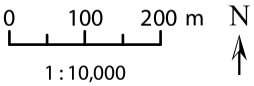

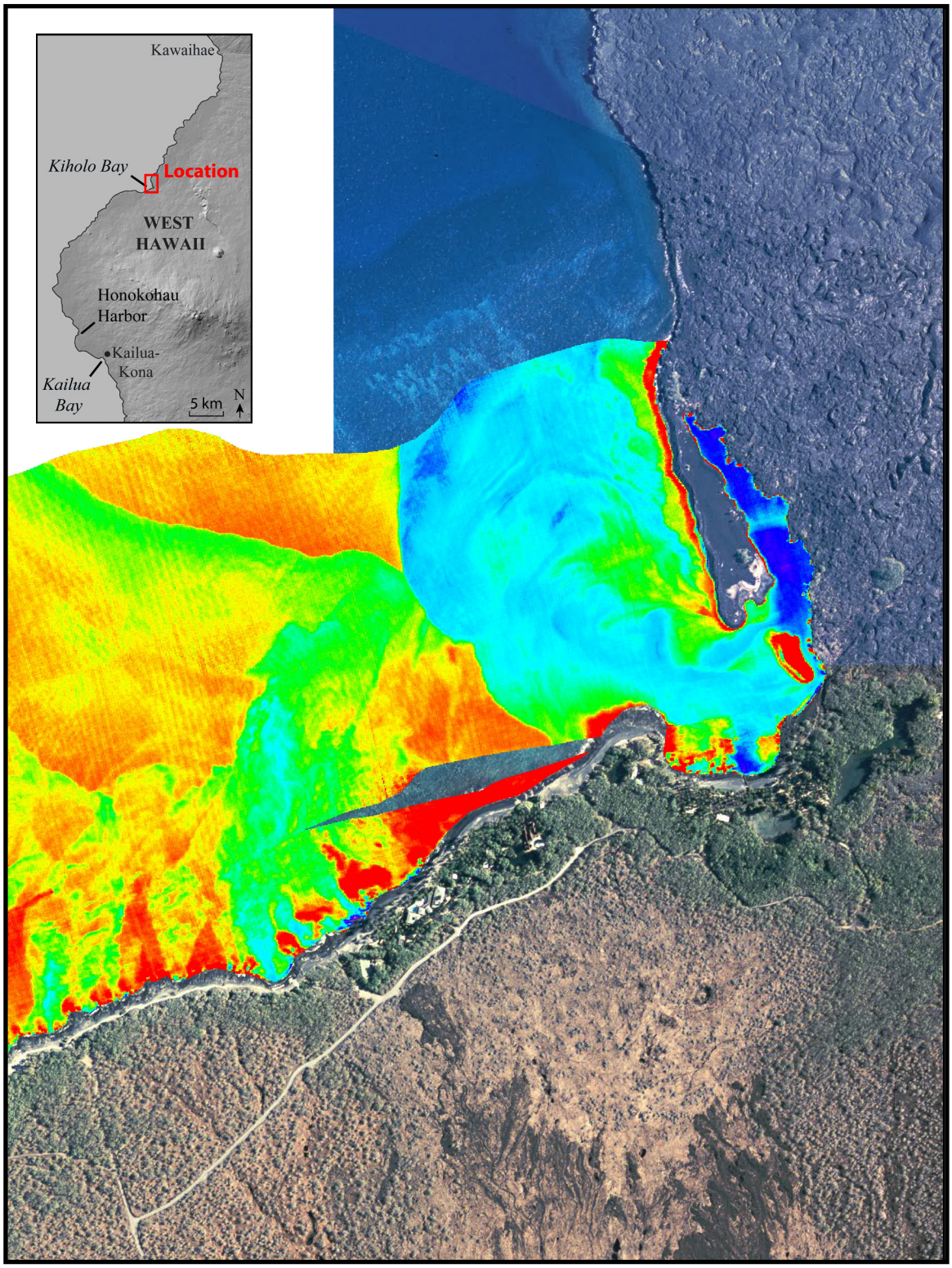

Panel 18.
NE Kiholo Bay (May 1)

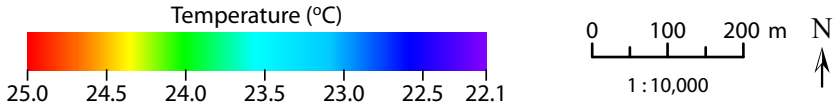

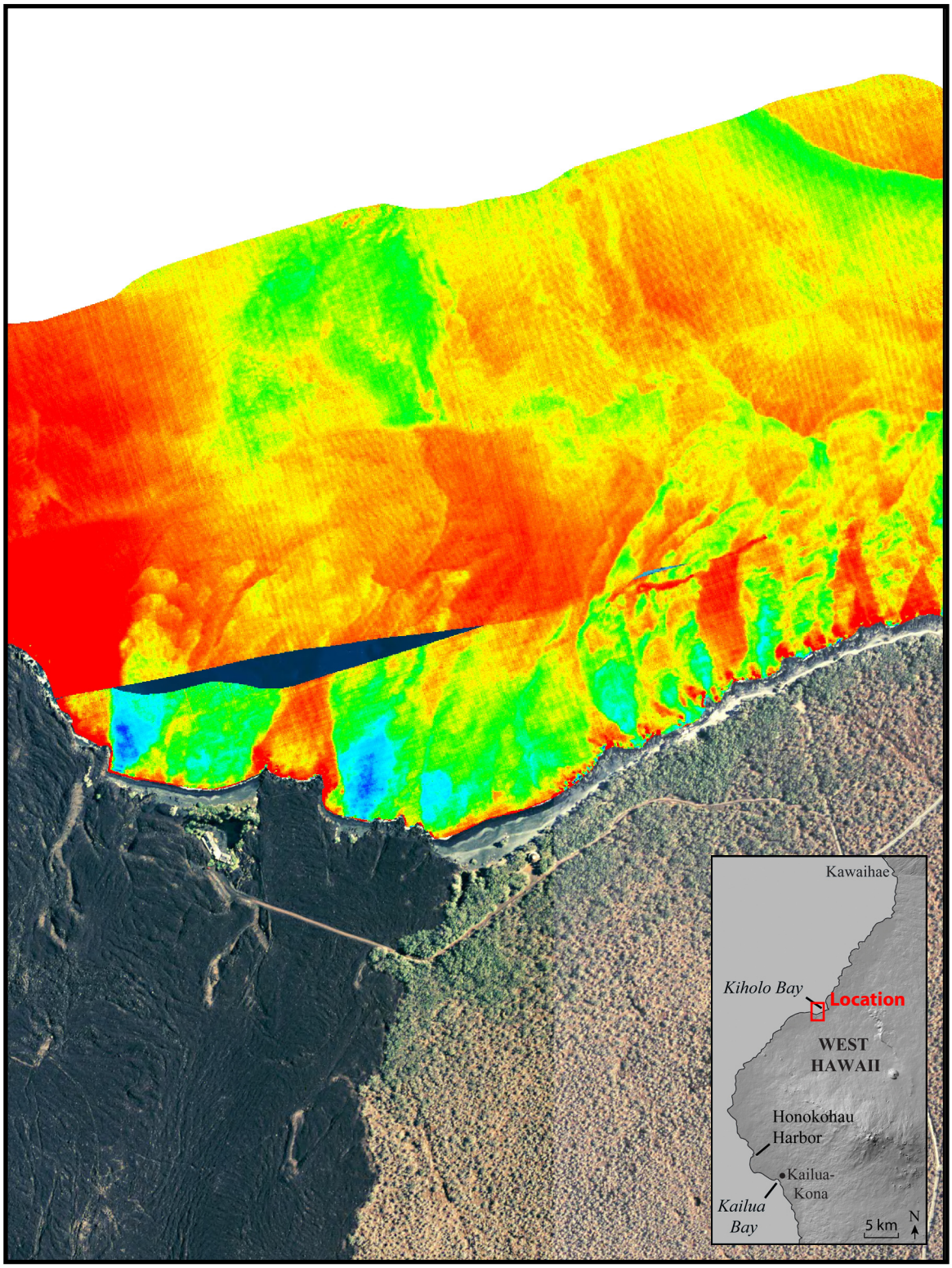

Panel 19.
SW Kiholo Bay (May 1)

Temperature (°C)
25.0 24.5 24.0 23.5 23.0 22.5 22.1

0 100 200 m
1 : 10,000
N

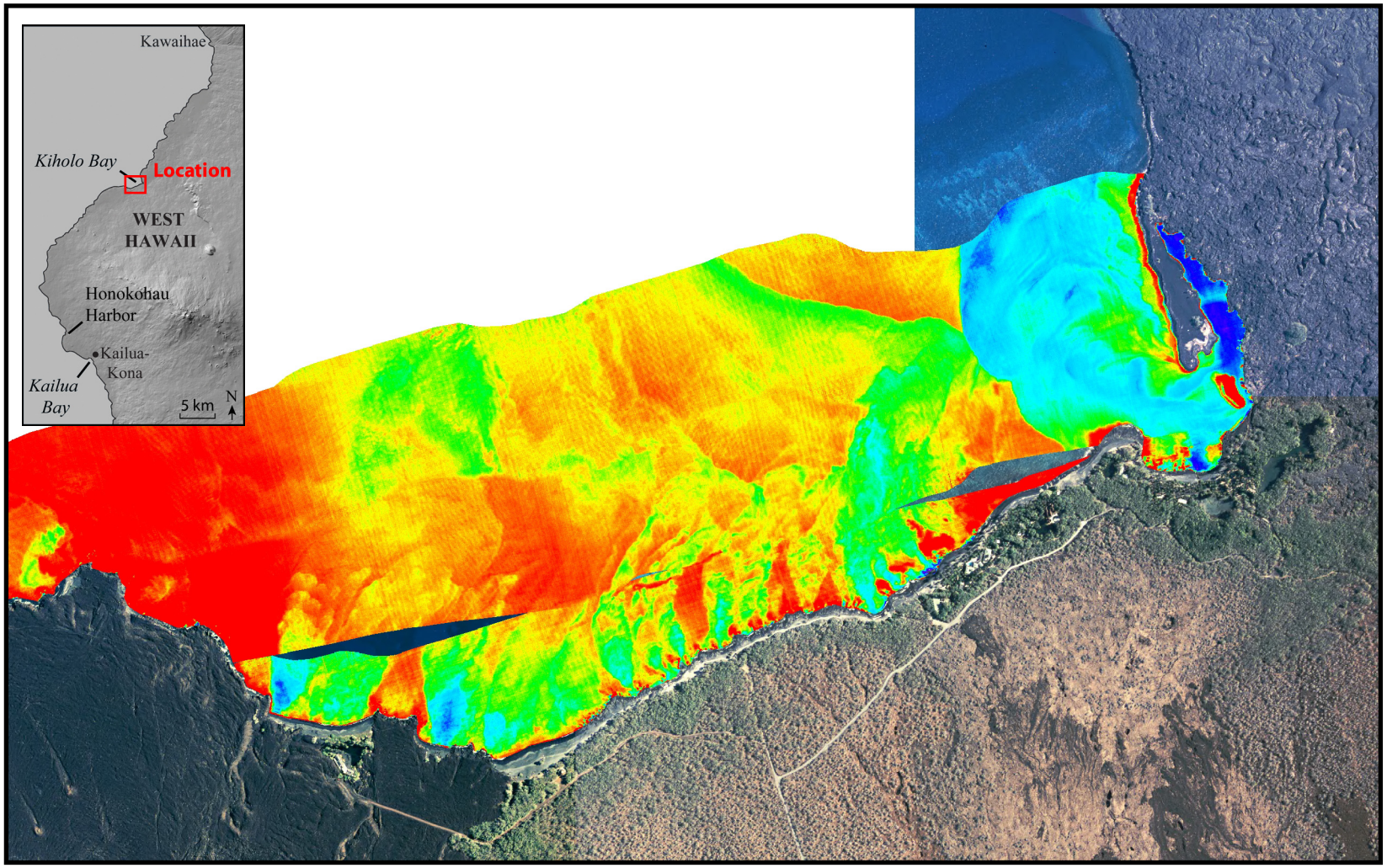

Panel 20.
Kiholo Bay (May 1)

Temperature (°C)
25.0 24.5 24.0 23.5 23.0 22.5 22.1

0 100 200 m
1 : 10,000
N

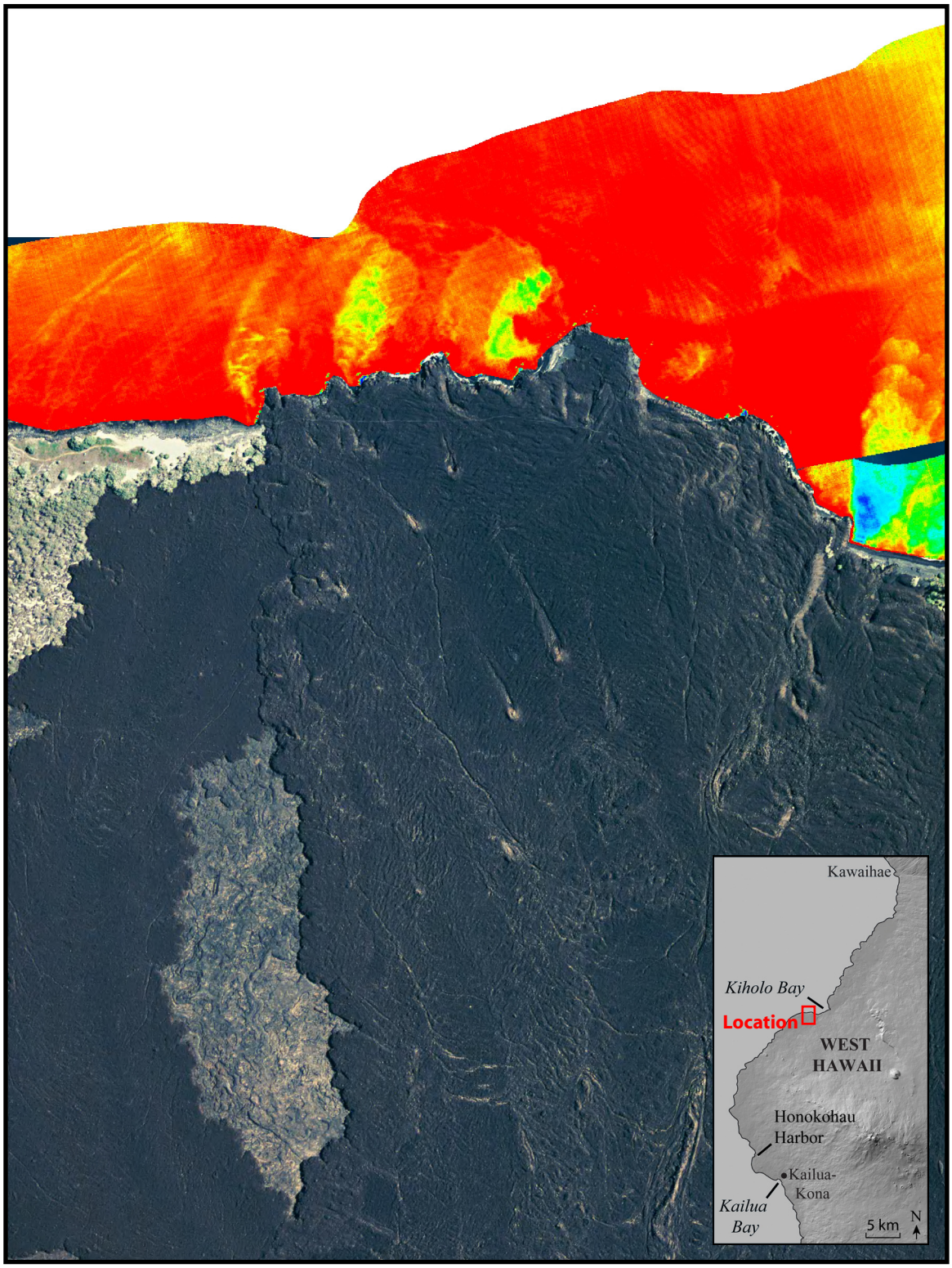

Panel 21.
1801 lava flow

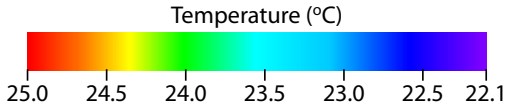

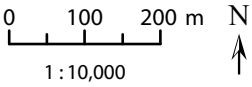

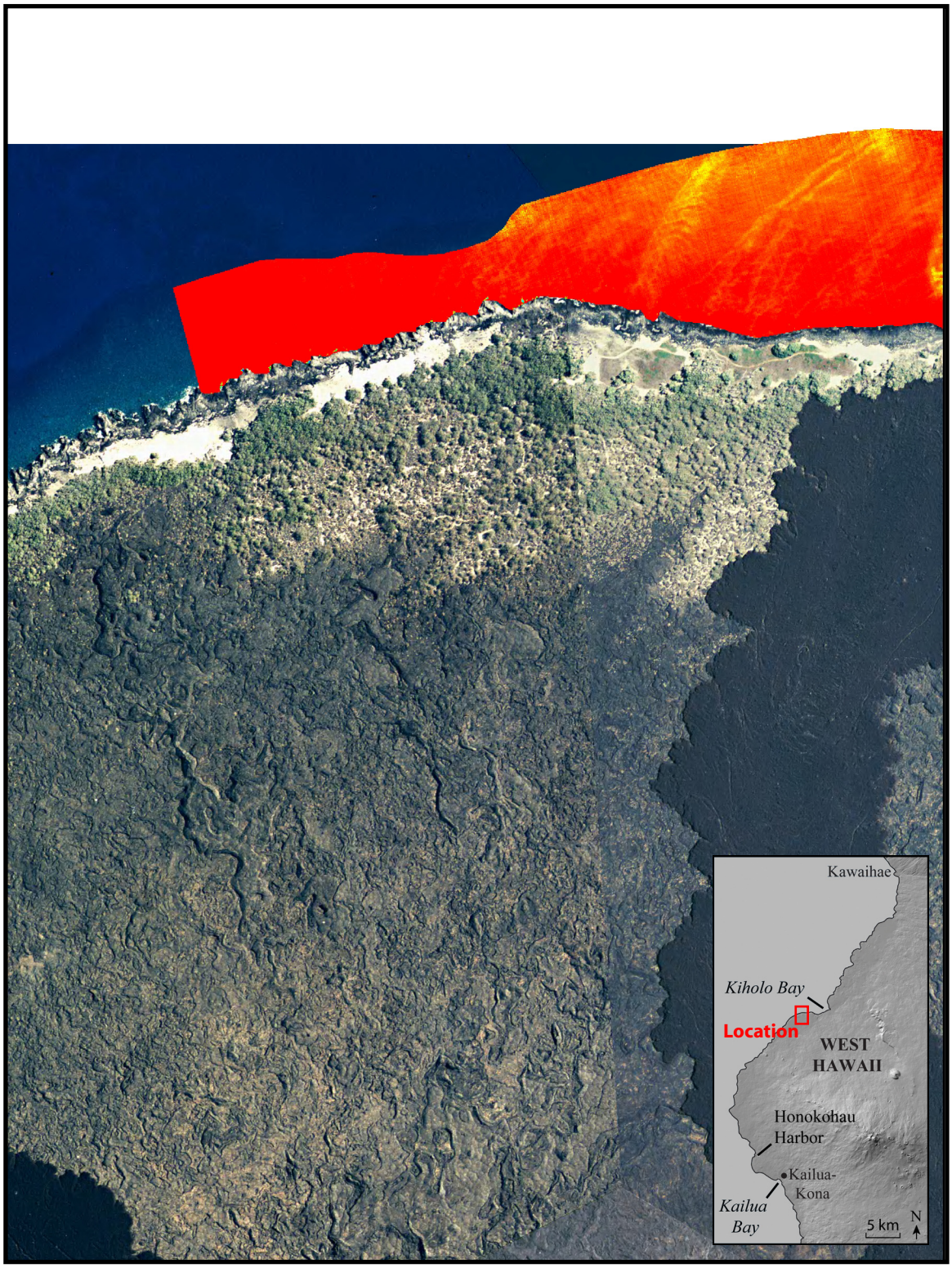

Panel 22.
Mano Pt.

Temperature (°C)

25.0 24.5 24.0 23.5 23.0 22.5 22.1

0 100 200 m

1 : 10,000

N

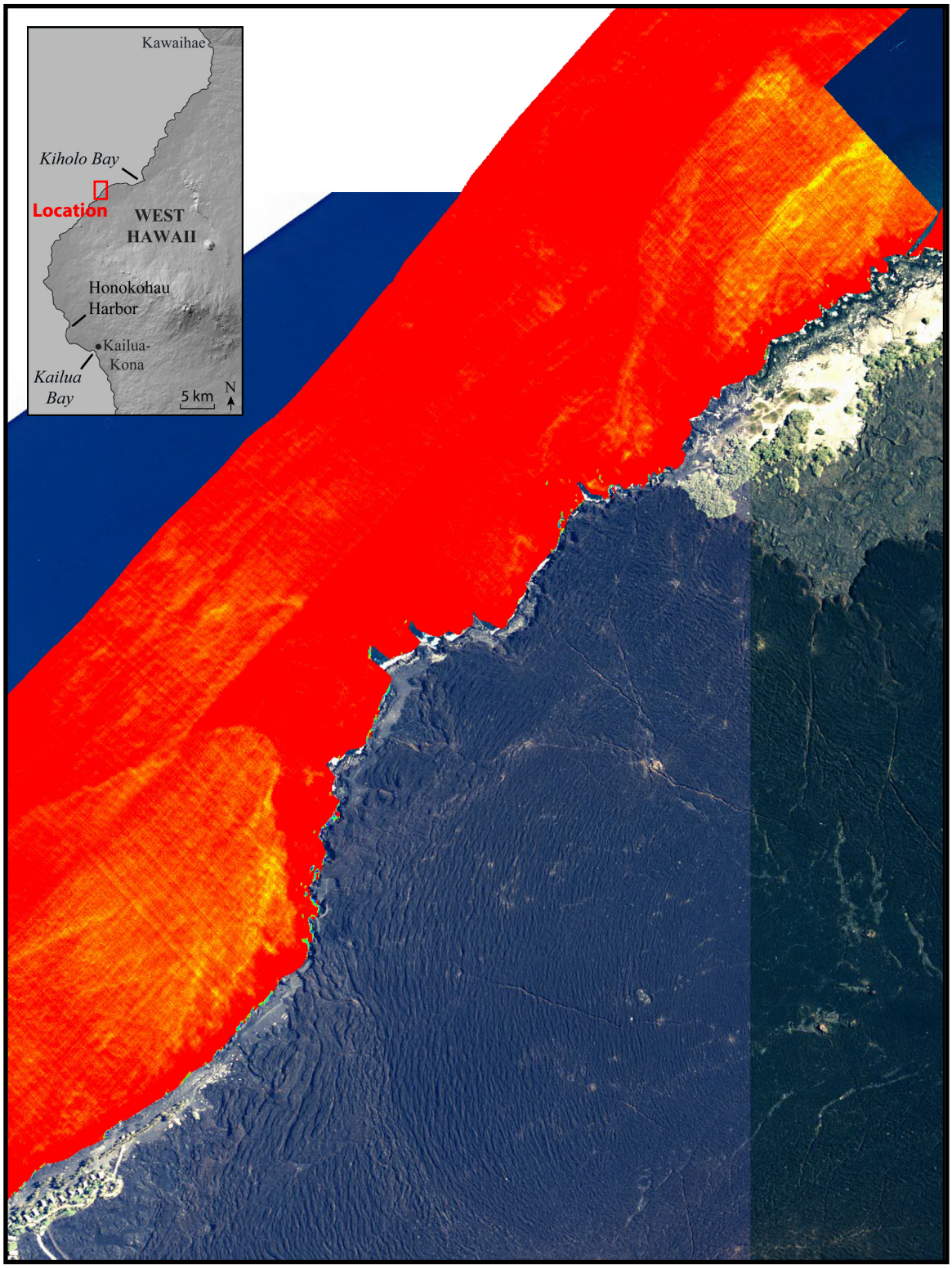

Panel 23.
Ala Kahakai

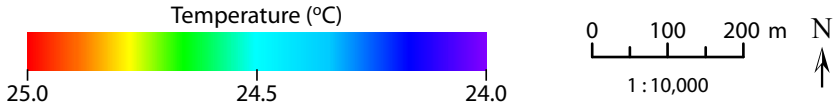

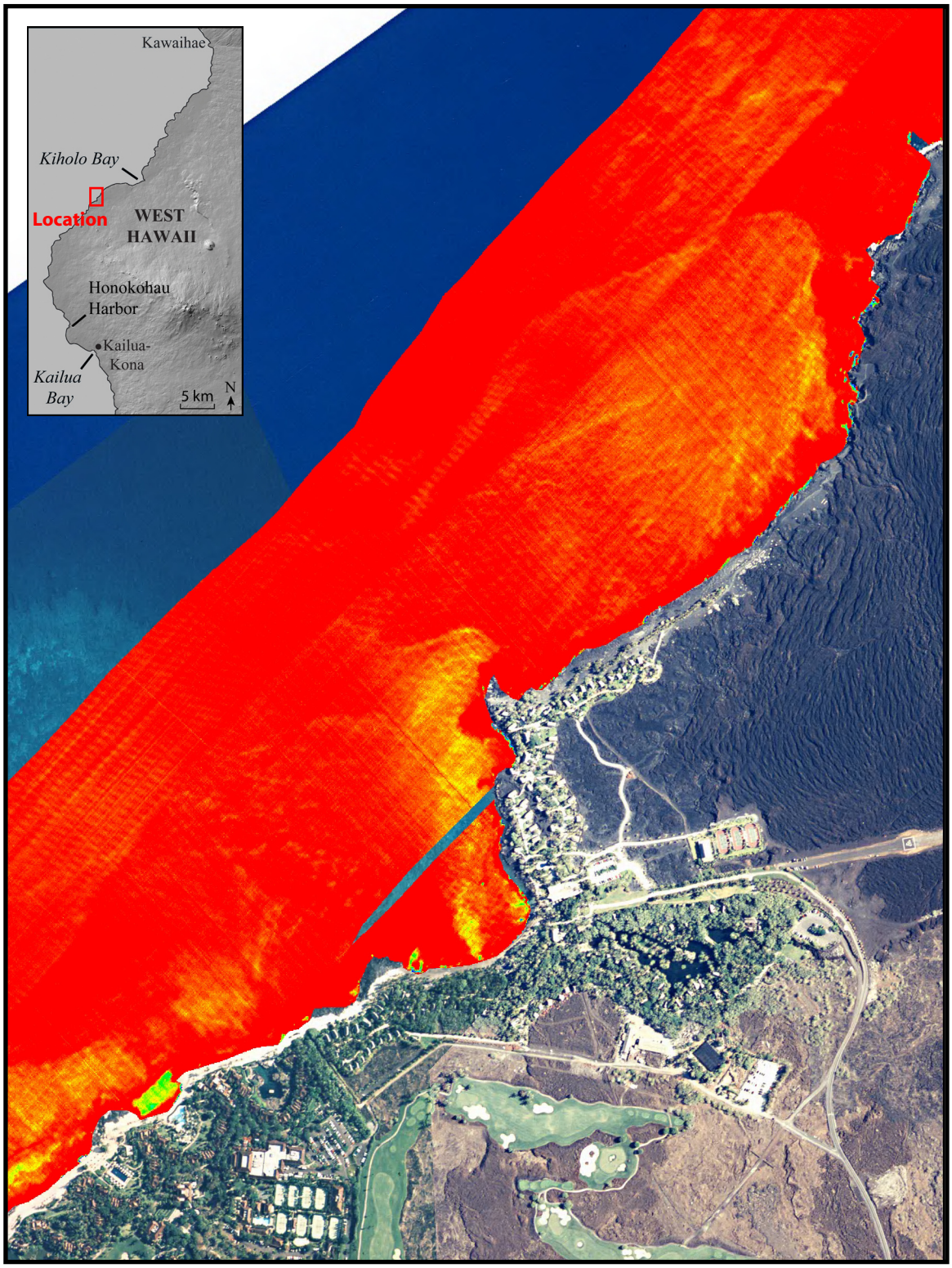

Panel 24.
Kahuwai Bay

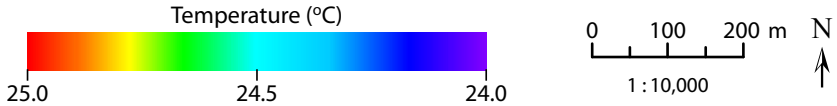

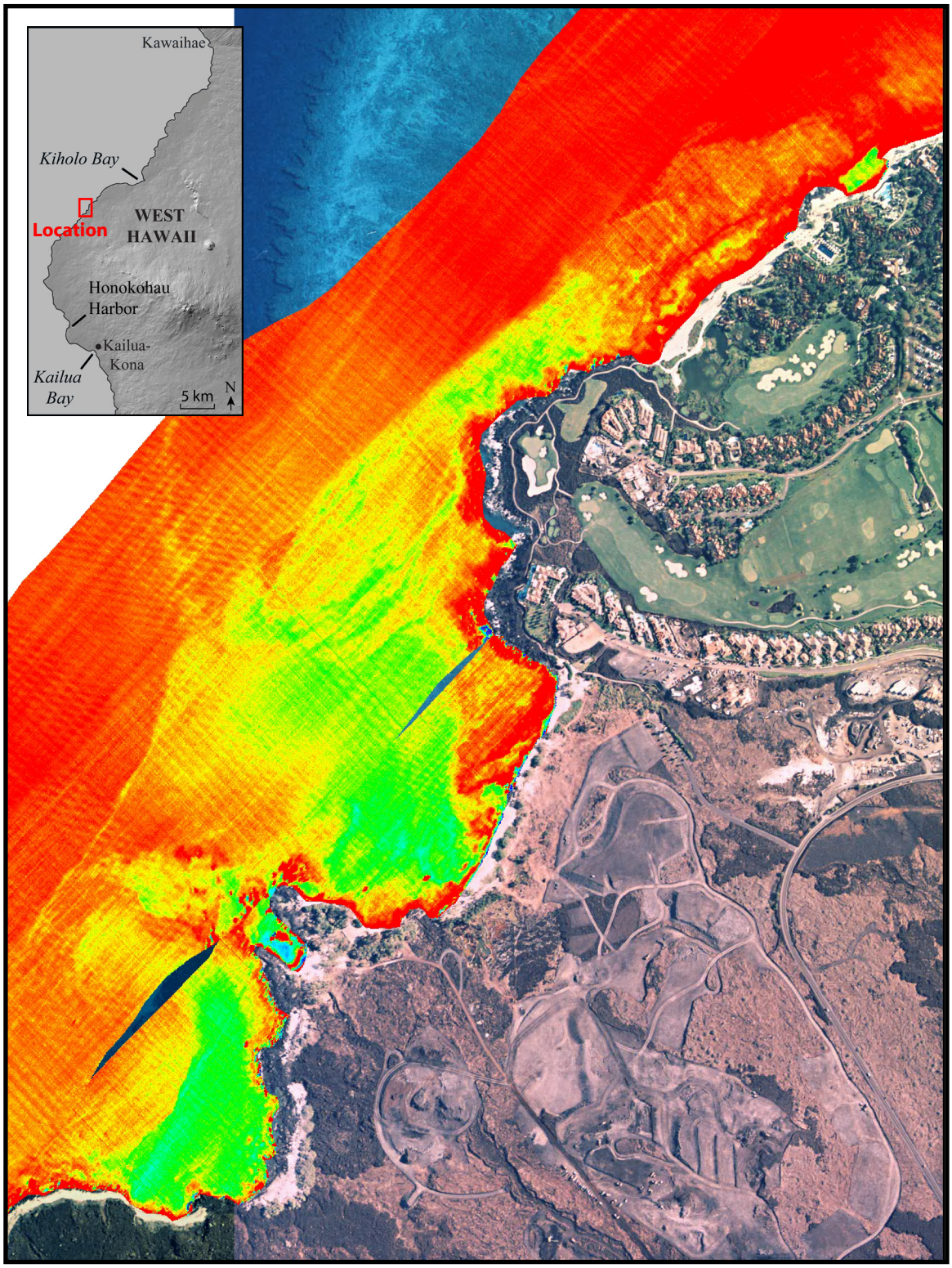

Panel 25.
Kukio Bay

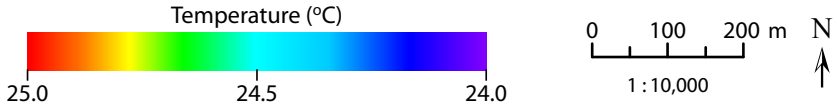

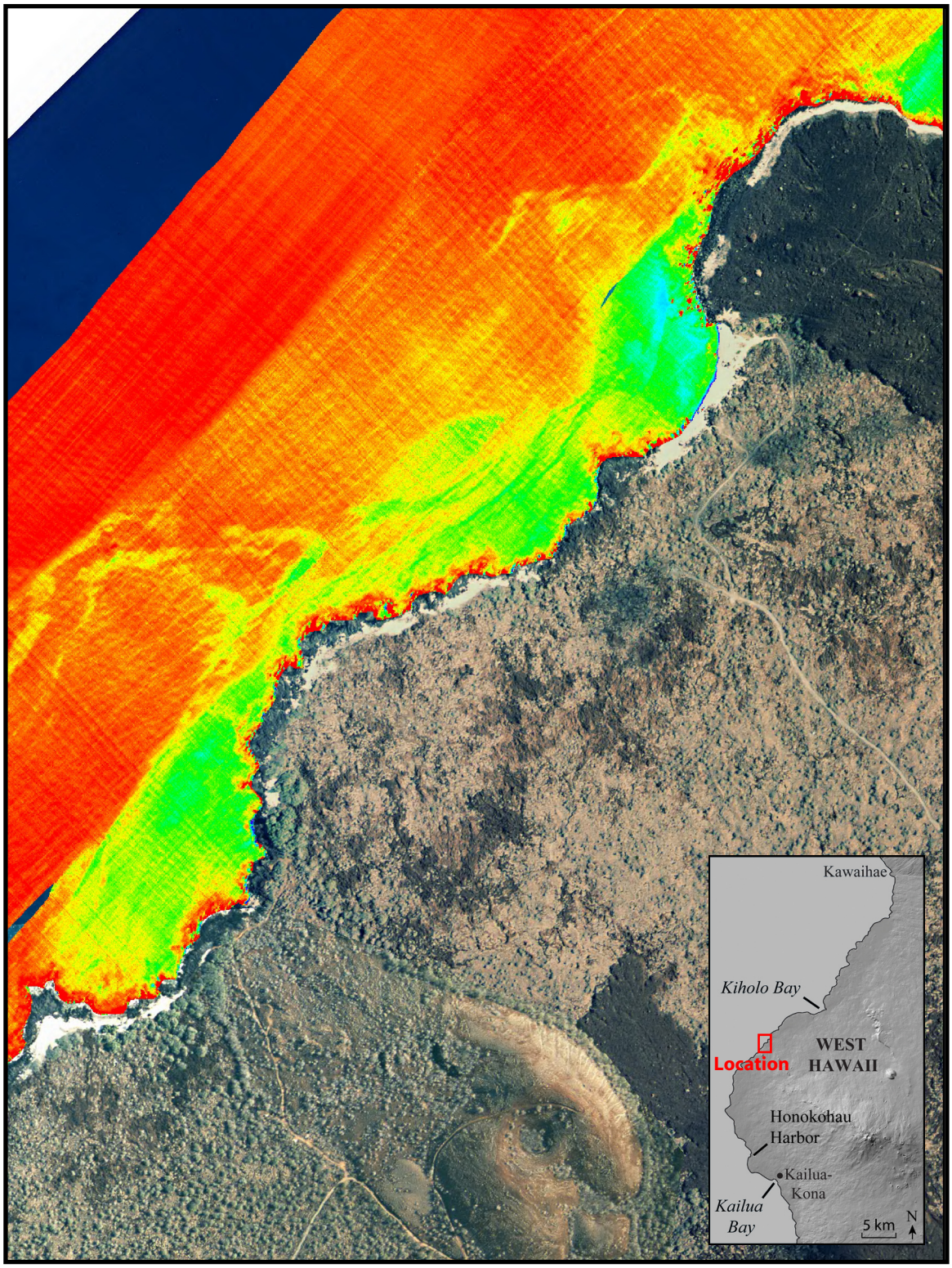

Panel 26.
Kua Bay

Temperature (°C)
25.0
24.5
24.0

0 100 200 m
1 : 10,000
N

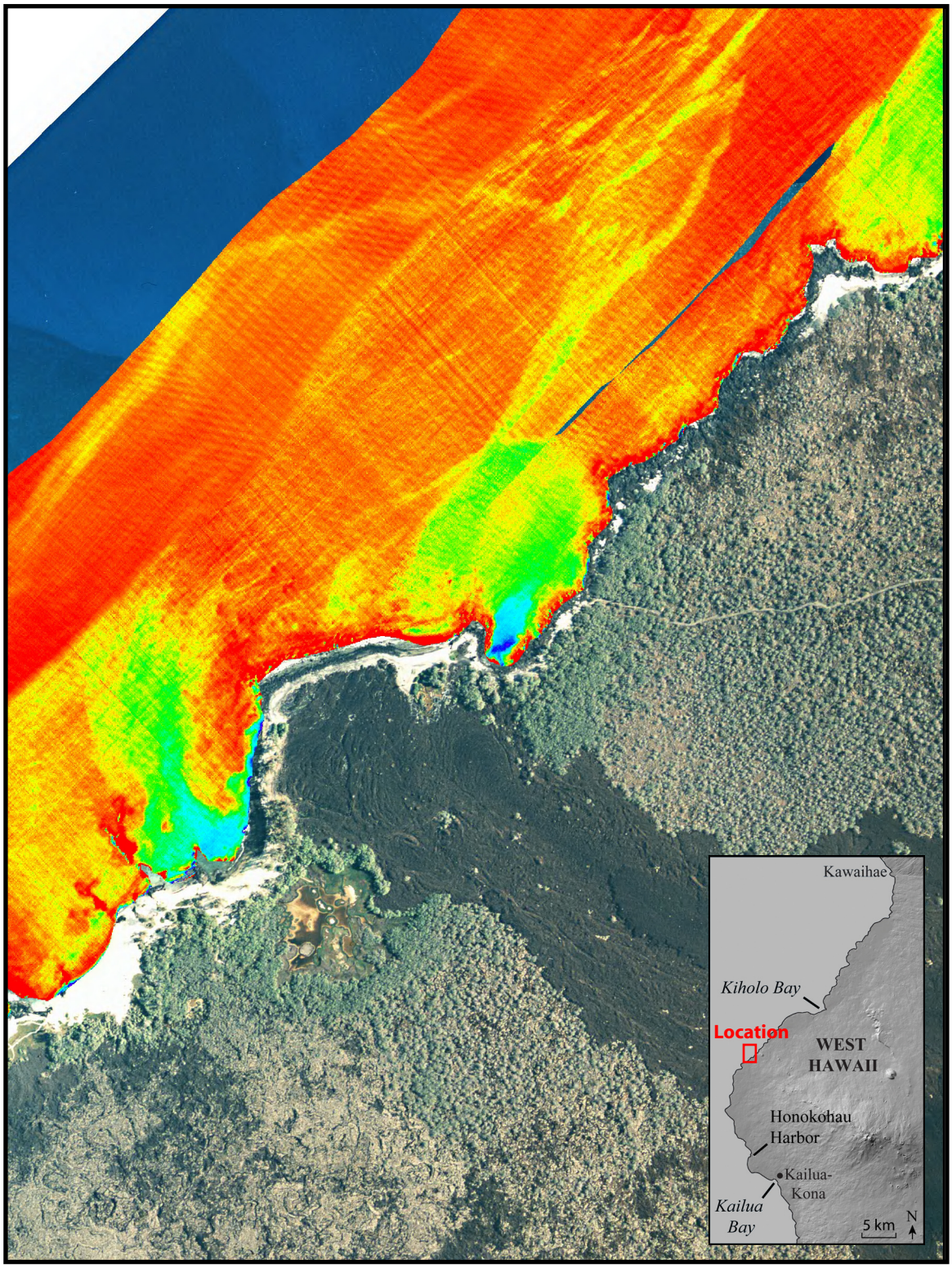

Panel 27.
Awakee Bay

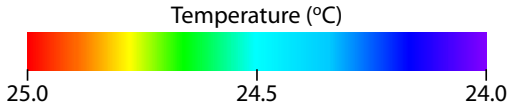

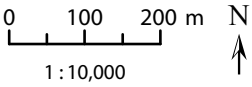

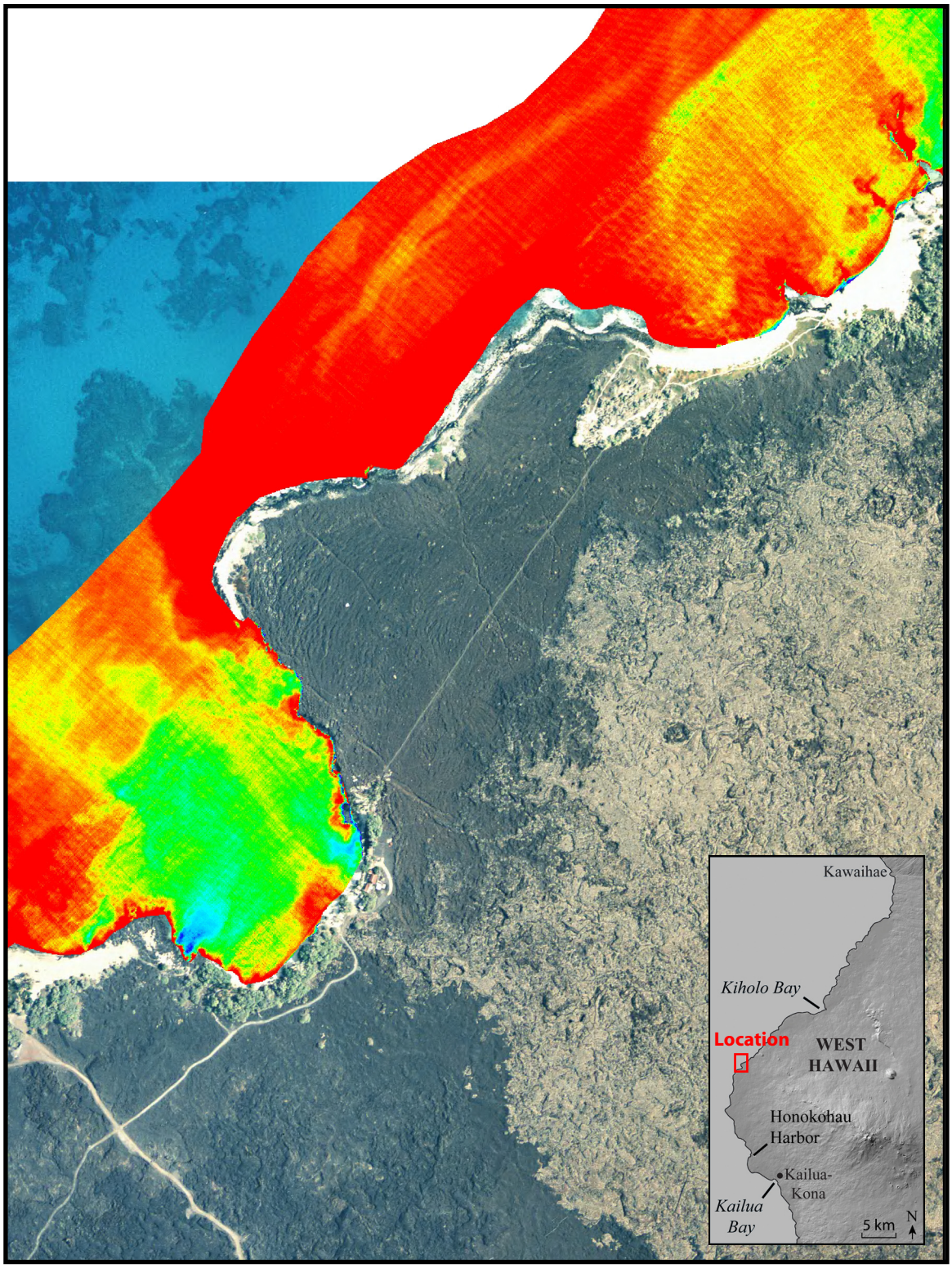

Panel 28.
Mahaiula Bay

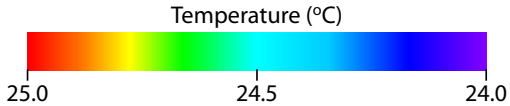

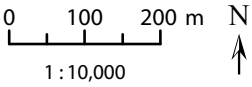

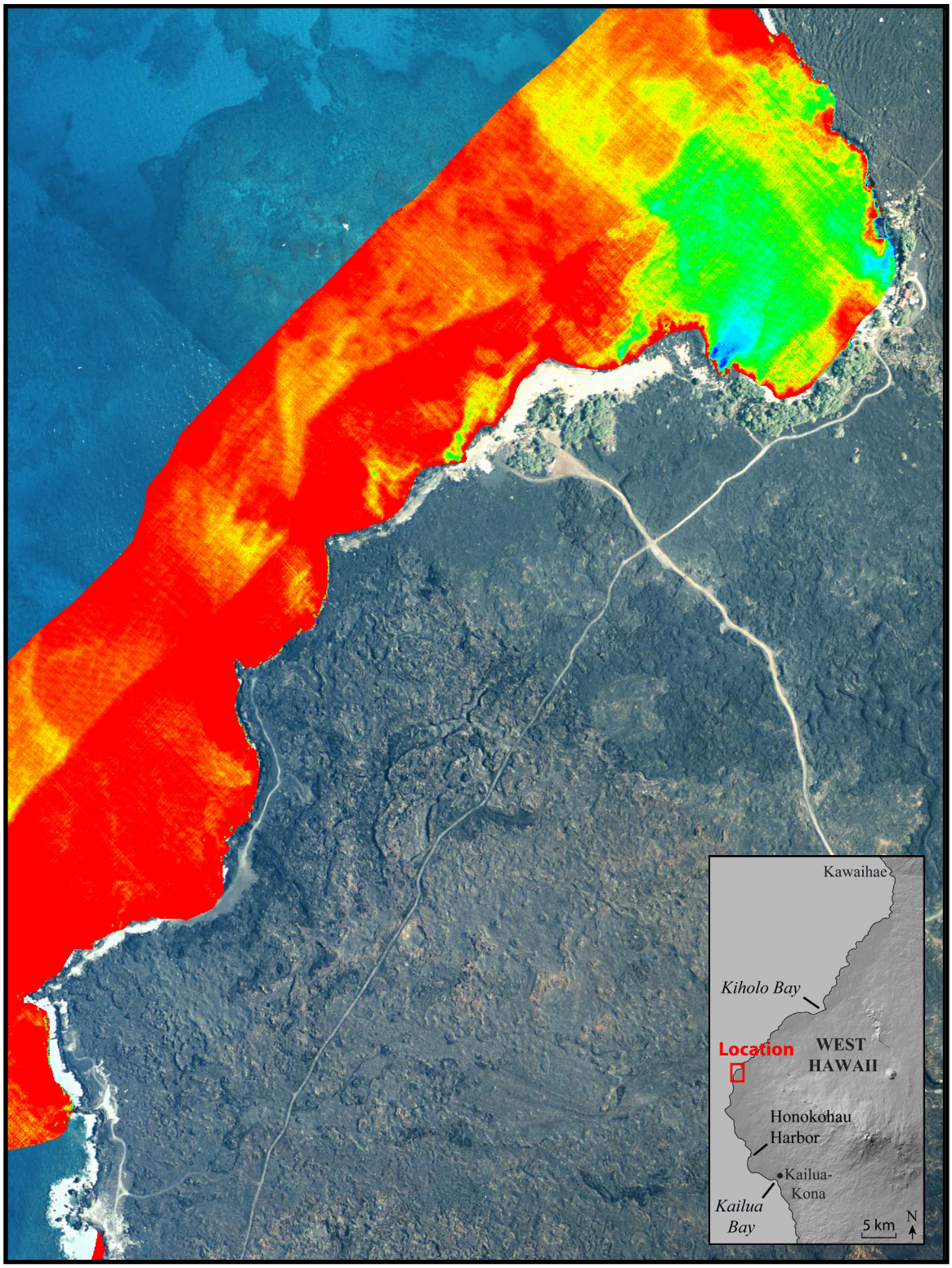

Panel 29.
Makolea Pt.

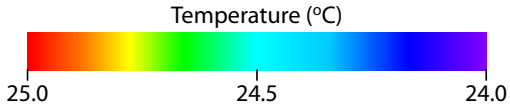

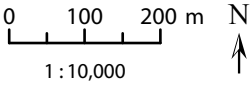

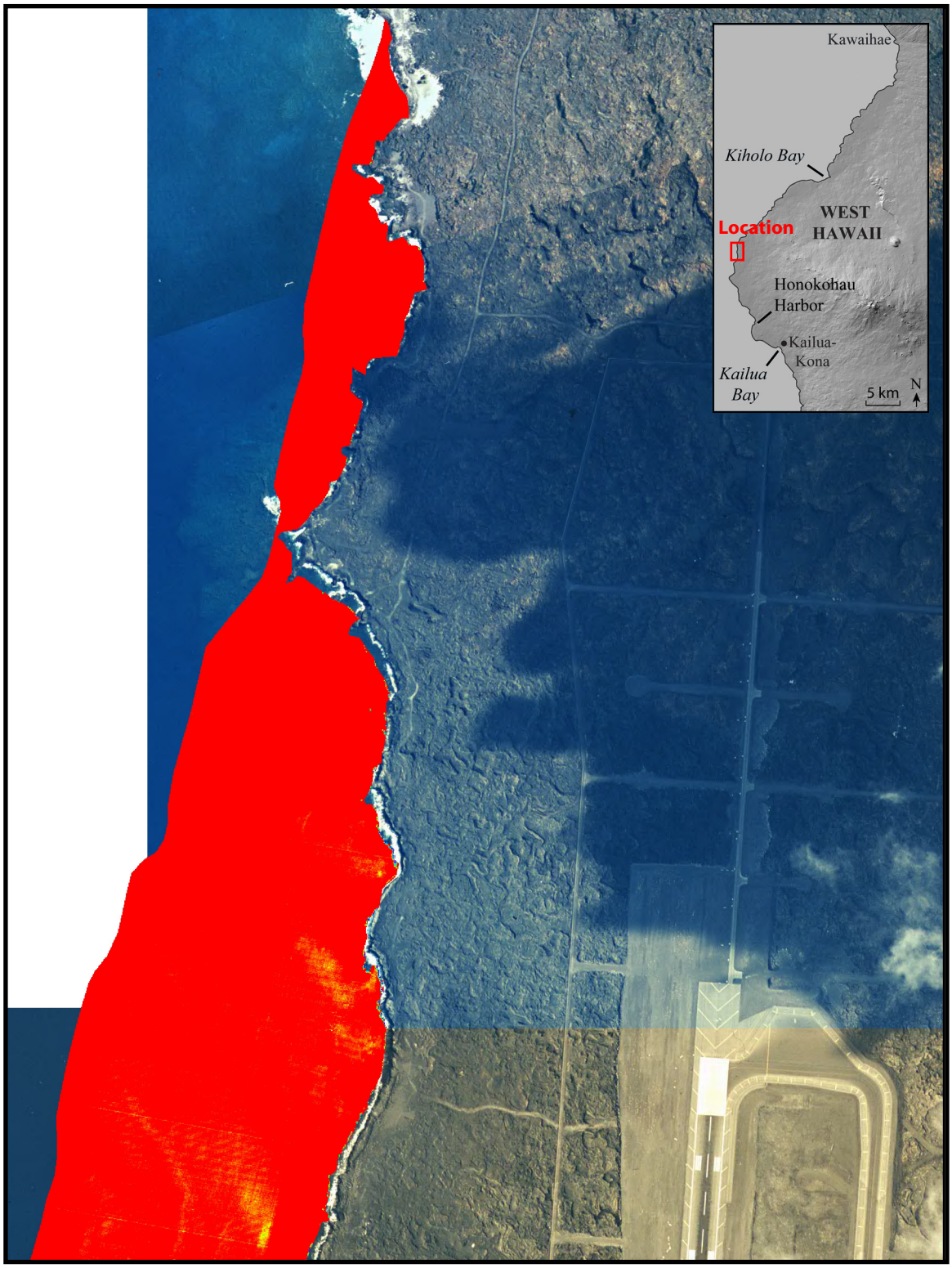

Panel 30.
Puu Kala Pt.

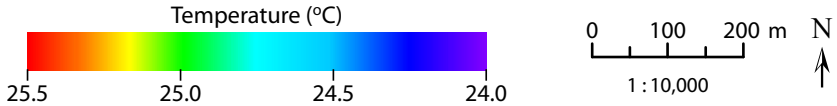

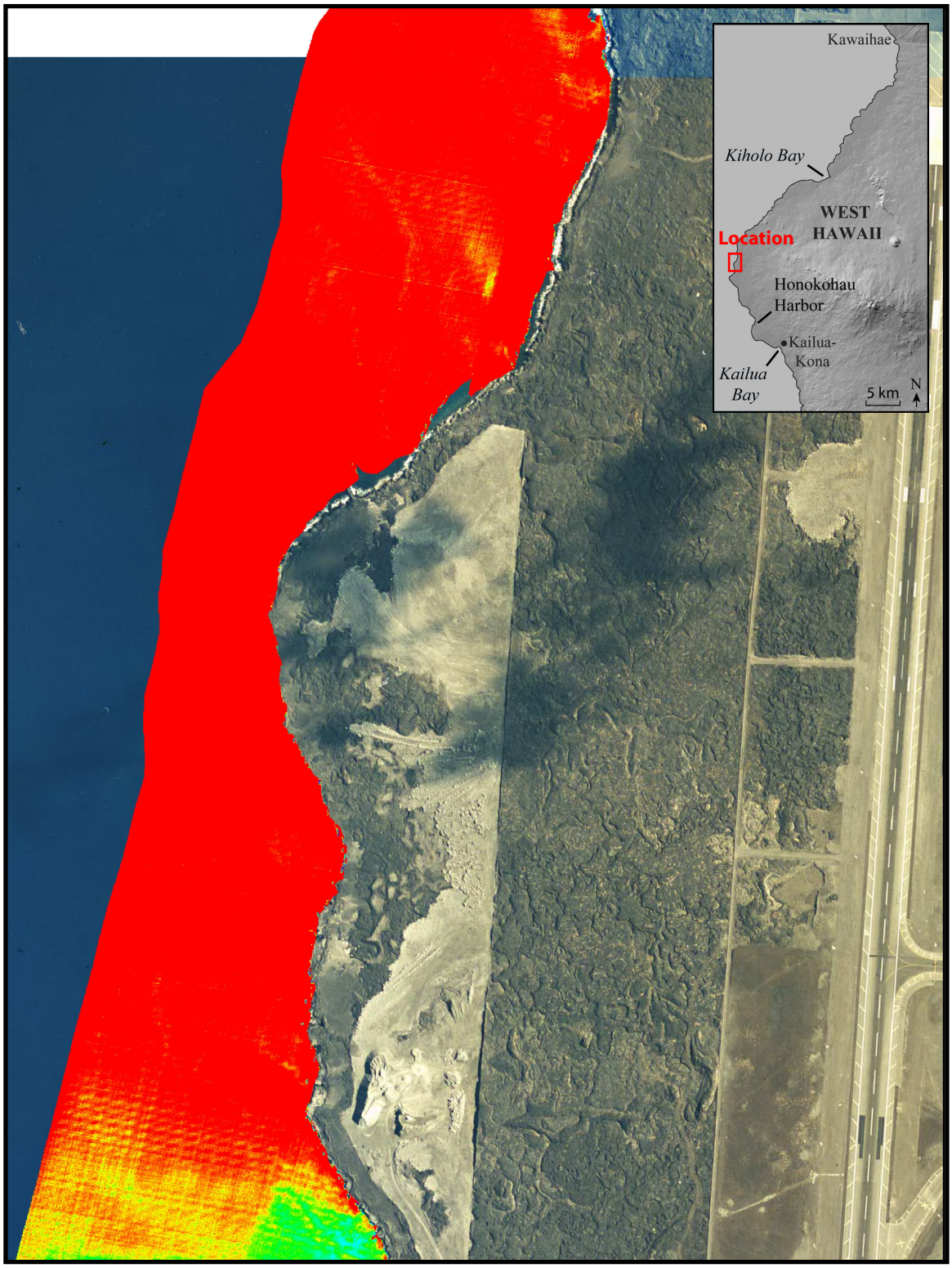

Panel 31.
Kona Airport

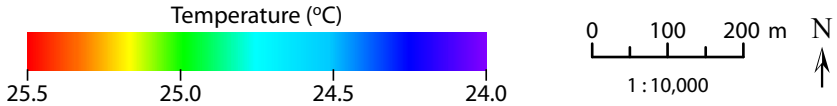

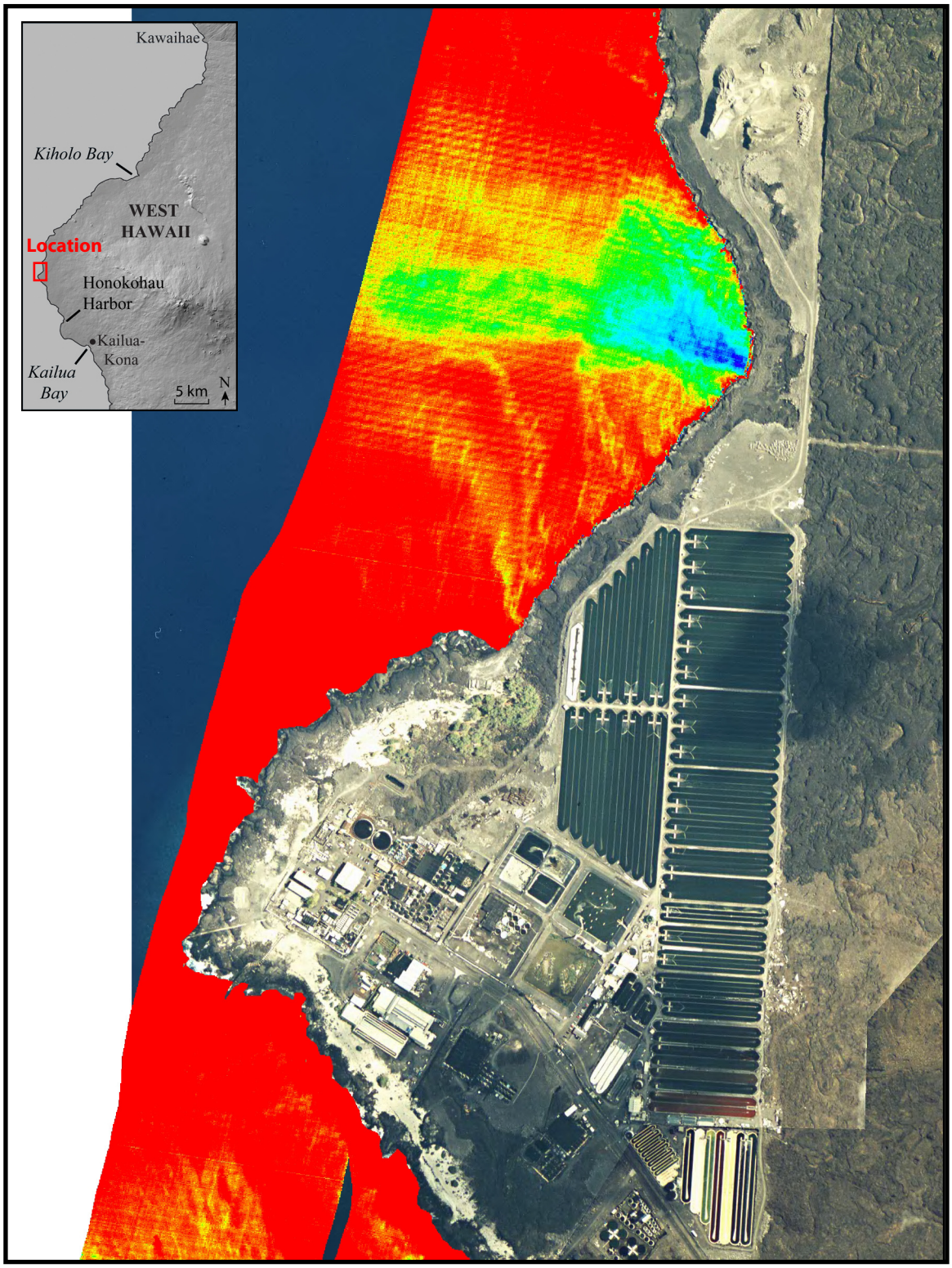

Panel 32.
Keahole Pt.

Temperature (°C)
25.5 25.0 24.5 24.0

0 100 200 m
1 : 10,000
N

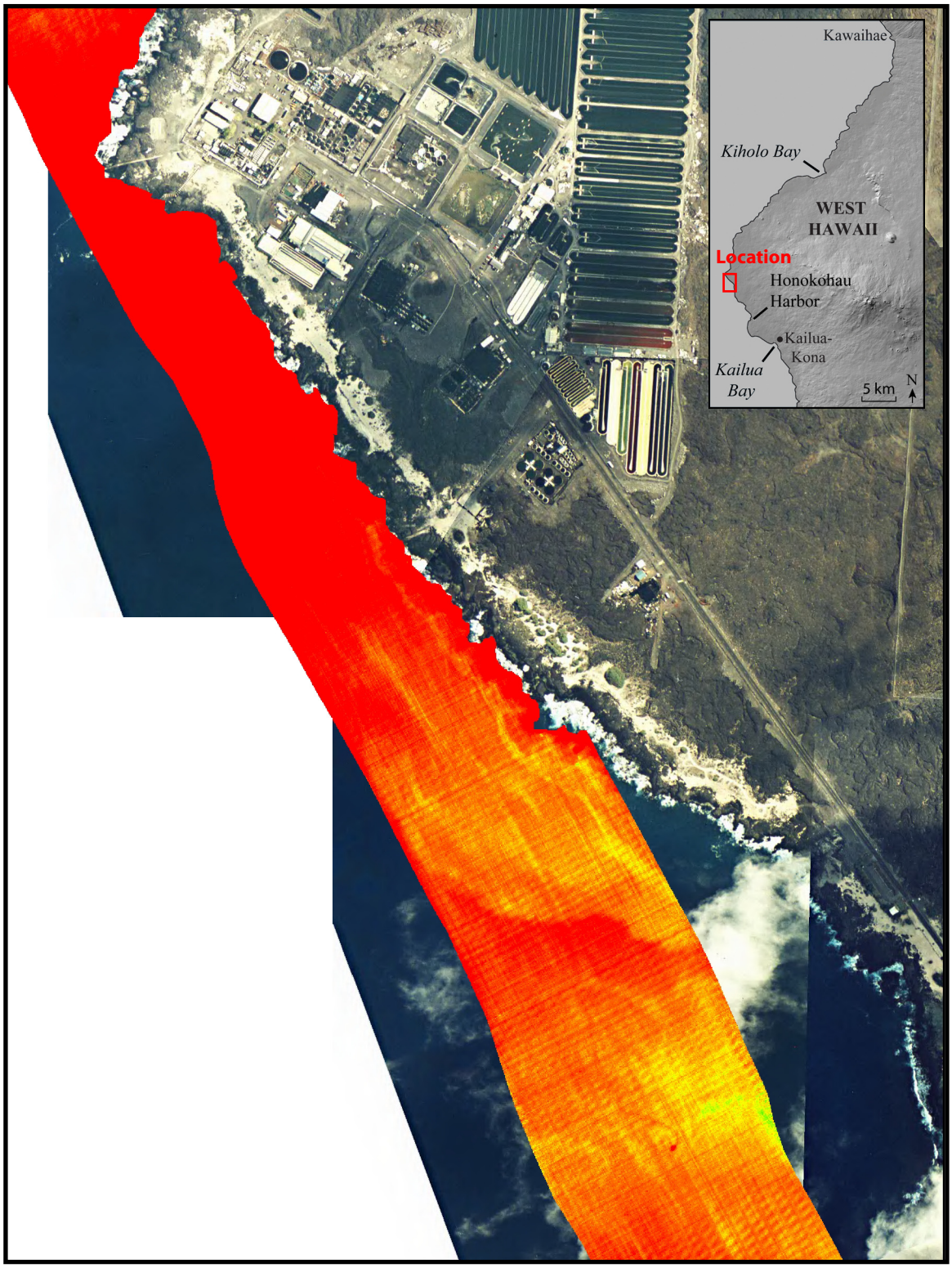

Panel 33.
Kalihi Pt.

Temperature (°C)
25.5 25.0 24.5 24.0

0 100 200 m
1 : 10,000
N

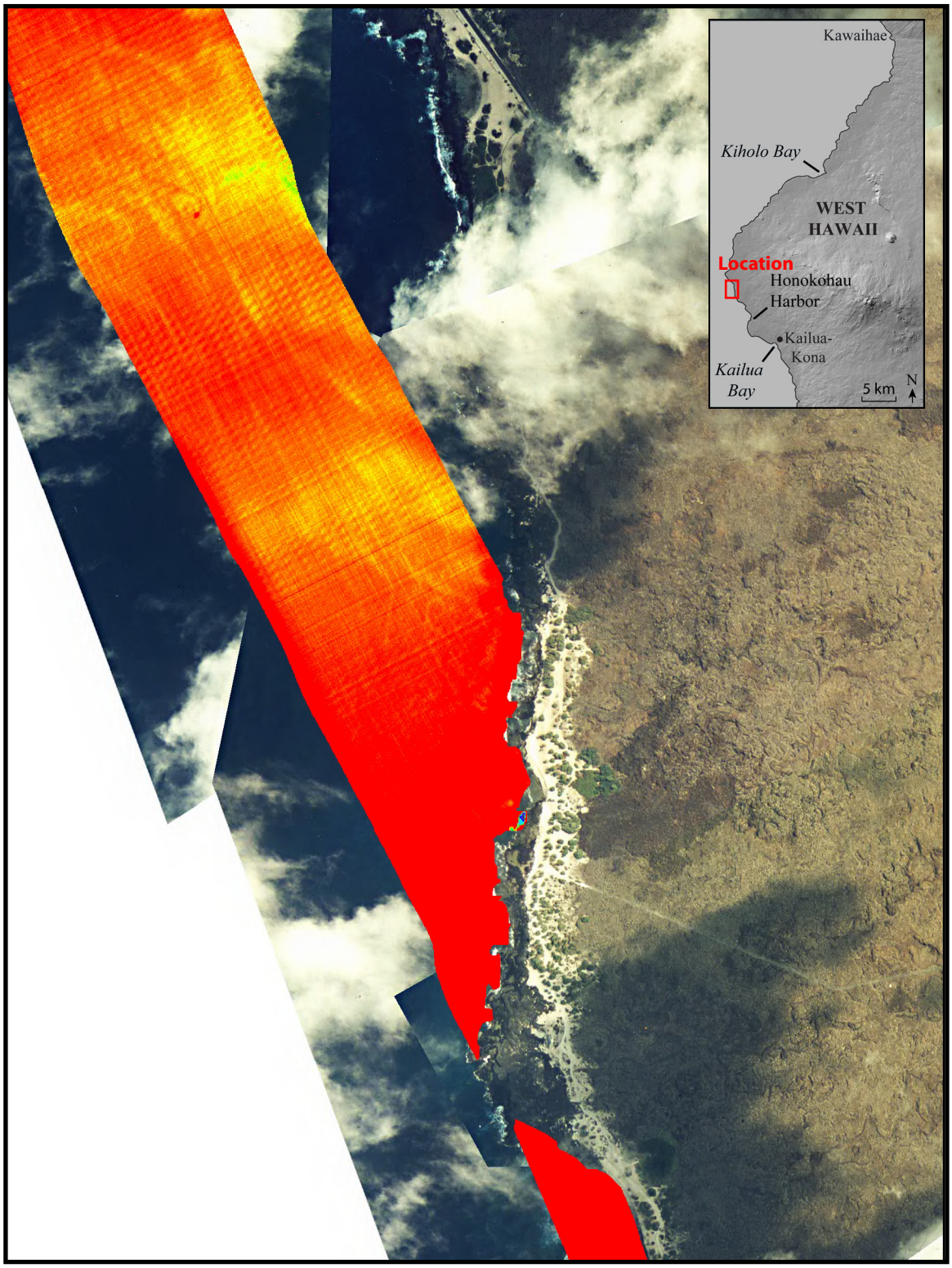

Panel 34.
Wawaloli Beach

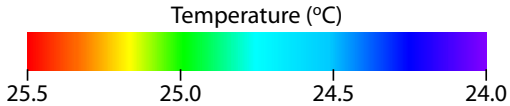

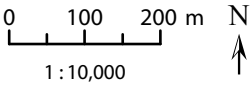

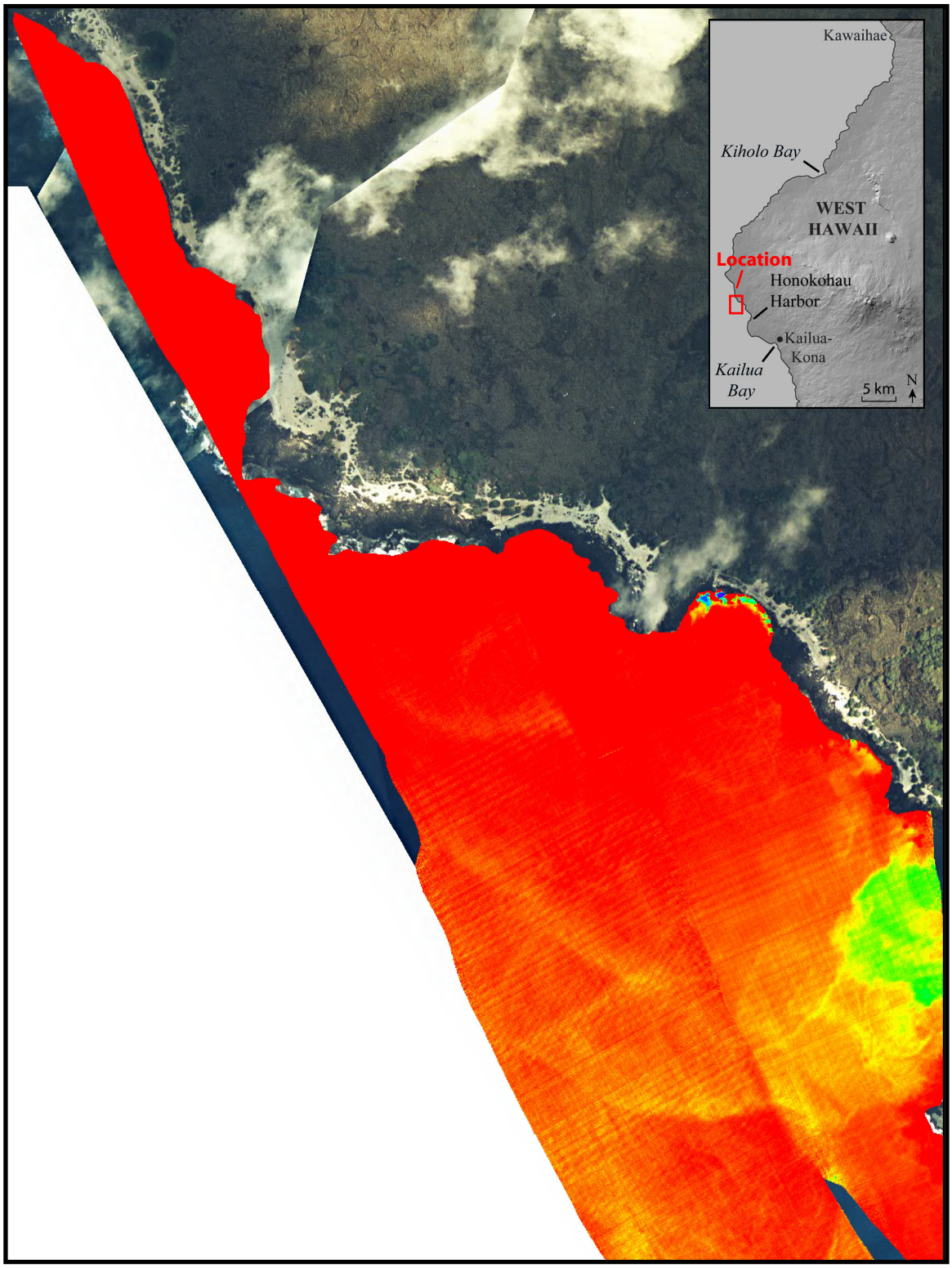

Panel 35.
Wawahiwaa Pt.

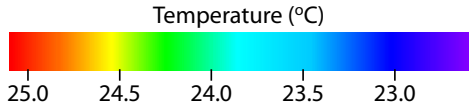

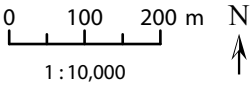

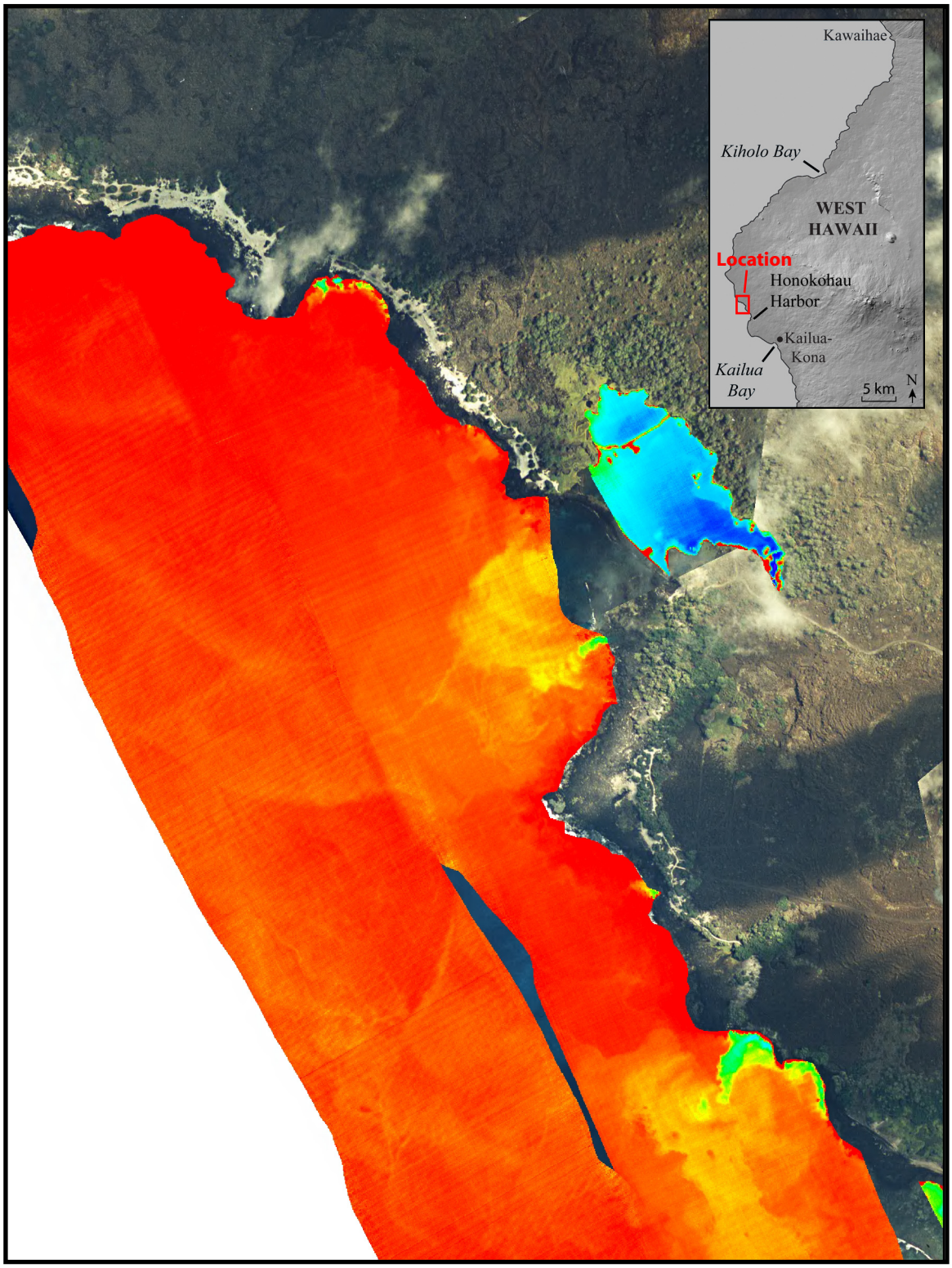

Panel 36.
Kaloko Pond

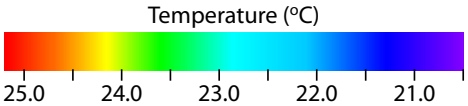

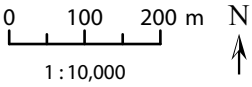

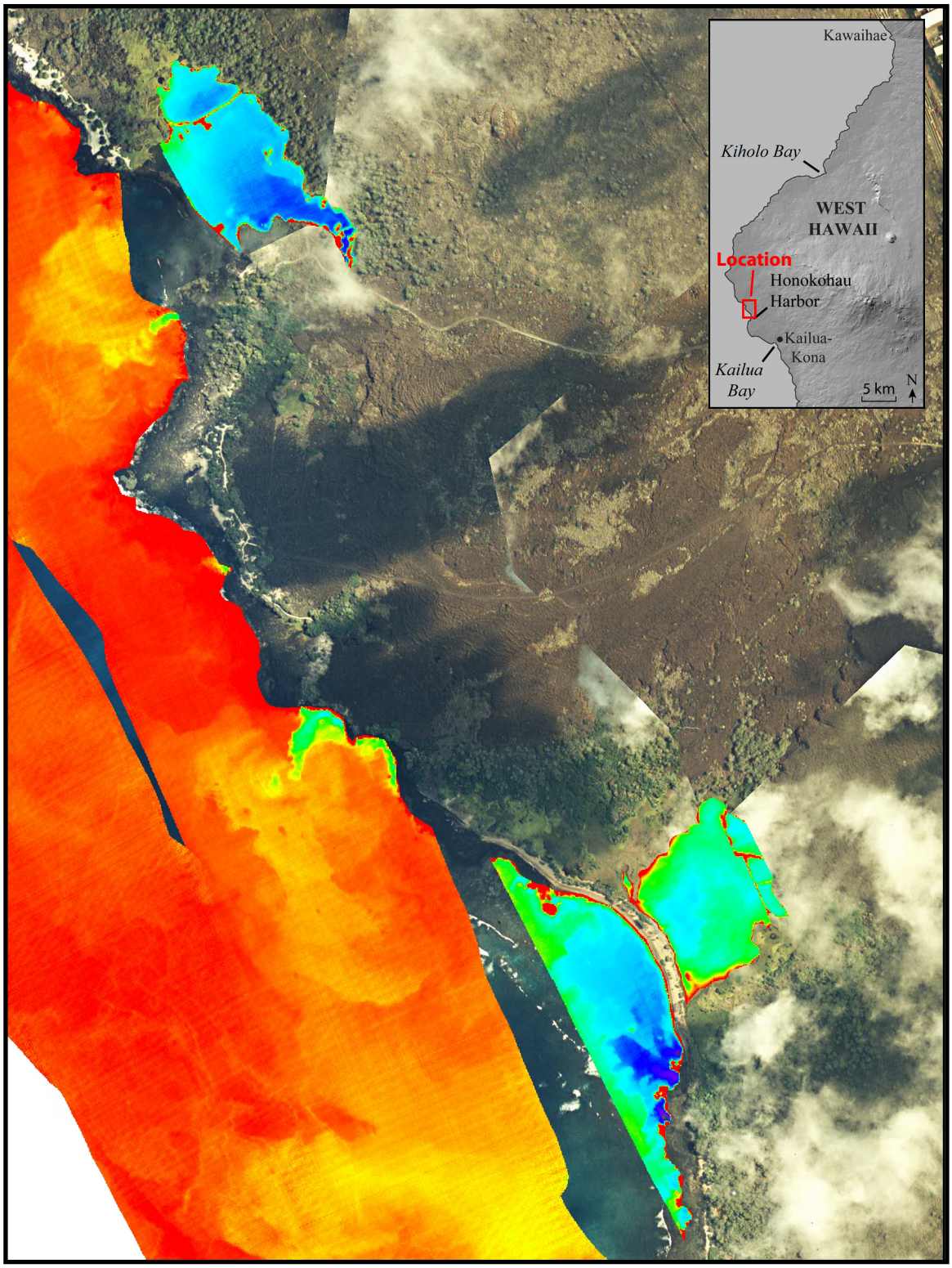

Panel 37.
Aimakapa Pond

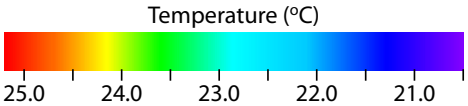

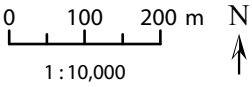

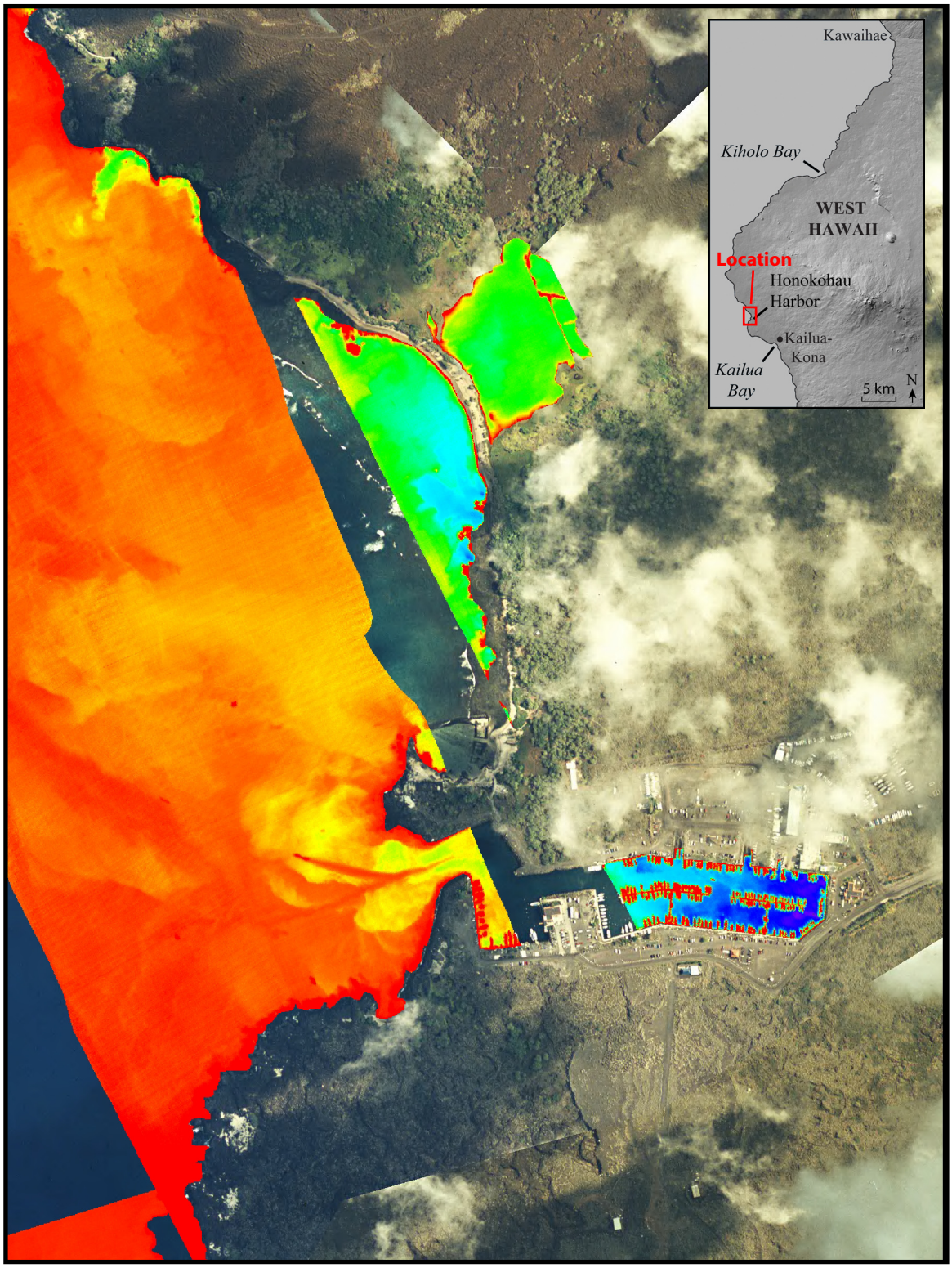

Panel 38.
Honokohau Harbor

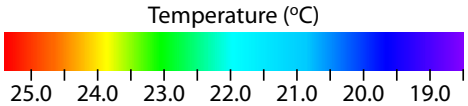

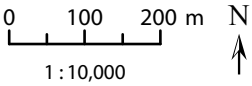

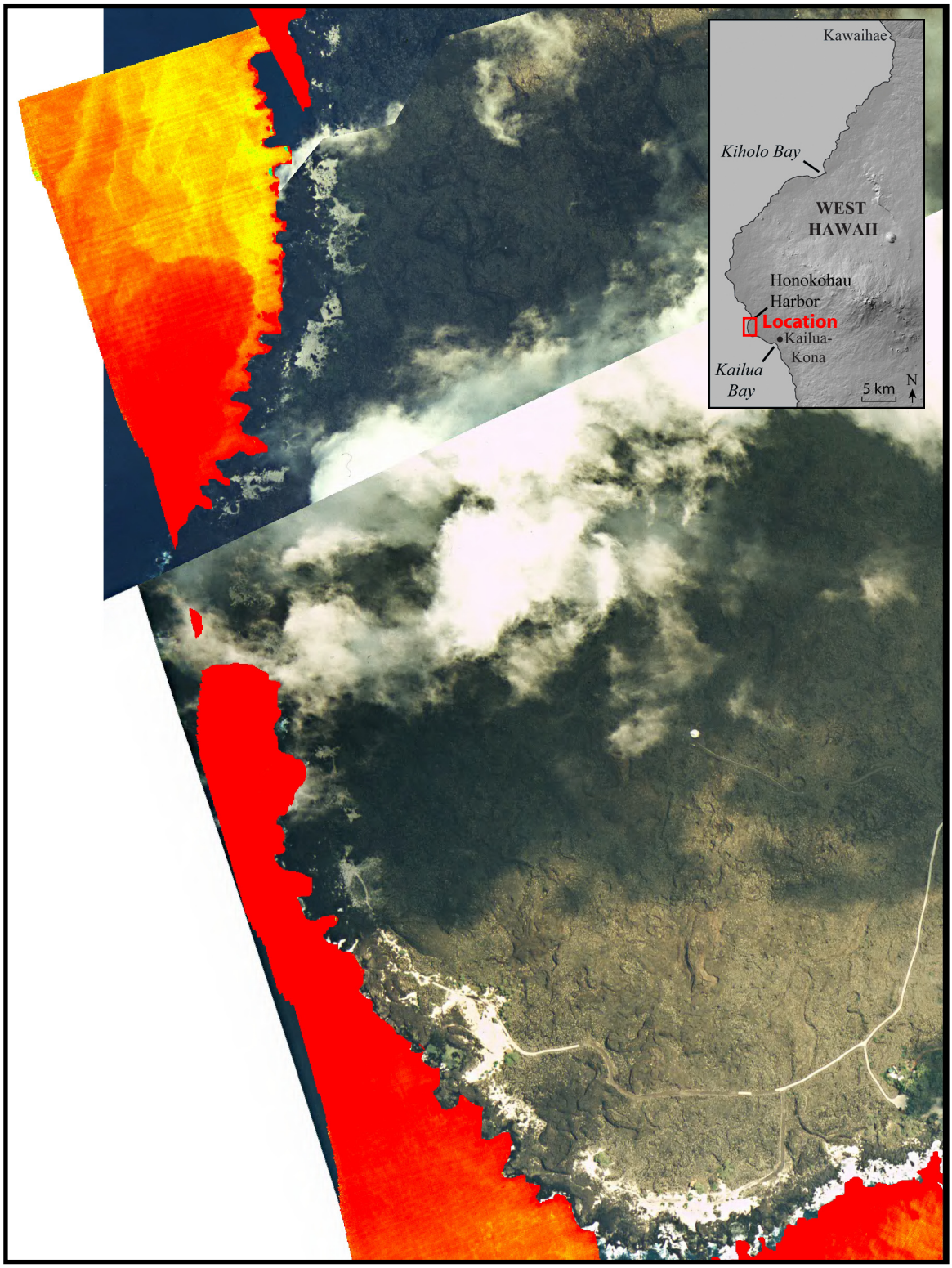

Panel 39.
Kaiwi Pt.

Temperature (°C)
25.0 24.5 24.0 23.5

0 100 200 m
1 : 10,000
N

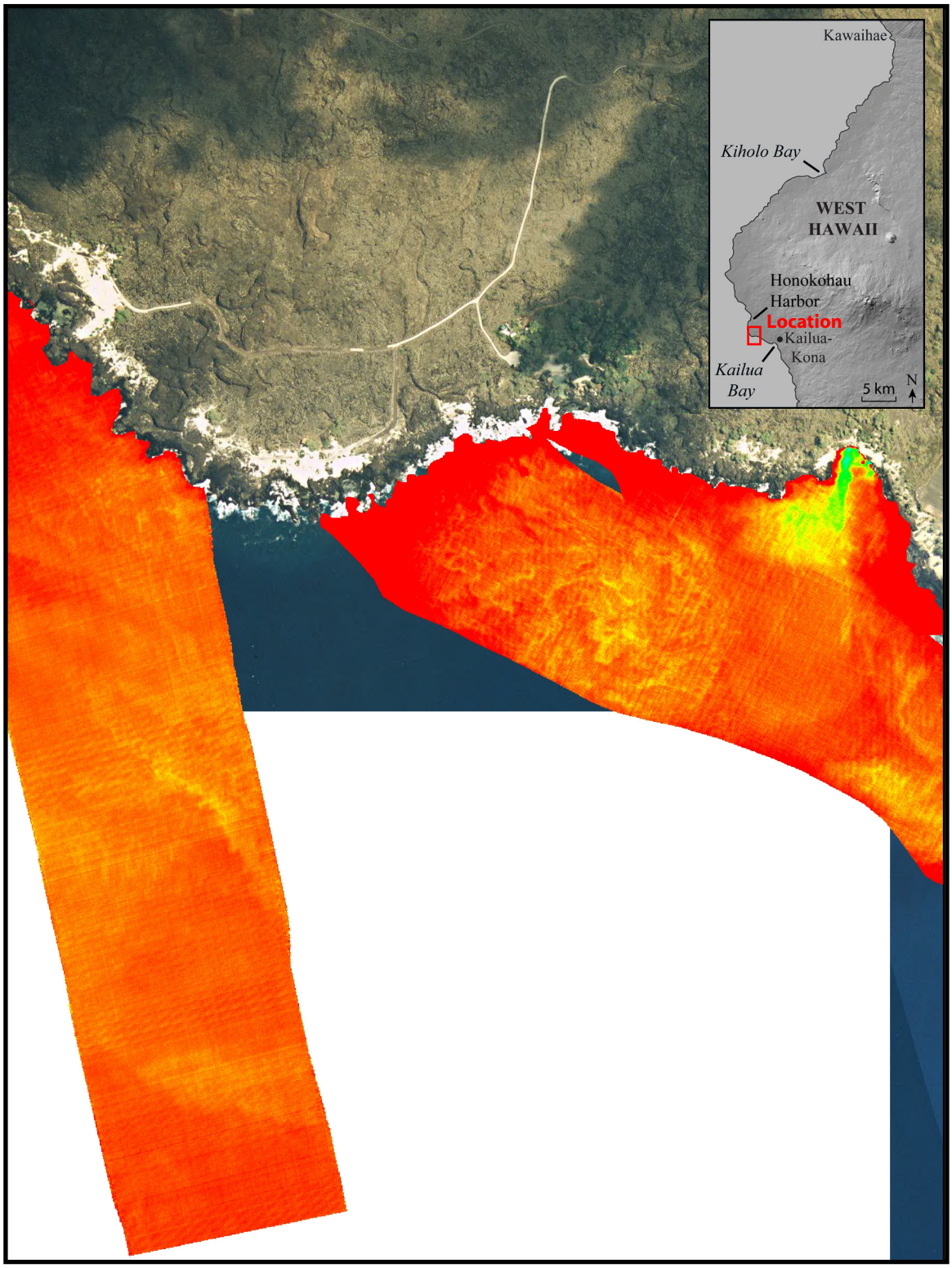

Panel 40.
Keahu o Lu Pt.

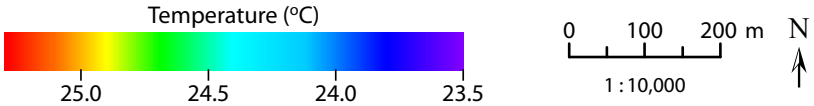

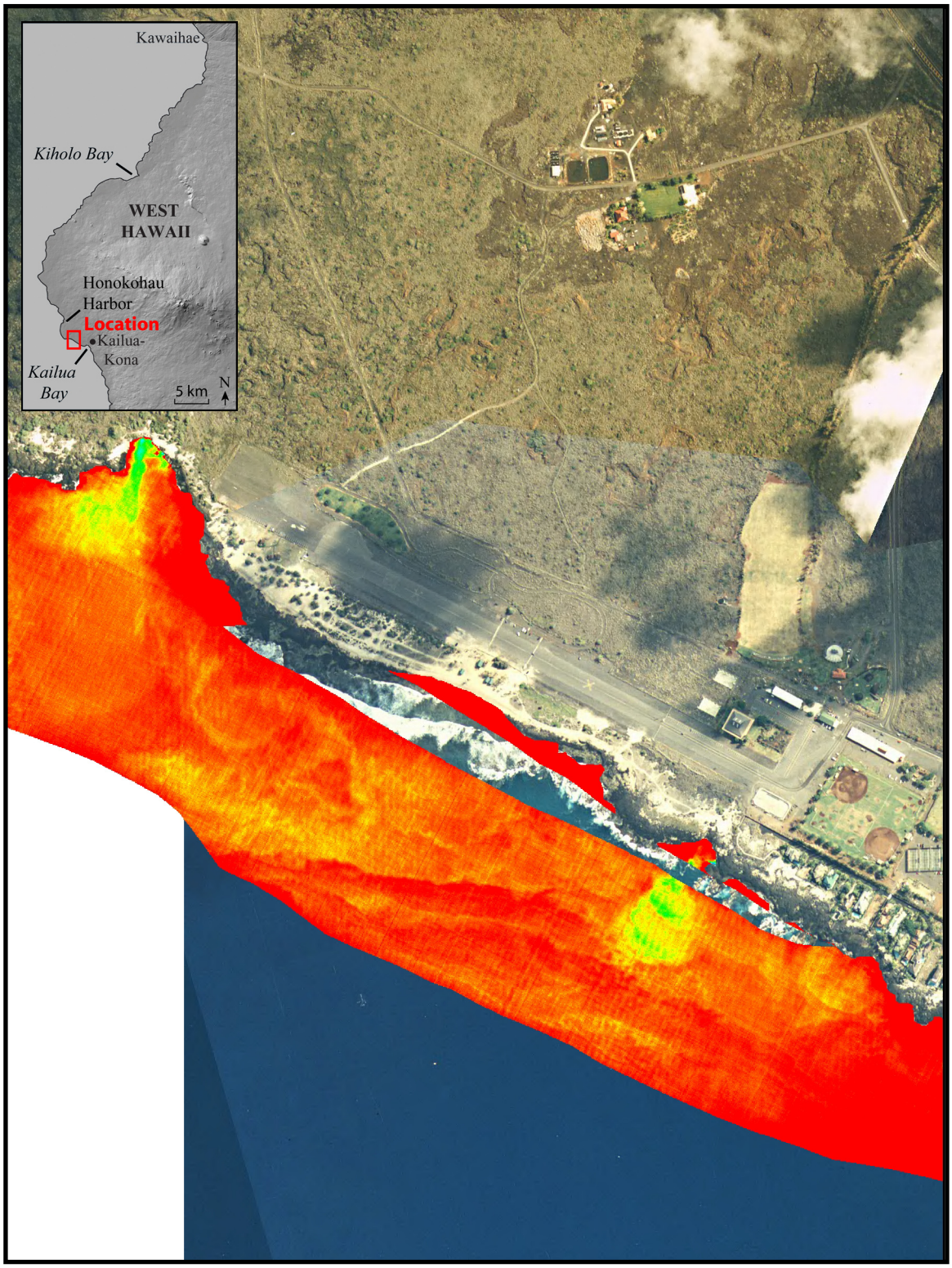

Panel 41.
Old Kona airport

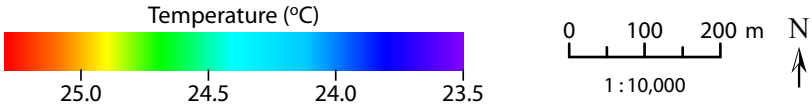

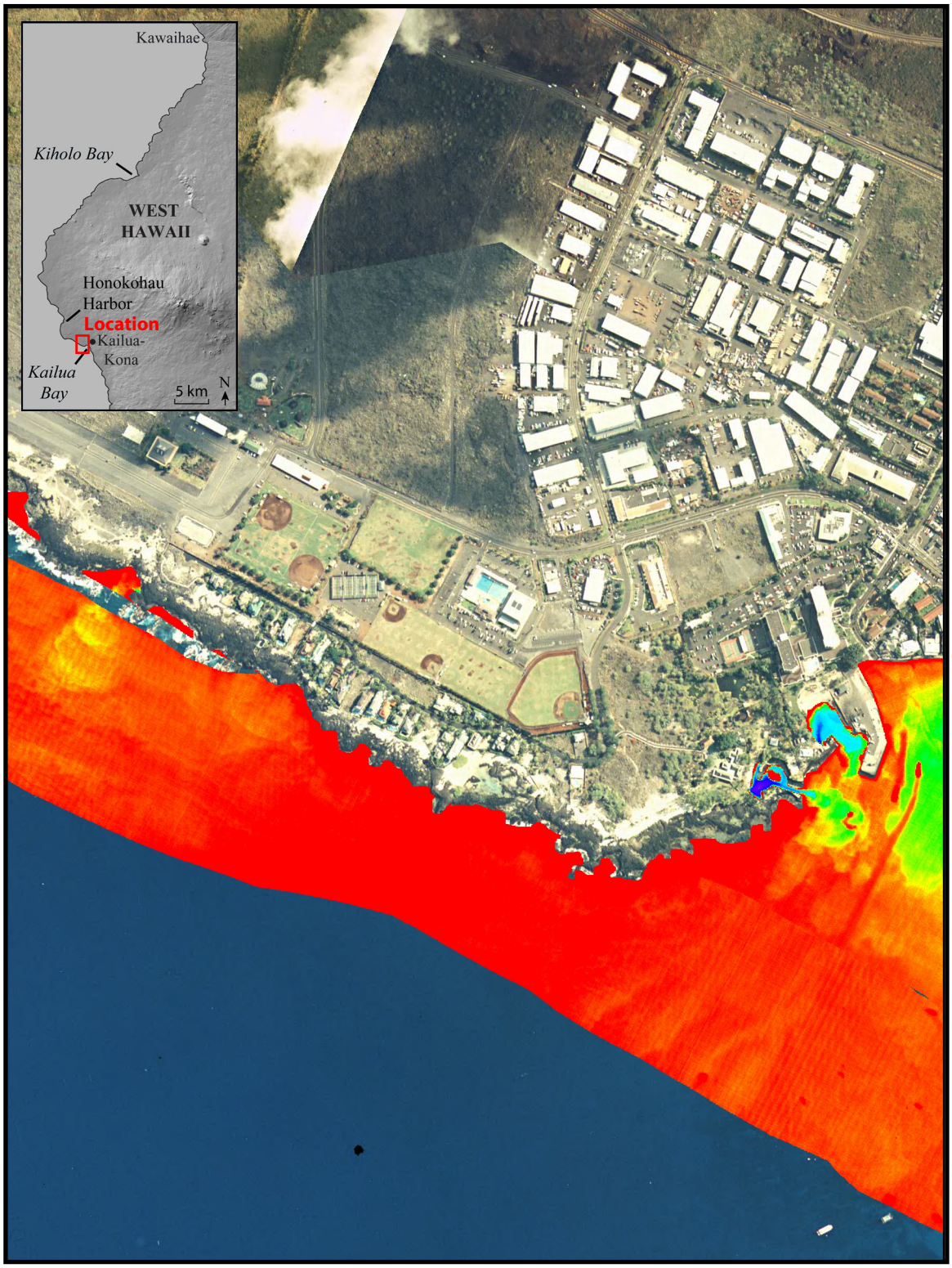

Panel 42.
Kuka'ilimoku Pt.

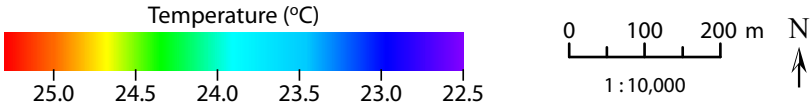

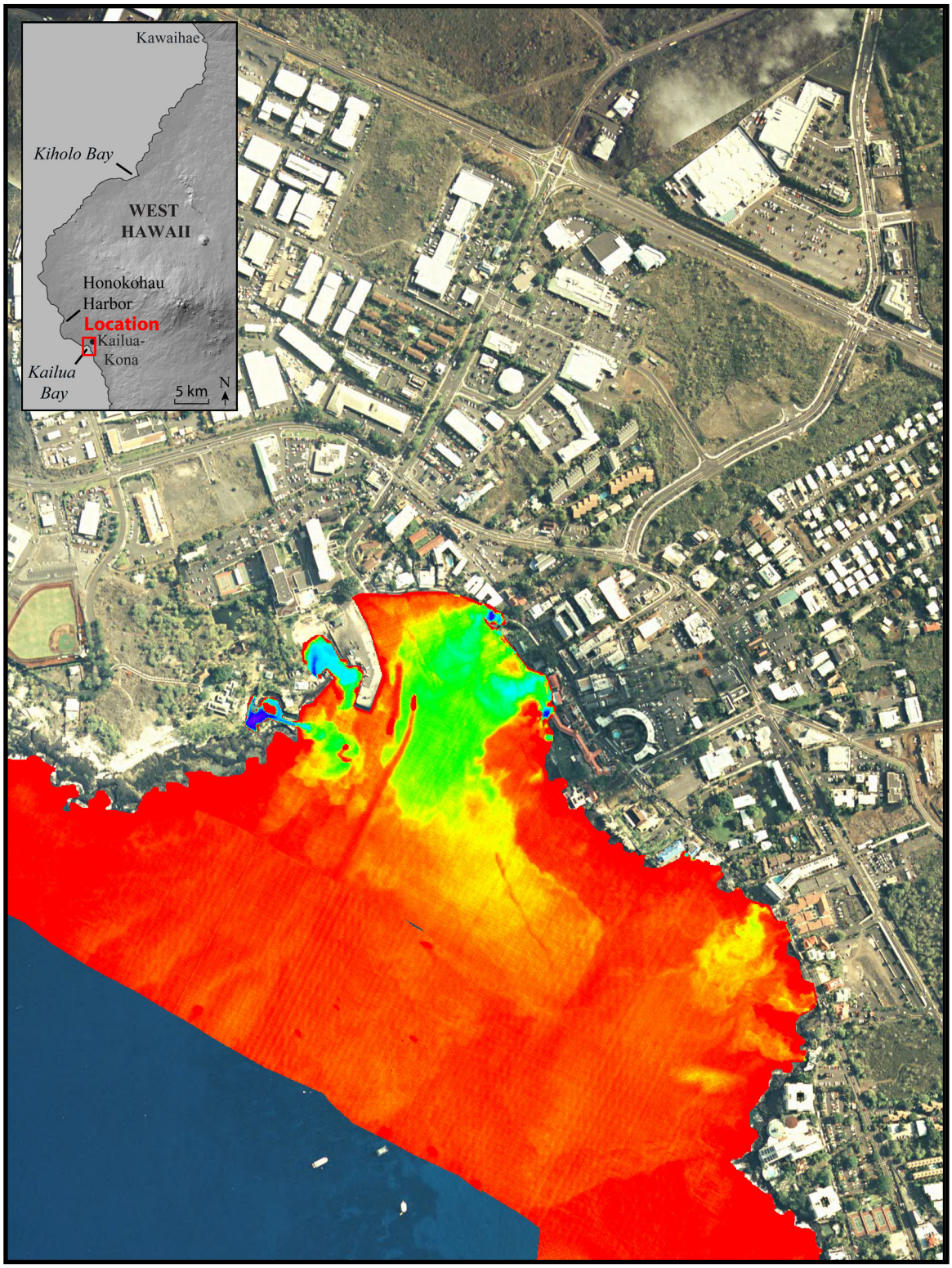

Panel 43.
Kailua Bay

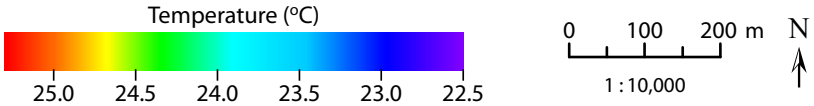

REFERENCES

Anderson, D. M., and D. L. Garrison. 1997. The ecology and oceanography of harmful algal blooms: Preface. Limnology and Oceanography **42:** i-ii.

Banks, W. S. L., R. L. Paylor, and W. B. Hughes. 1996. Using Thermal-Infrared Imagery to Delineate Ground-Water Discharge. Ground Water **34:** 434-443.

Bauer, G. R. 2003. A study of the ground-water conditions in North and South Kona and South Kohala Districts Islands of Hawai'i, 1991-2002: Commision on Water Resource Management Report, PR-2003-01., p. 94. State of Hawaii.

Bienfang, P. K. 1980. Water Quality Characteristics of Honokohau Harbor: A Subtropical Embayment Affected by Groundwater Intrusion. Pacific Science **34:** 279-291.

---. 1983. The Status of Water Quality, Water Circulation and Plankton Populations in Honokohau Small Boat Harbor, 1982, p. 11-31. A Decade of Ecological Studies Following Construction of the Honokohau Small Boat Harbor, Kona, Hawaii. U.S. Army Corps of Engineers (Honolulu District).

Boehm, A. B., G. G. Shellenbarger, and A. Paytan. 2004. Groundwater Discharge: Potential Association with Fecal Indicator Bacteria in the Surf Zone. Environmental Science & Technology **38:** 3558-3566.

Bowen, J. L. and others 2007. A review of land-sea coupling by groundwater discharge of nitrogen to New England estuaries: Mechanisms and effects. Applied Geochemistry **22:** 175-191. doi:110.1016/j.apgeochem.2006.1009.1002.

Breier, J. A., C. F. Breier, and H. N. Edmonds. 2005. Detecting submarine groundwater discharge with synoptic surveys of sediment resistivity, radium, and salinity. Geophysical Research Letters **32:** doi:10.1029/2005GL024639,022005.

Brown, C., L. N. Conner, J. L. Lillibridge, N. R. Nalli, and R. V. Legeckis. 2005. Remote Sensing of Coastal Aquatic Environments: An introduction to satellite sensors, observations and techniques.

Burnett, W. C. and others 2006. Quantifying submarine groundwater discharge in the coastal zone via multiple methods. Science of The Total Environment **367:** 498-543.

Burnett, W. C., H. Bokuniewicz, M. Huettel, W. S. Moore, and M. Taniguchi. 2003. Groundwater and pore water inputs to the coastal zone. Biogeochemistry **66:** 3-33.

Burnett, W. C., M. Taniguchi, and J. Oberdorfer. 2001. Measurement and significance of the direct discharge of groundwater into the coastal zone. Journal of Sea Research **46:** 109-116.

Burnett, W. C. and others 2007. Groundwater-derived nutrient inputs to the Upper Gulf of Thailand. Continental Shelf Research **27:** 176-190.

Cracknell, A. P., and L. W. B. Hayes. 1991. Introduction to Remote Sensing, 1st ed. Taylor & Francis.

Dollar, S. J., and M. J. Atkinson. 1992. Effects of nutrient subsidies from groundwater to nearshore marine ecosystems off the island of Hawaii. Estuarine, Coastal and Shelf Science **35:** 409-424.

Duarte, T. K. E., H. F. Hemond, D. Frankel, and S. Frankel. 2006. Assessment of submarine groundwater discharge by handheld aerial infrared imagery: case study of Kaloko fishpond and bay, Hawai‘i Limnology and Oceanography: Methods **4:** 227-236.

Gallagher, B. 1980. Physical Structure and Circulation in Honokohau, a Small Hawaiian Harbor Affected by Groundwater. Pacific Science **34:** 301-311.

Garrels, R. M., and F. T. Mackenzie. 1971. Evolution of sedimentary rocks. Norton and Co.

Giblin, A. E., and A. G. Gaines. 1990. Nitrogen Inputs to a Marine Embayment: The Importance of Groundwater. Biogeochemistry **10:** 309-328.

Gordon, D. C. J. and others 1996. LOICZ Biogeochemical Modeling Guidelines.

Hu, C., F. E. Muller-Karger, and P. W. Swarzenski. 2006. Hurricanes, submarine groundwater discharge, and Florida's red tides. Geophysical Research Letters **33:** L11601.

Juvik, J. O., and P. C. Ekern. 1978. A Climatology of Mountain Fog on Mauna Loa: Hawaii Island, p. 70. Water Resources Research Center Technical Report No. 118. University of Hawaii, Honolulu, Hawaii.

Kay, A. E., L. S. Lau, E. D. Stroup, S. J. Dollar, D. P. Fellows, and R. H. F. Young. 1977. Hydrologic and Ecologic Inventories of the Coastal Waters of West Hawaii, p. 94. Water Resource Research Center Technical Report 105. University of Hawaii.

Kelly, M. 1973. Historical background of Kekaha, North Kona, Hawaii. Honolulu, Dept. of Anthropology.

Kim, G., K.-K. Lee, K.-S. Park, D.-W. Hwang, and H.-S. Yang. 2003. Large submarine groundwater discharge (SGD) from a volcanic island. Geophysical Research Letters **30**.

Krest, J. M., W. S. Moore, L. R. Gardner, and J. T. Morris. 2000. Marsh Nutrient Export Supplied by Groundwater Discharge: Evidence From Radium Measurements. Global Biogeochemical Cycles **14:** 167-176.

Laroche, J., R. Nuzzi, R. Waters, K. Wyman, P. Falkowski, and D. Wallace. 1997. Brown Tide blooms in Long Island's coastal waters linked to interannual variability in groundwater flow. Global Change Biology **3:** 397-410.

Lee, D. R. 1977. A device for measuring seepage flux in lakes and estuaries. Limnology and Oceanography **22:** 140-147.

Lee, J.-M., and G. Kim. 2007a. Estimating submarine discharge of fresh groundwater from a volcanic island using a freshwater budget of the coastal water column. Geophysical Research Letters **34**.

Lee, Y.-W., and G. Kim. 2007b. Linking groundwater-borne nutrients and dinoflagellate red-tide outbreaks in the southern sea of Korea using a Ra tracer. Estuarine, Coastal and Shelf Science **71:** 309-317.

Macdonald, G. A., A. T. Abbott, and F. L. Peterson. 1983. Volcanoes in the Sea, 2nd ed. University of Hawaii Press.

Maciolek, J. A., and R. E. Brock. 1974. Aquatic Survey of the Kona Coast Ponds, Hawaii Island. Sea Grant Advisory Report.

Miller, D. C., and W. J. Ullman. 2004. Ecological Consequences of Ground Water Discharge to Delaware Bay, United States. Ground Water **42:** 959-970.

Mink, J. F., and L. S. Lau. 1993. Aquifer identification and classification for the island of Hawaii: Groundwater protection strategy for Hawaii, p. 31. University of Hawaii Water Resources Research Center Technical Report no. 188.

Mink, J. F., E. T. Murabayashi, and L. S. Lau. 1993. Five-year review of state land use districts: Protection of watershed and water resources in Hawaii, p. 31. Water Resources Research Technical Report No. 188. Universtiy of Hawaii, Honolulu, Hawaii.

Moore, W. S. 1996. Large groundwater inputs to coastal waters revealed by ^{226}Ra enrichments. Nature **380:** 612-614.

Moore, W. S., J. M. Krest, G. Taylor, E. Roggenstein, S. Joye, and R. Lee. 2002. Thermal evidence of water exchange a coastal aquifer: Implications for nutrient fluxes. Geophysical Research Letters **29:** 1704, doi:1710.1029/2002GL014923.

Moore, W. S., J. L. Sarmiento, and R. M. Key. 2008. Submarine groundwater discharge revealed by ^{228}Ra distribution in the upper Atlantic Ocean. Nature Geoscience **1:** 309-311. doi:310.1038/ngeo1183.

Mulligan, A. E., and M. A. Charette. 2006. Intercomparison of submarine groundwater discharge estimates from a sandy unconfined aquifer. Journal of Hydrology **327:** 411-425.

Oki, D. S. 1999. Geohydrology and Numerical Simulation of the Ground-Water Flow System of Kona, Island of Hawaii. U.S. Geological Survey Water-Resources Investigations Report 99-4073.

Oki, D. S., T. G. W., W. R. Souza, and E. L. Bolke. 1999. Ground-water resources in Kaloko-Honokohau National Historical Park, Island of Hawaii, and numerical simulation of the effects of ground-water withdrawls. U.S. Geological Survey Water Resources Investigation Report 99-4070.

Paerl, H. W. 1997. Coastal Eutrophication and Harmful Algal Blooms: Importance of Atmospheric Deposition and Groundwater as "New" Nitrogen and Other Nutrient Sources. Limnology and Oceanography **42:** 1154-1165.

Paytan, A., G. G. Shellenbarger, J. H. Street, and M. E. Gonneea. 2006. Submarine groundwater discharge: An important source of new inorganic nitrogen to coral reef ecosystems Limnology and Oceanography **51:** 339-342.

Peterson, R. N., W. C. Burnett, C. R. Glenn, and A. G. Johnson. 2008. Quantification of point-source groundwater discharges from western Hawaii. Limnology and Oceanography**:** submitted.

Peterson, R. N., W. C. Burnett, C. R. Glenn, and A. J. Johnson. 2007. A box model to quanitfy groundwater discharge along the Kona coast of Hawaii using natural tracers, p. 142-149. *In* W. Sanford, C. Langevin, M. Polemio and P. Povinec [eds.], A New Focus on Groundwater-Seawater Interactions. IAHS Press.

Pieters, C. M., and P. A. Englert. 1993. Remote geochemical analysis: elemental and mineralogical composition. Cambridge.

Rosenau, J. C., G. L. Faulkner, C. W. Hendry, and R. W. Hull. 1977. Springs of Florida. Florida Geological Survey Bulletin **31**.

Roxburgh, I. S. 1985. Thermal infrared detection of submarine springs associated with the Plymouth Limestone. Hydrological Sciences Journal **30:** 185-196.

Santos, I. R., W. C. Burnett, J. Chanton, B. Mwashote, I. G. N. A. Suryaputra, and T. Dittmar. 2008. Nutrient Biogeochemistry in a Gulf of Mexico Subterranean Estuary and Groundwater-Derived Fluxes to the Coastal Ocean. Limnology and Oceanography.

Schluessel, P., W. J. Emery, H. Grassl, and T. Mammen. 1990. On the Bulk-Skin Temperature Difference and Its Impace on Satellite Remote Sensing of Sea Surface Temperature. Journal of Geophysical Research **95:** 13,341-313,356.

Shaban, A., M. Khawlie, C. Abdallah, and G. Faour. 2005. Geologic controls of submarine groundwater discharge: application of remote sensing to north Lebanon. Environmental Geology **47:** 512-522.

Slomp, C. P., and P. Van Cappellen. 2004. Nutrient inputs to the coastal ocean through submarine groundwater discharge: controls and potential impact. Journal of Hydrology **295:** 64-86.

Stearns, H. T., and G. A. Macdonald. 1946. Geology and ground-water resources of the island of Hawaii.

Street, J. H., K. L. Knee, E. E. Grossman, and A. Paytan. 2008. Submarine groundwater discharge and nutrient addition to the coastal zone and coral reefs of leeward Hawai'i. Marine Chemistry **109:** 355-376. doi:310.1016/j.marchem.2007.1008.1009.

UNESCO. 1994. Protocols for the Joint Global Ocean Flux Study (JGOFS) Core Measurements. IOC Manual and Guides no. 29.

Valiela, I., J. Costa, K. Foreman, J. M. Teal, B. Howes, and D. Aubrey. 1990. Transport of Groundwater-Borne Nutrients from Watersheds and Their Effects on Coastal Waters. Biogeochemistry **10:** 177-197.

Valiela, I. and others 1992. Couplings of Watersheds and Coastal Waters: Sources and Consequences of Nutrient Enrichment in Waquoit Bay, Massachusetts. Estuaries **15:** 443-457.

Vitousek, P. M. 2004. Nutrient cycling and limitation: Hawaii as a model system. Princeton University Press.

Weigner, T. N. submitted. Limnology and Oceanography.

Wilkins, G. M. unpublished. 1992 Infrared video of volcano and fresh water, Hawaii.

Zekster, I. S. 2000. Groundwater and the Environment - Applictions for the Global Community. Lewis Publishers (CRC Press LLC).